SIMULTANEOUSLY COLLIERS AND COAL-FIRED WASTEWATER TREATMENT AS WELL AS ENERGY PRODUCTION THROUGH REVERSE ELECTRODIALYSIS

by

Thobeka Ngobese

This dissertation is submitted in the fulfilment of the requirements for the degree of Master of Engineering in Chemical Engineering to the Faculty of Engineering and the Built Environment at Durban University of Technology.

Supervisor: Dr. Peterson Thokozani Ngema

Co-Supervisors: Prof. Armel Tumba Kaniki

Dr. Nkululeko Nkosi

January 2024

PREFACE

This study was supervised by Dr. Peterson T. Ngema from Durban University of Technology (DUT), Department of Chemical Engineering in collaboration with co-supervisors (Prof. Armel T. Kaniki and Dr. Nkululeko Nkosi from Mangosuthu University of Technology (MUT), Department of Chemical Engineering. Experiments were carried out in the research laboratory in the Chemical Engineering research laboratory at MUT.

DECLARATION

I, **Thobeka Ngobese,** hereby declare that.

i. The research reported in this dissertation, except where otherwise indicated, is my original work.

ii. This dissertation has not been submitted for any degree or examination at any other university.

iii. This dissertation does not contain data, pictures, graphs, or other information belonging to other people unless specially acknowledged as being sourced from other persons.

iv. This dissertation does not contain the writing of others unless expressly acknowledged as being sourced from other researchers. Where other sources have been quoted, then

a) their words have been rewritten, but the general information attributed to them has been referenced.

b) Where their exact words have been used, their writing has been placed inside quotation marks and referenced.

v. Where I have reproduced a publication of which I am an author or co-author, I have indicated in detail which part of the publication was written by myself alone and have fully referenced such publications.

vi. This thesis does not contain text, graphics, or tables and is pasted from the internet unless expressly acknowledged, and the source is detailed in the thesis and the reference sections.

Signature of Candidate

25 /January /2024
Day/Month/Year

As the candidates' supervisors, we have approved the submission of this dissertation.

……	**……**	**……**
Supervisor (Dr. Ngema)	Co-supervisor (Prof. Kaniki)	Co-supervisor (Dr. Nkosi)
……../……./…….	**……../……./…….**	**……../……./…….**
Day/Month/Year	**Day/Month/Year**	**Day/Month/Year**

ACKNOWLEDGEMENTS

Working on this topic has been very rewarding and would not have been possible without the contribution of some wonderful souls.

- I would like to give credit to **Almighty God,** his presence may not be visible, but I trust that he is always by my side.
- A Special thanks to Prof. Armel T. Kaniki and Dr. Peterson T. Ngema for giving me the opportunity and guidance during the study period. I thank Dr. Nkululeko Nkosi for his valuable suggestions in my project. Their guidance helped me in the time of research and writing of this dissertation. Thank you for the opportunity bestowed on me to obtain this degree.
- I would also like to thank my friend, Miss Nompumelelo Lindiwe Ndebele, who is also my academic mentor, for her encouragement whenever I thought of giving up.
- A big thank you to the MUT Blue Energy team (Mfanelo Mbokwana and Lungisane Ngcobo); you were always there when I needed help.
- I sincerely thank the DUT for allowing me to obtain my master's degree. I would like to thank MUT for being the first university in Africa to introduce Blue Energy research. Thanks to the Chemical Engineering Department for providing a well-equipped resource to conduct my research.
- Most of all, I thank my husband, Zamokuhle Ngobese, my greatest supporter and smile keeper. Thank you for your immeasurable love and understanding.
- A big thank you to my parents (Musawenkosi, Samkelo, Debra, and Nokukhanya) whose faith in me never faded; their prayers keep me moving.
- My heartfelt gratitude goes to my children (Akhanya, Xoliso, and Yamihle) for always being patient with me and my studies.
- Lastly, my siblings (Scelo, Sipho, and Nomalungelo), for their words of wisdom, gave me strength every time I felt like giving up.

DEDICATION

I dedicate this work to honour my late mother-in-law, Hlengiwe Mamthethwa Ngobese.

ABSTRACT

One primary sector contributing to the country's economic development is coal mining. As the country's primary energy source, coal dominates the country's energy mix. Conversely, the devastating environmental impact of this industry cannot be ignored. An ever-increasing population and economic growth exacerbate this problem further. This energy resource, "coal", is mined using large quantities of water, resulting in salted wastewater and further contaminating groundwater. South Africa (SA) is experiencing water shortages because of climate change, which coal directly contributed to, so it has no choice but to implement mitigation plans instead of preventing it to ensure its sustainability.

Therefore, it is in this context that led to the motive for this current research. This study uses reverse electrodialysis (RED) technology to mitigate and address this environmental challenge sustainably. A vital advantage of this technology is its ability to produce power while purifying wastewater. This advantage makes it a valuable energy mix that can substantially reduce and alleviate coal-fired emissions. The study aimed to investigate the desalination and power generation process for treating synthesised coal mining and colliers using a RED stack.

The study's hypothesis was tested by using small laboratory-scale RED stacks. This study used synthetic wastewater to mimic SA's colliery mine and coal power plant wastewater. A performance assessment of the RED stacks was conducted under varying system temperatures, solution concentrations, and flow rates. 20 to 40 °C system temperatures, 1 to 2 mol/L solution concentrations, and 896 to 1550 mL/min flow rates were used. Within the specified experimental ranges, an empirical tool, response surface methodology (RSM), was used to minimise the number of experiments while obtaining sufficient experimental data. The selected process parameters were converted into dimensionless codified data in three levels. A general full factorial design type recommended 18 experimental runs. The influence of each selected parameter was examined individually in the first part of this study. A range of 2.31 to 10.75 W/m^2 and 3.94 to 16.13 wt.% power density and salt removal were obtained at the selected experimental ranges. These results corresponded to a membrane flux range used in this study. The membrane flux data was used to assess scale-up feasibility and cost estimation for the RED technology.

Statistical analysis was performed using the historical data design (HDD) option provided by RSM software to examine the combined influence of the investigated parameters on power density and salt removal. The results recommended that the 2FI model, as the highest order with significant terms, can describe the desalination and power density. A good agreement was found between experimental data and data generated by empirical models, with a less than 3% deviation. A regression (R^2) analysis was performed to determine the accuracy and reliability of the developed empirical models. An accuracy level of 95% was obtained in predicting experimental data within the experimental range for these models. Against this brief, the two-factor interaction (2FI) acquired by the model elucidates that this model is not recommended since it cannot make accurate predictions, as 0.6949 as well as 0.8704 for salt removal percentage and power density, respectively, indicate a relatively low value for regression. The combined effects and significance of input parameters were assessed with a three-dimensional surface (3-D) and a contour plot. The assessment revealed that power density and salt removal were less affected by the increase in flow rate than by solution concentration and system temperature.

The feasibility of the technology was further explored by optimising input variables since the membrane flux data alone cannot provide detailed information on the technology's potential. Increasing RED parameters, such as pumping at higher flow rates, frequently requires more energy; therefore, pumping costs may increase if the operating parameters necessitate higher solution flow rates, affecting the RED system's overall running costs. The temperature, concentration, and flow rate were optimal through RSM software at 40℃, 1.93 mol/L and 896 mL/min. This high temperature will accelerate scaling effects, leading to technical failure if the technology is used to treat or produce electricity on a large scale. Consequently, this technology would be more expensive. However, this does not exclude the possibility of replacing current conventional technologies with this technology. After RED technology has been conceptually designed and cost analysis, including sensitivity analysis, has been conducted, a realistic conclusion can be drawn.

The effect of divalent ions was investigated in further detail using these optimal conditions. The synthetic coal mine wastewater was prepared by adding Ca^{2+} and SO_4^{2-}, maintaining NaCl concentration and increasing divalent ions. Deionised water simulating lower concentrations likely affected the overall performance of the RED stack in this study. In this case, further investigation into the effect of lower concentrations should be recommended to examine

improving the performance of RED stacks at even lower concentrations. It will also be possible to assess if they are effective on wastewater containing low salt levels. This study does not recommend the HDD method for optimising the experimental results. However, further investigation should be conducted to accurately develop models that would produce a reliable model with acceptable prediction ability. In this manner, similar experimental investigations can be conducted more quickly.

RESEARCH OUTPUT

Conference proceedings:

Peer-reviewed

T. Ngobese, P.T. Ngema, A.T. Kaniki, N. Nkosi 'Progress on strategies to maximize reverse electrodialysis power density using industrial and municipal effluents' in JCBEE-23 Nov. 16-17, 2023, Johannesburg (South Africa). International Institute of Chemical, Biological & Environmental Engineering, pp. (162-164). https://doi.org/10.17758/IICBE5.C1123044

Proceeding only

T. Ngobese, P.T. Ngema, A.T. Kaniki, N. Nkosi. 'Decarbonization by desalination with reverse electrodialysis: A comparative study', in FRD-23 Oct. 23, Durban (South Africa). Faculty of Engineering and the Built-Environment Research Day.

TABLE OF CONTENTS

LIST OF FIGURES

CHAPTER 2 - LITERATURE REVIEW

CHAPTER 3 -THERMODYNAMICS FUNDAMENTAL

CHAPTER 4 – EXPERIMENTAL METHODOLOGY

CHAPTER 5 - RESULTS AND DISCUSSION

APPENDIX C

APPENDIX D

APPENDIX E

APPENDIX F

LIST OF TABLES

APPENDIX B

APPENDIX C

APPENDIX D

NOMENCLATURE

English letters

A	Area
F	Flowrate
T	Temperature
R	Resistor
E	Energy
v	Velocity

Greek letters

α	Membrane Permselectivity
β	Spacer Masking Factor
γ	Activity Coefficient
ε	Spacer Porosity
μ	Dynamic Viscosity
ρ	Density
υ	Number of Ions into which a Molecule Dissociates
ϕ	Mole Ratio

Latin Letters

$Vstack$	Voltage Across the RED Stack
$\Delta Gmix$	Gibbs Free Energy of Mixing
$\Delta Gmix, VA$	Gibbs Free Energy of Mixing per Volume of Solution A
$Ncell$	Total number of cells
Nm	Total number of membranes
$Pnet$	Net Power
$Ppump$	Pumping Power

$Pstack$	Power Produced by the RED Stack
Δp	Change in Pressure
$Rgas$	Ideal Gas Constant
RBl	Boundary Layer Resistance
$R\Delta C$	Resistance Due to the Concentration Drop Along the Channel
$Relec$	Electrode Resistance
$Rload$	Load Resistance
$Rohmic$	Ohmic Resistance

Superscripts and subscripts

A	Solution A
B	Solution B
Cell	Cell pair
Low	Dilute Solutions
High	Concentrated Solutions

Abbreviation

AEM	Anion Exchange Membrane
ANOVA	Analysis of Variance
CEM	Cation Exchange Membrane
DOE	Design of experiments
ERS	Electrode rinse solution
IEM	Ion Exchange Membrane
OCV	Open-circuit voltage (V)
PRESS	Predicted Residual Error Sum of Squares
RED	Reverse Electrodialysis
RSM	Research Surface Methodology
SGP	Salinity Gradient Powe

CHAPTER 1 - INTRODUCTION

Chapter Overview

Desalination has been considered the solution to freshwater salinization caused by coal wastewater. However, when applied on larger scales, it typically requires a substantial amount of energy, which has been a drawback regarding economic and environmental concerns. Reverse electrodialysis (RED) technology, a green technology, can generate electricity while producing fresh water due to the migration of ions. As a result, reverse electrodialysis desalination is being developed to reduce contaminants (salt wastewater) in coal-generated wastewater and provide a more environmentally friendly alternative electricity source that desalination plants can offer, thereby saving Eskom and the water industry. A well-articulated motivation, rationale, study aims, hypotheses, research questions, and objectives are also provided. In this chapter, the significance of the study is also explained. Lastly, another purpose of this chapter is to provide a comprehensive dissertation overview.

1.1. Background into wastewater from coal

Life depends on water, the most valuable natural resource (Kurz *et al.* 2005; Hossain 2015). Consequently, clean water is scarce due to contamination caused by industrial, mining, agriculture, and human waste disposal (Schwarzenbach *et al.* 2010; Du Plessis and du Plessis 2019). The coal mining industry also contributes to this concern due to its environmental impact, including generating large quantities of wastewater (Pan et al. 2012; Rashed 2013; Wang et al. 2018; Palani et al. 2021). Pollutants in this wastewater pose a threat to human health and ecosystems.

It is common for coal mining wastewater to be discharged as combined effluent, containing discharges from various sources, including mine water (MW), acid mine drainage (AMD), coal washery effluent, and coke plant wastewater. These inorganic compounds, such as high levels of chlorides and sulphates, result in vast amounts of salt load each year because they contain many inorganic compounds (Kotelo 2013; Pondja 2013; Hareesh 2015; Maiti *et al.* 2019).

Large land areas are often disturbed during surface coal mining, which generates significant amounts of wastewater. Coal-fired power plants generate wastewater when flue gas desulfurization (FGD) systems cool and treat flue gas. Heavy metals, trace elements, and

dissolved salts are among the pollutants in this wastewater. As a result of bioaccumulation and exposure, these pollutants can pose a risk to aquatic life and human health. For this reason, it is crucial to develop effective methods to treat coal wastewater to minimize its effect on health and the environment.

1.2. Background into RED technology

In recent years, coal mining and coal-related industries have used several conventional treatments to remove salt from wastewater. These techniques include ion exchange membrane (Geise *et al.* 2014; Tanaka 2015; Ran *et al.* 2017), reverse osmosis (Wenten 2016; Ismail, Khulbe and Matsuura 2018; Kucera 2023), and thermal technology (Mabrouk and Fath 2015; Feria-Díaz *et al.* 2021). These techniques have advantages and limitations, including the following:

a) **High Energy Consumption**: Thermal distillation and reverse osmosis are both energy-intensive desalination processes. Since these technologies heavily depend on fossil fuels, carbon emissions increase, creating more environmental challenges.
b) **Cost:** Desalination plants' construction, operation, and maintenance require much capital. For countries with limited financial resources, desalinated water is often less economically viable than traditional water sources, such as rivers or groundwater.

However, salt removal from wastewater treatment is energy-intensive since external energy is required. There has been much interest in using membrane technology such as reverse osmosis for desalination because of its high removal efficiency (Obotey *et al.* 2020). However, membranes are costly to operate and maintain, making them an uneconomical waste treatment option. It is therefore recommended that we shift to an emerging technology like RED, which produces power and desalinates water simultaneously, thereby reducing the use of external power. In consequence, RED will be able to minimize adverse environmental impacts in coal mining and coal power plants as RED, as a renewable energy source, addresses environmental mitigation goals.

The RED technology generates electricity by harnessing the differences in salinity between saltwater and freshwater, thus desalinating the saltwater solution. RED uses ion-selective membranes to separate freshwater and saltwater to balance the salinity gradient so that ions

naturally flow from the higher concentration side (saltwater) to the lower concentration side (freshwater). The passage of ions across membranes creates an electric potential. An electric current can be created by connecting electrodes on either side of the membranes, which can then be captured and converted into electricity.

The RED system is complex, has poor ion-selective membrane performance, and is costly despite its potential as a sustainable energy source. Its innovative energy generation and desalination approach is continuously evaluated and improved to reduce costs, improve efficiency, and explore practical applications. Due to its potential for clean and sustainable energy production and desalination, this technology may become more viable as it develops.

1.3. Study Rationale

There is a need for wastewater effluent quality management in South Africa. Compliance is essential to mitigate the impact of these regulations on the environment. In the coal mining and coal power industries, environmental problems are associated with the discharge of saline wastewater. The methods for removing salt from wastewater cannot address the saline wastewater problems. Engineers and researchers have no option but to establish an efficient and effective alternative desalination method because of these technologies' high energy intensity and complexity.

This is where RED, also known as Blue Energy, comes into play as an alternative technology to mitigate the environmental and technical challenges mentioned before. In South Africa, this technology is relatively new. In most studies conducted outside of South Africa, RED stacks have been applied to generate electricity from seawater and river water. However, desalination of coal-based wastewater using RED has not been studied extensively. Thus, this study seeks to fill this research gap by exploring the possibility of desalinating coal-based wastewater using RED technology, which will benefit both industry and research. In addition to minimizing energy costs for coal-related industries, this desalination technique can also solve saltwater problems created by these industries. The RED technology can alleviate the energy-intensive desalination processes used by coal mining and power plants, which would be a serious drawback. Due to the electrical power production that thereafter powers the process, the RED stack offers a cost-saving alternative to these industries.

1.4. Hypotheses and research questions

The following hypothesis was developed as part of this research:

- by using reverse electrodialysis stacks, coal mines and power plant wastewater can be stripped of salt (NaCl) while generating electric power simultaneously.

This study supports the hypothesis and addresses the following questions:

- can coal-fired power stations and collieries provide sustainable energy and desalination processes through industrial wastewater?
- what are the best conditions for maximizing power production and salt removal?

1.5. Aim and objectives of the study

This study aims to investigate the simultaneous colliery (as well as a coal-fired power station) wastewater treatment and renewable energy production by RED to improve process economics and carbon footprint.

Objectives were as follows:

- to investigate the desalination process for the treatment of synthesized coal mining and coal power plants using RED stack.
- to investigate the effects of various factors on Reverse Electrodialysis (RED) stack performance.
- to assess the permeation flux of RED and the impact that various parameters have on permeation flux.
- to optimize the desalination and power production with the RED process utilizing response surface methodology (RSM). Input factors evaluated were concentration, flow rate, and temperature as a function of salt removal efficiency and power density.
- to compare and validate the desalination and power production under the optimum conditions.
- to investigate the effect of divalent ions ($CaCl_2$ and Na_2SO_4) based on optimum conditions.

1.6. Outline of the Dissertation

There are six chapters in this dissertation, which are briefly summarized below:

Chapter One: Presents an introduction to the study.

Chapter Two: A literature review focuses on conventional desalination techniques used in

coal mines and power plants for wastewater treatment. The study's knowledge gap is highlighted by a summary of emerging RED technology and previous studies on RED.

Chapter Three: A literature review focuses on conventional desalination techniques used in coal mines and power plants for wastewater treatment. The study's knowledge gap is highlighted by a summary of emerging RED technology and previous studies on RED.

Chapter Four: All steps involved in the laboratory experiment are presented in this chapter. It provides process optimization, analytical, and model development approaches.

Chapter Six: The conclusions derived from the acquired results are presented in this chapter. Future research recommendations are also provided.

CHAPTER 2 - LITERATURE REVIEW

Chapter overview

This chapter reviews an overview of the coal mining and power plant industries, desalination treatment processes such as thermal technology, membrane technology, ion exchange and electrodialysis and their advantages and disadvantages. This chapter also assesses reverse electrodialysis works, emphasising the wastewater treatment process. A brief review of response surface methodology is highlighted as an optimisation tool used in this study. An in-depth critical review is provided to highlight the knowledge gaps that laid the groundwork for this work.

2.1. Overview of coal mines

South Africa is one of the world's top coal-producing countries. The country relies mainly on coal fuel for electricity generation, steel manufacturing, and production of petrochemicals. Therefore, coal mining is the backbone of the country's economy. However, the country suffers from regional water scarcity and pollution caused by coal mining (Konovšek *et al*. 2017; Polisi *et al*. 2021; Bulmer *et al.* 2021).

The country has 19 coalfields (as shown in Figure 2-1), and most collieries in South Africa are located in the Mpumalanga Province. They are particularly prevalent in the towns of Emalahleni. (Formerly Witbank), Middelburg, Ermelo and Secunda). Coal mining in the Mpumalanga province dates from the late 1800s. South Africa's mining history has generated vast economic benefits and still plays a vital role in ensuring the country's position in the global market (Steyn 2019). Over 90% of the coal used on the entire African continent is produced in South Africa, providing nearly 80% of South Africa's energy demands. Eskom states that coal is the most widely used primary fuel internationally, accounting for approximately 36% of the world's electricity production (Marais *et al.* 2019).

The coal mining industry encountered various environmental challenges ranging from acid mine drainage (AMD), subsiding ground, pollution of streams, and the exacerbation of potentially harmful elements (PHEs) and their effects on aquatic ecosystems. These environmental woes are experienced during active mining operations and are worse in

abandoned mines where less maintenance and environmental stewardship are implemented (Mahlase 2021).

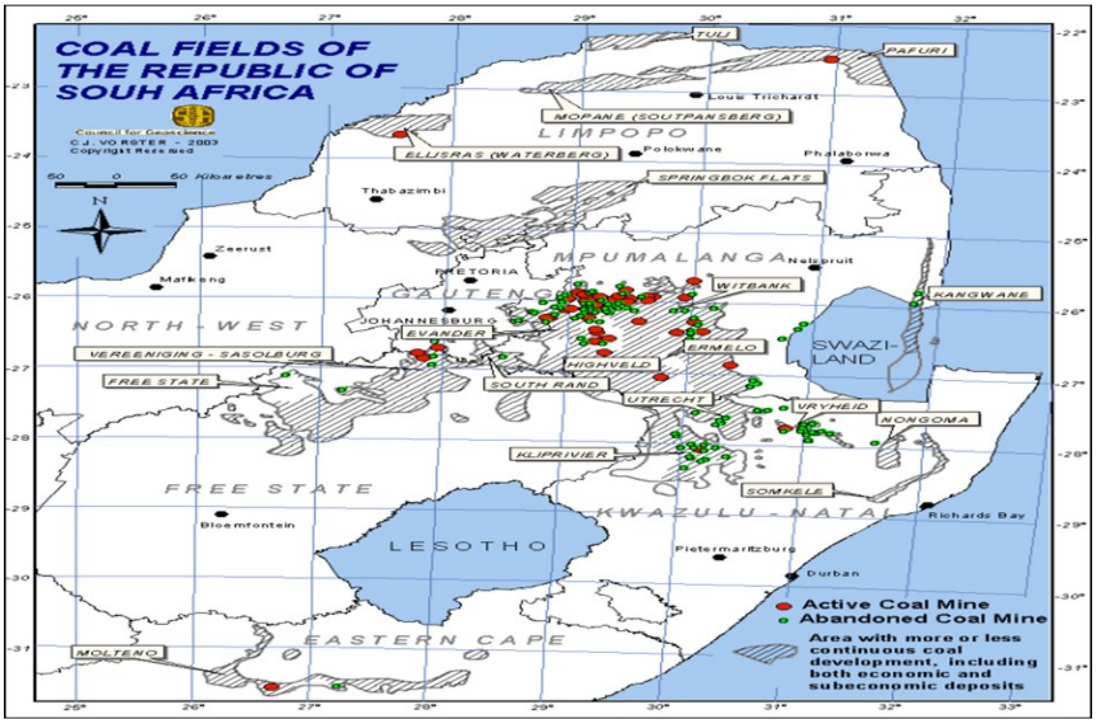

Figure 2- 1: South African's coal field (Adapted from Hancox and Götz (2014)).

Therefore, it is of great significance to treat wastewater from these industries efficiently as coal industries will continue to impact the environment negatively since our country still relies more on Eskom, which utilises coal for electricity production.

2.2. Mining legislation in South Africa that protects the environment.

South Africa is a country with a limited supply of water, and the quality of the water influences its usefulness for various uses. The report by (Mabiletsa and du Plessis 2001) indicated that exploiting South Africa's natural resources through mining contributes to the country's economic development. However, mining is an activity that has possible impacts on the environment. Section 24 of the Constitution of the Republic of South Africa, 1996, states as follows:

Everyone has the right -

a) to an environment that is not harmful to their health or well-being, and
b) to have the environment protected for the benefit of present and future generations through reasonable legislative and other measures that -

1. prevent pollution and ecological degradation.
2. promote conservation, and
3. secure ecologically sustainable development and use of natural resources while promoting justifiable economic and social development.

In general, mining is one of the activities that severely impacts the environment. In order to protect people's health, general well-being, and the natural resources that development depends on, it is also important to prevent the environment's continuous degradation (Mabiletsa and du Plessis 2001).

In 2017, The Department of Water and Sanitation (DWS) constituted a regulation that demands mine operations to monitor their surrounding water resources in the capacity of a potential recipient of pollutants from the mining operation (Lebepe 2022). The sampling is done as follows:

- Quarterly surface water, groundwater, and wastewater sampling.
- Quarterly groundwater level measurements.

The outcomes often display the information gathered throughout the mine's operation and demonstrate the estimated or anticipated possible effects of the adjacent mining activities. In determining the quality and water use, specific parameters must be analysed, i.e. pH, Aluminium (mg/L), Calcium (mg/L), Chloride (mg/L), Fluoride (mg/L), Iron (mg/L), Magnesium (mg/L), Manganese (mg/L), Potassium (mg/L), Sodium (mg/L), Sulphate (mg/L), Total dissolved solids (mg/L) and Suspended solids (mg/L). In 2019, DWS set wastewater discharge limits for coal-related industries, as presented in Table 2-1.

Table 2- 1: Discharge limits for coal-related industries set by DWS (Adapted from Maiti *et al.* (2019)).

Parameters	Discharge limits
pH	4–12
Colour, Hazen unit	<5–15
Turbidity, NTU	1–5
Odour	Agreeable
Total suspended solids	15–50
Total dissolved solids	1,000–2,000
Chloride	350–700
Sulphate	300–500
Sodium	200
Magnesium	150–200
Calcium	150–200

2.3. Background of the study

Over the years, the water quality crisis has remained the world's most challenging concern, emanating from rapid population growth (Cosgrove and Loucks 2015; Reid *et al.* 2019). The growing demand for safe and affordable clean drinking water globally has necessitated adequate wastewater treatment for discharge and recycling to prevent the projected water crisis and reduce environmental pollution (Raimi *et al.* 2019; Onu *et al.* 2023).

Another world problem is the energy crisis (Halkos and Zisiadou 2023; Skrzyniarz *et al.* 2023). Energy derived from the combustion of fossil fuels not only has a severe harmful influence on human health but also greatly contributes to climate change. In this vein, while desalinating with waste-to-energy (WtE) technologies such as RED, usable energy (electricity and heat) can be converted in a safe and environmentally friendly way (Kamal 2012).

2.4. Conventional methods for mine wastewater treatment

Mine waters unsuitable for discharge into natural waterways are typically strongly acidic or alkaline and carry high concentrations of salts, trace metals, suspended solids, and organic compounds (Cogho, 2012). There are various techniques for treating mine waters, depending on the amount of effluent, the kinds of contaminants present, and their concentrations. Mine

water composition depends on the mined ore, and the chemical additives utilised in mineral and hydrometallurgical processing (Thiruvenkatachari *et al*. 2011). This implies that mine waters do not often have a particular composition, so the classification of mine water based on its composition is challenging (Madzivire 2009).

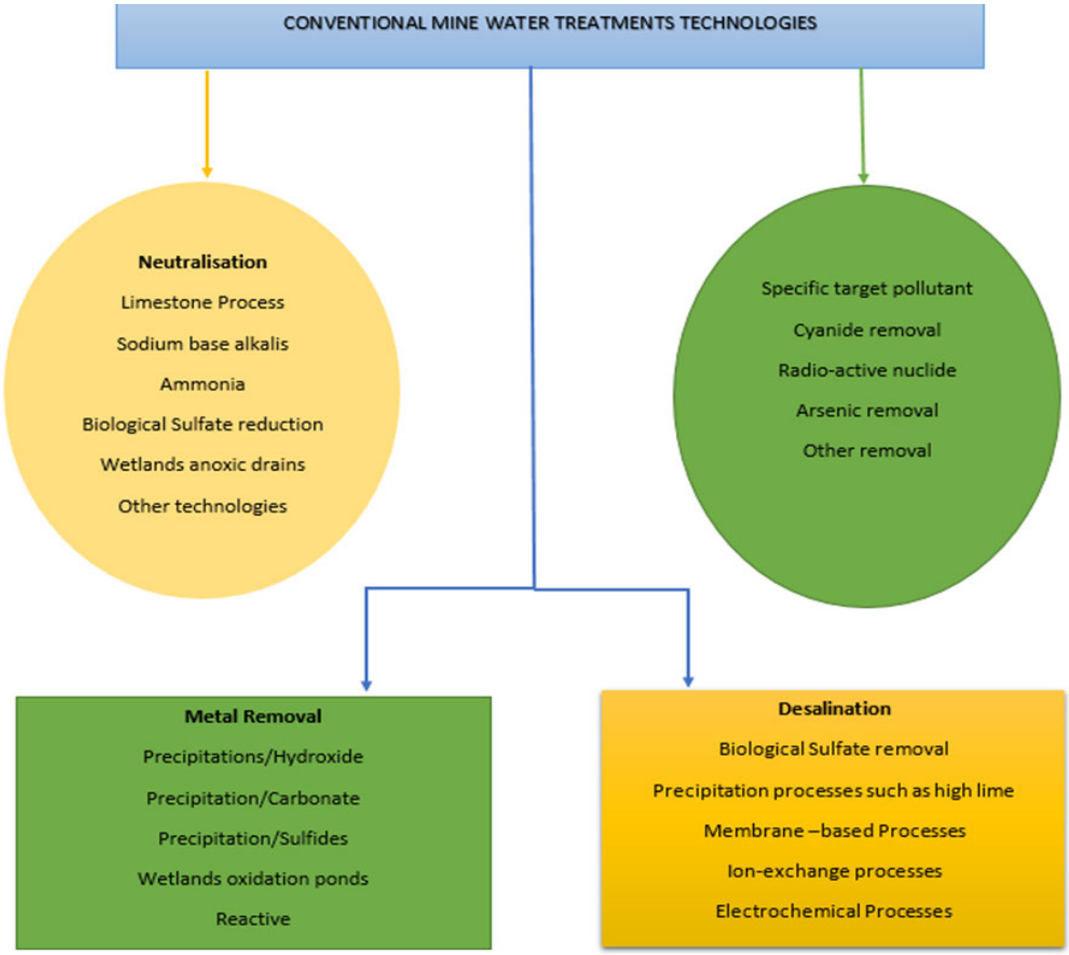

Figure 2- 2 : Conventional mine water treatment technologies (Adapted from Zhang *et al.* (2020)).

The kind of wastewater produced by mines mostly depends on the chemical characteristics of the geological elements that come into contact with the water. The concentrations of salts and other constituents frequently render such waters inappropriate for direct discharge to the river systems, except during heavy rain when sufficient diluting capacity is the regulatory authorities permit present and controlled release. Mine wastewater treatment is a possible solution to prevent or minimise the pollution of water resources (Iakovleva and Sillanpää 2013). However, it has become costly to treat the water to a condition acceptable for release into natural watercourses (Annandale *et al.* 2007).

2.5. Desalination process

Desalination is a general term for the process that removes dissolved solids and produces fresh water from feed waters such as seawater, brackish water, and inland water and increasingly to reclaim recycled water. The desalination of water has been done since ancient times but was not widely utilised due to technological limitations, the prohibitive high capital costs, high energy consumption, and finally, the exceptionally high unit cost of water compared to conventional water development (Karagiannis and Soldatos 2008) Typically, a desalination plant consists of : (Karagiannis and Soldatos 2008)

- Intake, made up of pumps and pipes to take water from the source (sea or brackish water)
- Pre-treatment comprised of filtration of raw water to remove solid components and the addition of chemical substances to reduce the salt's precipitation and the corrosion inside the desalination unit.
- Desalination, where freshwater is extracted from saltwater.
- Post-treatment for pH correction by adding selected salts to meet the requirements of the final uses.

Desalination requires enormous energy to separate the undesired particles from the water molecules (Broggi 2013; Härtel *et al.* 2015; Darre and Toor 2018). Desalination has attracted a lot of attention recently due to its potential for recovering potable water from sewage and turning brackish and seawater, which is why it is seen to be crucial in supplying the world's water needs (Papapetrou *et al.* 2017; Danaeifar *et al*. 2023). There are multiple desalination technologies, but each one's applicability heavily depends on the type of water to be desalinated. The other main factors in choosing the best desalination technology for a particular application include energy availability, the intended use for the produced water, and the required treatment capacity (Asadollahi *et al*. 2017). Various desalination processes have been developed; some are currently under research and development (Mabrouk and Fath 2015; Ali *et al.* 2018; Gebreeyessus 2019; Saleem *et al.* 2023).

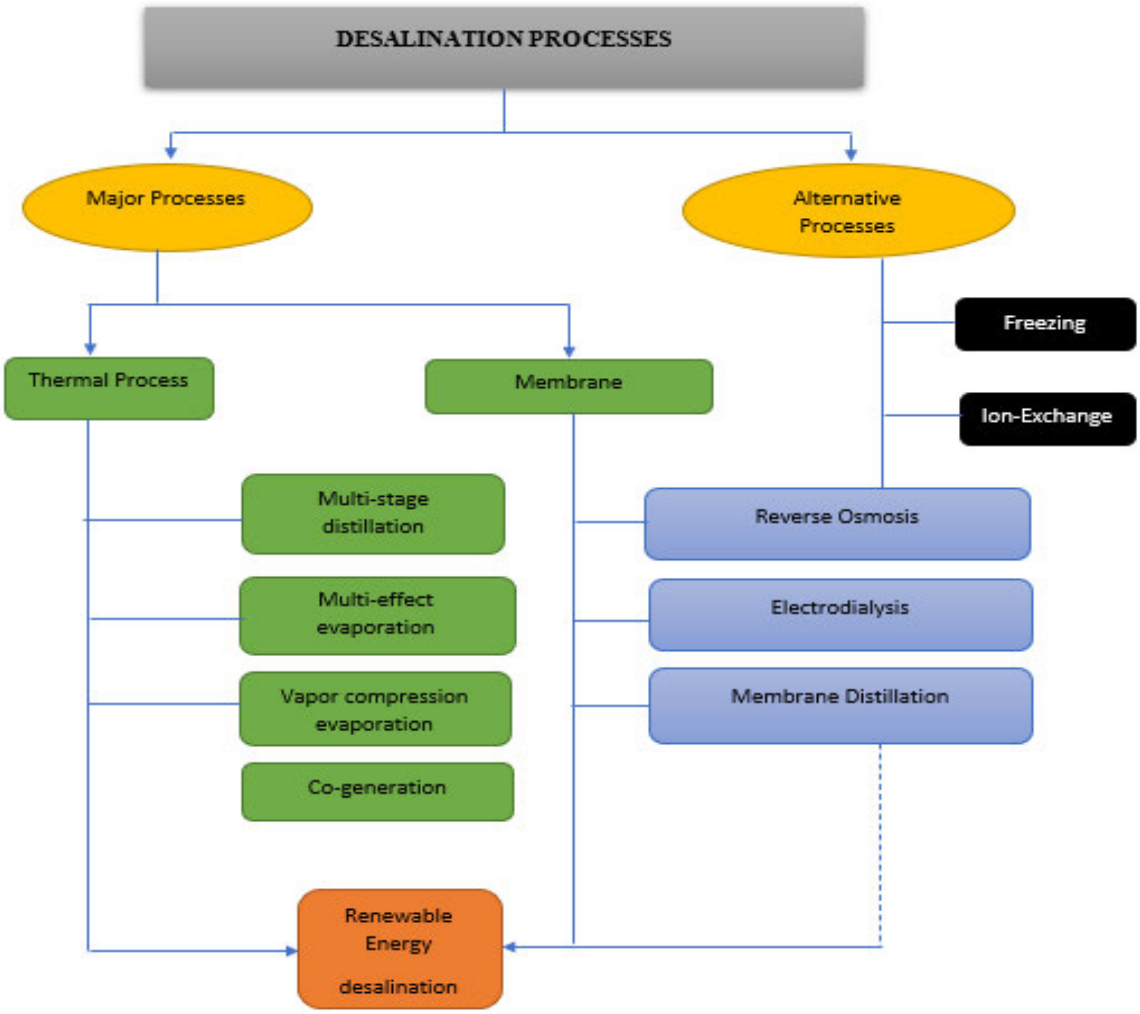

Figure 2- 3: Classification of water desalination technologies (Adapted from Shatat and Riffat (2014)).

2.6. Thermal Technology

Thermal technologies are based on the concept of using evaporation and distillation processes, which are common distillations used for desalination worldwide. There are three common thermal technologies used, which mainly include multi-stage flash (MSF), multiple effect distillation (MED), and vapour compression (VC) (He *et al.* 2022). Heat drives thermal processes, which induce a phase change in water, which causes it to vanish, evaporate, and leave dissolved solids behind. Due to the effort required to accomplish this, thermal techniques are not usually used for brackish water treatment due to their high cost. However, these technologies produce water with shallow levels of TDS, and they are used extensively in the Middle East, where there are plenty of sources of fossil fuels (Jaberi and Ghassemi 2015)

2.6.1. Multi-Stage Flash (MSF)

This distillation process combines many flashing stages and is one of the world's most reliable thermal seawater desalination plants. MSF strictly separates heat transfer and evaporation, minimising the risk of scaling and significantly reducing maintenance costs. Furthermore, MSF can handle large capacities. Given that it can operate at high temperatures and pressure, its limitation and disadvantage is that it requires the highest amount of energy (El-Ghonemy 2018; Hamed 2020).

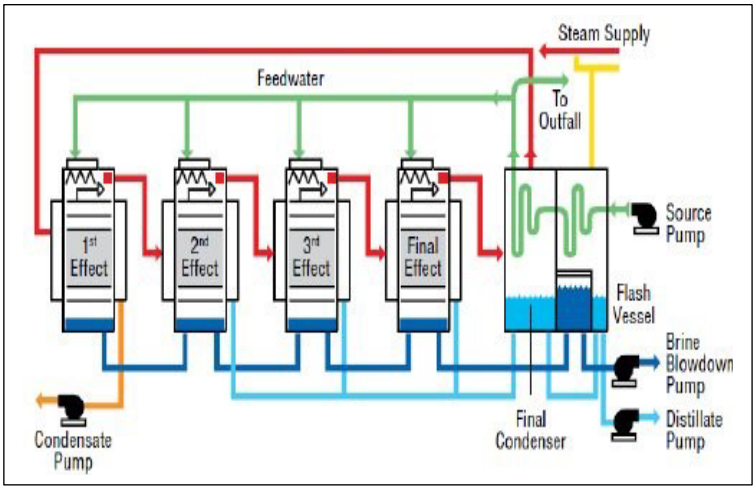

Figure 2- 4: Multi-Stage Flash process (Adapted from Lawal *et al.* (2023)).

2.6.2. Multiple Effect Distillation (MED)

This process is the oldest in desalination. MED contains numerous chambers in a single vessel, which improves the MED efficiency. Significant features of the MED process are low primary energy consumption due to a lower top brine temperature in the MED, low heat transfer area, and high gain ratio. However, the use of MED is limited because it has less production capacity (Al-Shammiri and Safar 1999; Thimmaraju *et al.* 2018; Al-Hotmani *et al.* 2020).

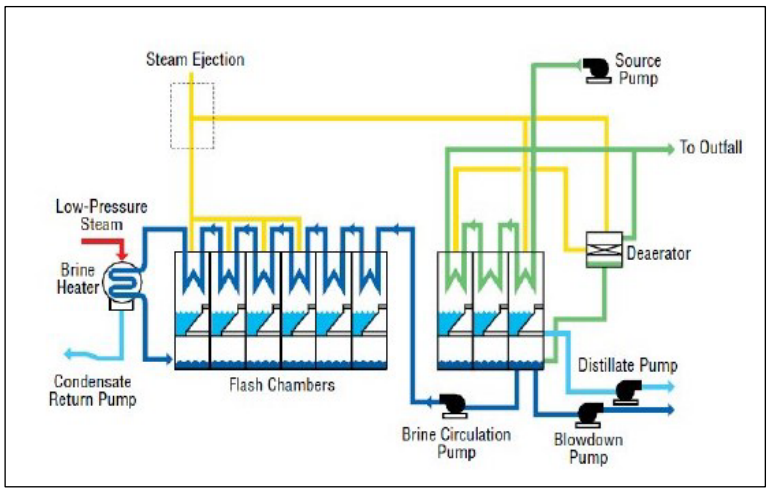

Figure 2- 5: Multiple effect distillation processes (Adapted from Alhaj *et al.* (2017)).

2.6.3. Vapor Compression (VC)

This distillation process is much more efficient in distilling water than other older technologies, whereby fresh water from saline water is produced by developing heat by vapour compression. Vapor compression distillation has many advantages, including the compressor being driven by electricity or a diesel engine. However, it is limited as the boiler scaling is severe and is used for small-scale desalination (Zheng *et al*. (2017)).

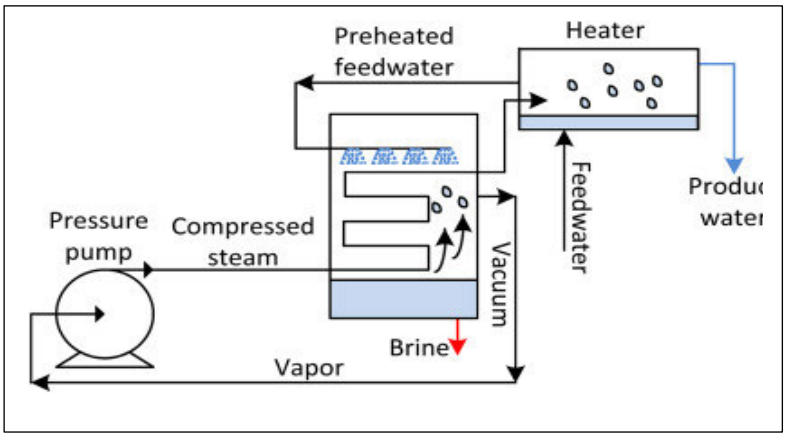

Figure 2- 6: Vapor Compression process (Adapted from Alhaj *et al.* (2017)).

2.7. Membrane technology for desalination

It offers several appealing characteristics that make any saline stream's desalination reasonably affordable compared to thermal desalination processes. These techniques rely on hydraulic pressure to achieve separation (Yan 2022). There are four main types of these processes. These are microfiltration (MF), ultrafiltration (UF), nanofiltration (NF), and reverse osmosis

(RO)(Goh *et al.* 2016). However, MF, UF, and NF can only remove other particles (as shown in Figure 2-7) than salts (Brover *et al.* 2022). Reverse Osmosis is considered effective in salt removal, and in 2012, it was regarded as a popular desalination technology with 60% of the total global desalination capacity (Jaberi and Ghassemi 2015).

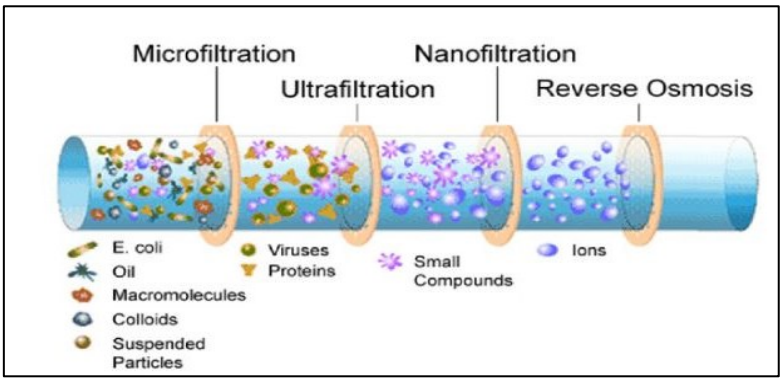

Figure 2- 7: Membrane technology process (Adapted from de Pinho and Minhalma (2019)**).**

2.7.1. Ion Exchange Membrane

Ion-exchange membranes are used to desalinate and remove heavy metals and organic compounds from industrial effluents and are favourable to many industries. Ion exchange membranes contain high concentrations of fixed charges, allowing specific ions to pass through while blocking others (as shown in Figure 2-8). The membrane separates dissolved ions in a liquid (Hassanvand *et al.* 2017). This type of membrane can be best described as the interchange of ions between a solid and liquid phase surrounding the solid. However, their disadvantage and limitations are their high operational costs and failure to remove all contaminants at low concentrations (Tanaka 2012).

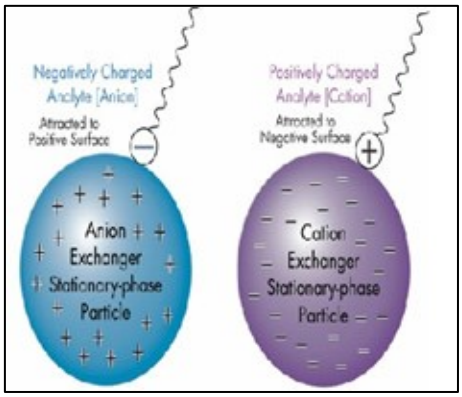

Figure 2- 8: Ion Exchange Membrane process (Adapted from Tanaka (2012)).

2.7.2. Electrodialysis

Electrodialysis is utilised widely today for desalination of brackish water, and in some areas of the world, it is the primary process used to produce potable water. The operation of ED is driven by the development of ion exchange membranes that produce high water recovery and do not require phase change, reaction, or chemicals. Membranes can be constructed to permit the selective passage of either cations or anions, as shown in Figure 2-9 (Al-Amshawee *et al.* 2020). ED has the capability of high recovery in terms of more freshwater products and less brine. ED is limited because desalination of water with concentrations of dissolved solids higher than 30 g/l, like seawater, is possible, but it is not economically viable, and energy usage is proportional to the salts removed (Shatat and Riffat 2014).

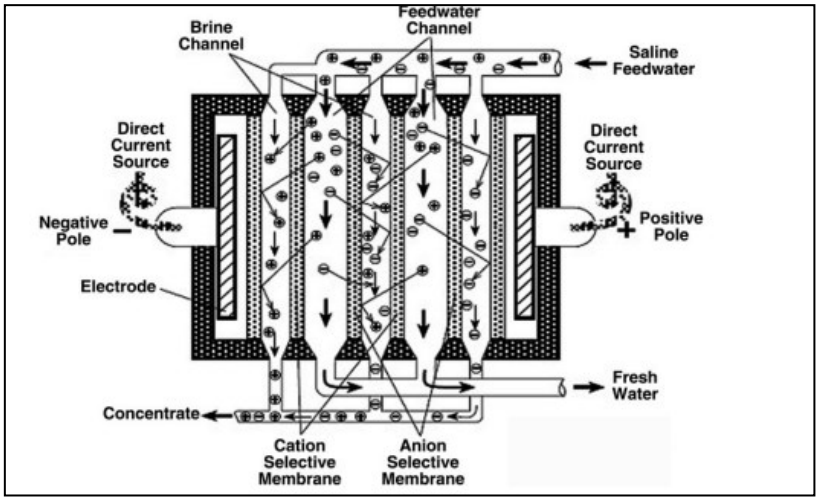

Figure 2- 9: Movement of ions in the ED process (Adapted from Shatat and Riffat (2014)).

2.7.3. Reverse Osmosis

Reverse osmosis (RO) is the common method of purifying water that uses a semi-permeable membrane to separate water molecules from other materials. RO applies pressure to overcome osmotic pressure that favours even distributions.RO is gaining popularity in the chemical and environmental engineering fields due to its high removal efficiency and ability to remove various metallic ions (Qasim *et al.* 2019). RO is today the leading desalination technology and accounts for more than 20% of the restoration world's desalination operations because of pumping pressures, semi-permeable membrane regeneration, and restoration. RO is highly known for its efficiency in separating small particles, including bacteria and monovalent ions like sodium and chloride ions, up to 99.5% (Qasim *et al.* 2019). The disadvantage and

limitation of RO is its high power consumption because of pumping pressures, semi-permeable membrane regeneration, and restoration (Joo and Tansel 2015).

2.8. Emerging desalination technique

Even though the use of membrane processes guarantees the removal of at least 95% of contaminants that any treatment process can achieve due to its energy intensity, shifting to a technology that could work as a desalination process while also generating electricity simultaneously will reduce negative environmental impact and minimising cost of electricity.

2.9. Reverse electrodialysis

The idea was formulated for the first time in 1954 by R. Pattle in Nature (Wick 1978; Cipollina *et al.* 2016; Tian *et al.* 2020). RED, a reverse desalinisation process, is a technology that generates electricity using the entropy of mixing sea and river water (Mei and Tang 2018). Salinity gradient energy (SGE) capture by reverse electrodialysis (RED) is an emerging technology to advance the phaseout of conventional water-intensive energy sources in the desalination industry (Tristán *et al.* 2020a). It is also inherently clean and sustainable. In addition, energy can theoretically be produced 24 hrs per day and 365 days a year (Post 2009). In a RED system, which is a reverse of an electrodialysis system, several cation and anion-exchange membranes are stacked in an alternating pattern between a cathode and an anode, as depicted in Figure 2-10. Feed waters, such as seawater and river water, flow alternatingly through the feed compartments between the membranes. The salinity gradient over each ion exchange membrane generates a voltage difference (the Donnan potential), which propels the process. This voltage differential builds up when alternating CEMs and AEMs are stacked. When the RED stack is connected to an external load, this driving force results in a flux of ions through the membranes. An electrode is in contact with the membrane stack's ends to allow the ionic flux, and a redox couple recirculates between the electrodes to transform the ionic flux into an electrical current (Vermaas *et al.* 2013; Moreno *et al.* 2018).

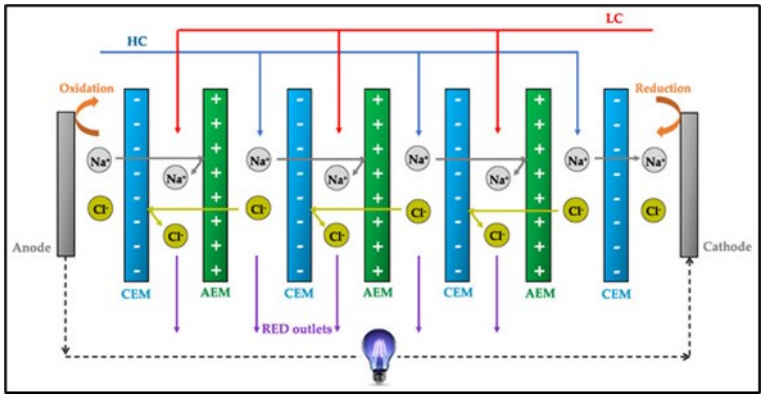

Figure 2- 10: Reserve electrodialysis process (Adapted from Güler *et al.* (2013)).

The compartments between the membranes are alternately filled with a concentrated salt solution and a diluted salt solution, as Figure 2-11 demonstrates.

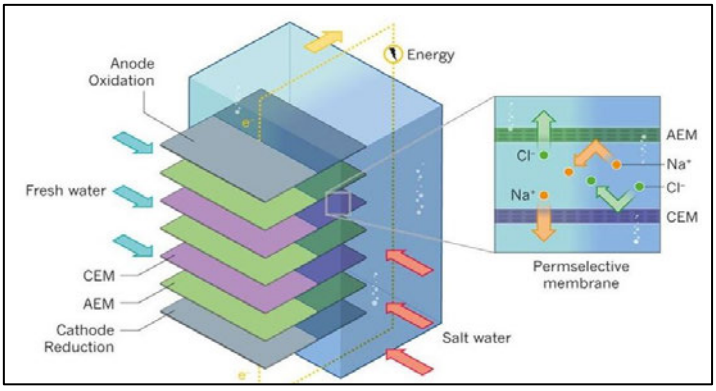

Figure 2- 11: Shows several cation and anion-exchange membranes are stacked in an alternating pattern (Adapted from Güler *et al.* (2013)).

Theoretically, approximately 0.8 kWh is obtainable when 1 m^3 of freshwater flows into the sea, translating into nearly 2 TW of SGP based on the total freshwater flow of the significant rivers worldwide (Mei and Tang 2018). RED enables energy harnessing from abundant yet largely untapped sources, such as industrial effluents, thus providing energy and emission savings from an otherwise waste stream, conforming with the waste-to-wealth concept (Tristán *et al.* 2020b).

2.10. Comparative Analysis of Desalination Technologies

2.10.1. Advantages and disadvantages of Desalination technologies

Table 2- 2: Advantages and disadvantages of Desalination technologies (Adapted from El-Ghonemy (2018); Lawal *et al.* (2023); Alhaj *et al.* (2017); Jaberi and Ghassemi (2015); Tanaka (2012); Pathak (2020) and Tristán *et al.* (2020a)).

Process	Advantage	Disadvantage
Multi-stage flashing	MSF plants are relatively simple to construct and operate	It is considered an energy-intensive process, which requires both thermal and mechanical energy, but it can be overcome by the cogeneration system
Multi-effect distillation	The MED process is designed to operate at lower temperatures of 708 °C (1588 °F). This minimises tube corrosion and the potential of scale formation around the tube surfaces	The multi-effect flash system operates at high temperatures that increase corrosion and scale formation.
Vapor-compression evaporation	The low operating temperatures (below 708 °C) reduce the potential for scale formation and tube corrosion.	The simplicity and reliability of plant operation make it an attractive unit for small-scale desalination units.
Reverse osmosis	The use of energy recovery devices that are connected to the concentrated stream as it leaves the pressure vessel.	Membrane scaling caused by the precipitation of salts is a common problem in the RO process and high operating cost.
Electrodialysis	Energy usage is proportional to the salts removed.	ED is feasible for brackish water with a salinity of, 6 g/l of dissolved solids, but not suitable for water with dissolved solids of, 0.4 g/l.
Membrane distillation	The main advantages are its simplicity and the low operating temperature it requires to operate.	The MD process requires that the feed water should be free of organic pollutants; this explains the limited use of this method.
Reverse electrodialysis	The main advantage is operating simultaneously in the desalination of water and the production of clean energy to feed the desalination process.	High capital costs of membranes

In the past decade, the study of reverse electrodialysis has received great interest because its adoption can overturn energy challenges in the world and is of great interest for clean electrical power (Siemens 2023). Less than five salinity gradient power stations operate worldwide (Tumba). However, there are reports of ongoing projects in numerous coastal countries. One of the pilot plants in the Netherlands uses fresh Ijsselmeer water and salt water from the Wadden Sea. The test site was built in 2006 but was put into service on 26 November 2014 and produced 50 kW of electricity (Cipollina *et al.* 2016). This plant generally uses fresh water flowing from the Rhine and seawater, as shown in Figures 2-12**,** to produce power, discharging the brine back into the sea to prevent the dam from flooding.

Figure 2- 12: RED pilot plant located in the Netherlands (Adapted from Tedesco *et al.* (2016)).

2.11. Development of RED stack in South Africa

Blue energy is a recently established field of study in Southern Africa and all of Africa. No pilot unit has been built as African researchers take their first steps in the field. Mangosuthu University of Technology is Africa's sole university working on blue energy research. Blue Energy has great potential in combining wastewater and electricity generation in both operational and abandoned mines, Coupling desalination and reverse electrodialysis, etc. (Tumba). The researcher further highlighted the challenges identified in South Africa, including a lack of data that can be used in simulations (flow rates, salinity, water availability).

2.12. Challenges, Advantages, and Disadvantages of RED Stack

Table 2- 3: Challenges, Advantages, and Disadvantages of the RED stack (Adapted to Tumba; Zhou et al. (2018)); Guler and Nijmeijer (2018)).

Challenge	• Small number of researchers involved in the field. • Lack of membranes specifically designed for RED. e.g., Improved monovalent selectivity, antifouling properties, and target-ion-selectivity for non-sodium chloride ions
Advantages	• Southern Africa is likely to claim the largest share of blue energy potential among all the major African regions. • There is room for plenty of innovation through RED research. • Blue energy adoption can overturn energy challenges in the region. • Not dependent on seasonal climate changes • RED stack can simultaneously produce energy while treating wastewater.
Disadvantages	• High capital costs involved

2.13. Energy Savings to Desalination from RED

Desalination plant capacity will define absolute GHG emission reduction. RED's salinity gradient energy retrieval from desalination's concentrate effluent is a viable strategy for balancing carbon emissions from the energy-intensive sector; this is particularly true for those locations deeply reliant on fossil fuel. RED's ability to cut down desalination's carbon emissions hinges on

- The technical and environmental performance of RED
- The energy required to drive desalination.

Tristán *et al.* (2020b) performed a study examining the relevant factors in reverse electrodialysis (RED) application in desalination plants to reach a more sustainable and clean water supply. The comparison was done to determine the potential reduction in energy

consumption and carbon emissions gained from RED integration in 20 medium-to-large-sized seawater reverse osmosis (SWRO) desalination plants spread worldwide. The research was conducted to quantify the grid mix share of the SWRO plant's total energy demand and emissions RED would abate. Results indicated that RED plant could a) abate roughly 10% of desalination plant emissions, b) potentially abate 0.32 to 1.18 Mt CO_2-eq per year, c) deliver high specific energy to the least energy-intensive SWRO plants, and d) be integrated into the most emission-intensive SWRO plants which could relieve up to 1.95 kg CO_2-eq m^3.

2.14. Comparison of Salinity gradient energy from RED stack to other marine renewable energy.

Table 2- 4: Comparison of various types of renewable energy (Adapted from Stages (2012); Dolan and Heath (2012) ; Smoot (2022) ; Farquharson *et al.* (2017) ; Tristán *et al.* (2020b)).

Unit Source	Global warming potential (g CO_2-e/kWh)	Availability of renewable sources
Photovoltaic	~40	Weather dependent
Wind	11-12	Weather dependent
Hydro	27.2-226	Always available
Geothermal	38	Weather dependent
Coal	~1000	Non-renewable
Natural Gas	490	Non-renewable
SGP (RED)	<10	Always available but not in non-coast countries
SGP (PRO)	<10	Always available but not in non-coast countries

2.15. Factors Affecting RED Stack

Various operational parameters affect the process of desalination and power production on the RED stacks. Each of these variables influences the effectiveness and efficiency of the wastewater desalination and power production process.

2.15.1. Temperature

The temperature has a significant impact on the transport properties of the membrane and solution. The feed stream temperature can strongly influence RED performance (Benneker *et al.* 2018). Increasing temperature may result in more power density and a high percentage of salt removal (Mehdizadeh *et al.* 2019). However, temperatures above 40 °C might affect the stability and durability of IEMs. Therefore it was reported by (Fontananova *et al.* 2014) and

many researchers that a 45% increase in the maximum power density was observed when the feed temperature was increased from 20 to 40 °C.

2.15.2. Concentration

Regarding operational variables, the feed solutions considerably impact the stack's internal resistance and provide the electromotive force. The ion removal rate and the total ion removal are highly dependent on ionic concentration and composition. Increasing the salinity difference between the high and low-concentration solutions often improves RED performance (Ortiz-Martínez *et al.* 2020). However, the high concentration of multivalent ions in the highly concentrated compartment could cause salt to precipitate on the IEM. Therefore, higher NaCl increases the ion removal rate, and total ion removal rises as the applied voltage impacts more ions, but as opposed to that, power density increases when higher salinity gradients are used. The effect of concentration bulk solution, spacers, and boundary layer resistances are more pronounced for less concentrated and lower gradients, whereas high ion concentrations have a significant impact on membrane resistance. Based on findings by numerous researchers, power generated by the RED stack enlarged when 0.6 to 3.6 M of higher NaCl concentrations were utilised. As a result of IEMs' capacity restrictions, the power stayed constant after that (Zhou *et al.* 2018).

2.15.3. Flow rate

According to (Tufa *et al.* 2018), velocity is the mean velocity inside the single spacer–filled channel which affects the RED system's hydrodynamics and chargers' mass transfer. The flow rate of the solution directly affects the ion transport rate. An experiment conducted by (Tedesco *et al.* 2016) indicated that higher velocity ranges from 2-3 cm/s reduce the diffusion boundary layer thickness as the solution mixing rate increases, resulting in negative net power output. General velocity in a 0.5 – 1.9 cm/s range does not influence the RED stack since it increases process efficiency. Furthermore, (Othman *et al.* 2022) highlighted that higher feed velocity had positive impacts on sodium and sulphate removal but negligible effects on calcium and chloride removals, which might explain the differences in the initial concentration. The flow of feed solutions reduces locally at the regions where fouling accumulates, and the effective membrane area decreases. Thus, it is also crucial to figure out the cleaning intervals of a RED stack to maximise the gross power (Rahman 2023).

2.15.4. Divalent ions

Magnesium ions can strongly influence the performance of the RED stack. Many researchers indicated that a high concentration of multivalent ions in the highly concentrated compartment could lead to salt precipitation on the IEM, thus limiting output power. A study by (Othman *et al.* 2022) indicated that the ion removal rate and the total ion removal highly depend on ionic concentration and composition.

Concerning the hydrated radius and hydration-free energy, as shown in Figure 2-13, (Kang *et al.* 2014) categorised ionic hydrations according to the hydrated radius and hydration-free energy:

1. Small, hydrated ions with strong hydration shells (SS).
2. Small, hydrated ions with weak hydration shells (SW).
3. Large, hydrated ions with strong hydration shells (LS).
4. Large, hydrated ions with weak hydration shells (LW).

It is reported that the more the ion charge density increased, the more the hydration free energy increased, and the smaller one for ions with the same charge would be hydrated firmer than the other. Thus, it is worth noting that Mg^{2+}, which belongs to LW, has the highest impact on power output.

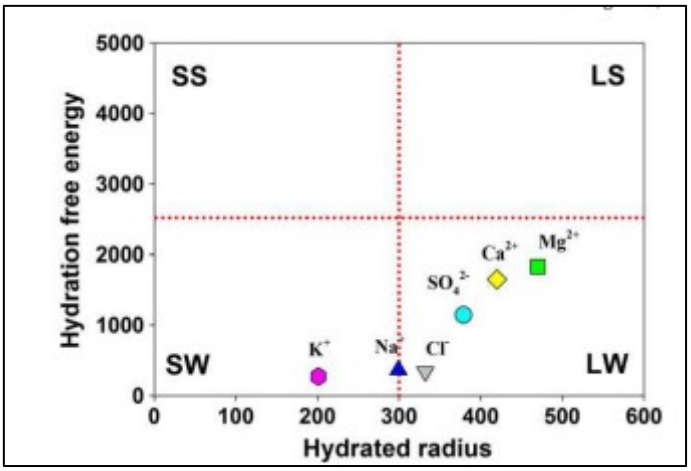

Figure 2- 13: Ionic behaviour in terms of hydration-free energy and hydrated radius. There are four groups: small, hydrated ions with strong hydration shells (SS), small, hydrated ions with weak hydration shells (SW), large, hydrated ions with strong hydration shells (LS), and large hydrated ions with weak hydration shells (LW).

In a study by Avci *et al.* (2016) investigated the impact of Mg^{2+} on the performance of RED using a stack of (10 x 10 cm^2) area with 25 pair cells. Based on the first experiment, feed solution containing synthesised pure NaCl solution (HCC: 4M NaCl &LCC:0,5M NaCl), a notable 1.06 W/m^2 power density was observed as presented in Figure 2-13. However, a drastic drop in power density was reported when synthesised pure $MgCl_2$ was used. As a result, it was reported that the presence of magnesium ions had an impact on the performance of RED even at a lower content.

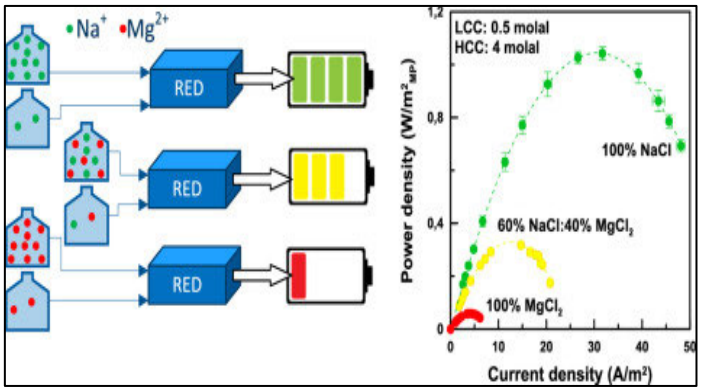

Figure 2- 14: Impact of Mg^{2+} on RED stack (Adapted from Avci *et al*. (2016)).

In General, the transport phenomenon is quite complex due to the presence of both monovalent and multivalent ions on both sides of the IEM (Besha *et al.* 2019). In this case, the uphill transport can be best defined as two Na^+ ions being transported in the opposite direction to the Mg^{2+} ions. The Na^+ and Mg^{2+} start moving until the overall E_i is balanced, reaching an equilibrium ($E_{Na^+} = E_{Mg^{2+}}$), at this point, the uphill transport stops.

According to Křivčík *et al.* (2015), highlighted that divalent anions do not cause a noticeable increase in resistance in anion exchange membranes. Measures of an ion's interaction with the surrounding water, such as hydrated radius and hydration-free energy, show less difference between anions and cations (Tansel 2012; Pintossi *et al.* 2020). These factors lead one to believe that cations have the greatest impact on performance.

2.16. Challenge on commercialising RED process

To date, RED application on a large scale has not been initiated as this technology still encounters challenges such as high capital costs for infrastructure etc. A recent paper by Chae *et al.* (2023) reported that this technology is nearly commercialised. However, the high cost,

current performance of membranes, and fouling issues hinder their widespread deployment.

2.17. Enhancing the RED performance

Enhancing the performance of the RED involves various methods. Research into RED is still ongoing to improve the performance, such as membrane development, electrode optimisation, scaling up system design, fouling mitigation, salinity gradient enhancement, temperature control and energy recovery method etc. Several researchers have done research to ascertain the best selection for enhancing the RED performance.

2.17.1. System Design

Co-counter, counter-current, and cross-flow operation modes are three different flow configurations utilised in the transfer process to feed solutions with different salt concentrations, as Figure 2-15 demonstrates. The difference between the three only lies in the flow path's direction.

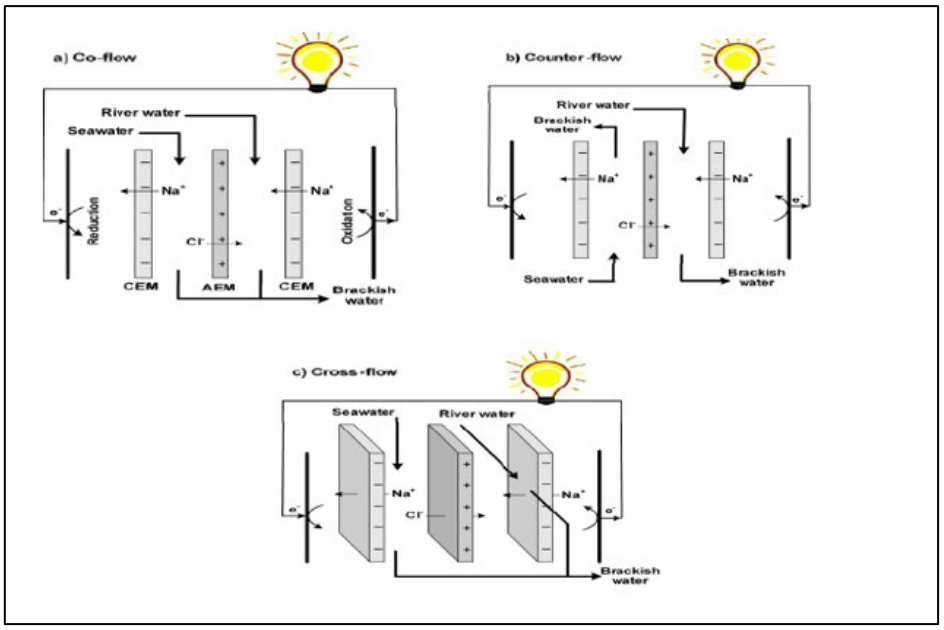

Figure 2- 15: Principle of RED using co- (a), counter- (b) and cross-flow (c) (Adapted from Ortiz-Martínez *et al*. (2020)).

The flow design affects the cells' average salinity gradient, affecting the system's energy effectiveness. Mainly, counter-flow is the channel configuration with the maximum efficiency. Despite identical outflow concentrations, a salinity gradient exists throughout the membranes

because the outflows are on various sides of the channels and exist throughout the entire channel.

A study by Cui *et al.* (2022) aimed to understand the response of salinity gradient power generation by utilising different flow modes. The study's objective was to explore the influence of co-counter and counter flow on the performance of the RED stack. Based on their findings, as illustrated in Figures 3-6, a notable high-power density in co-counters that are in counter-flow is reported. This proves that counter-flow causes the internal resistance of the membrane to squeeze and bend at the entrance and exit, as reported in the literature, thus decreasing the power output (Veerman 2020; Gao *et al.* 2023). Co-counterflow, also known as co-flow mode, has been chosen in this study because of these benefits.

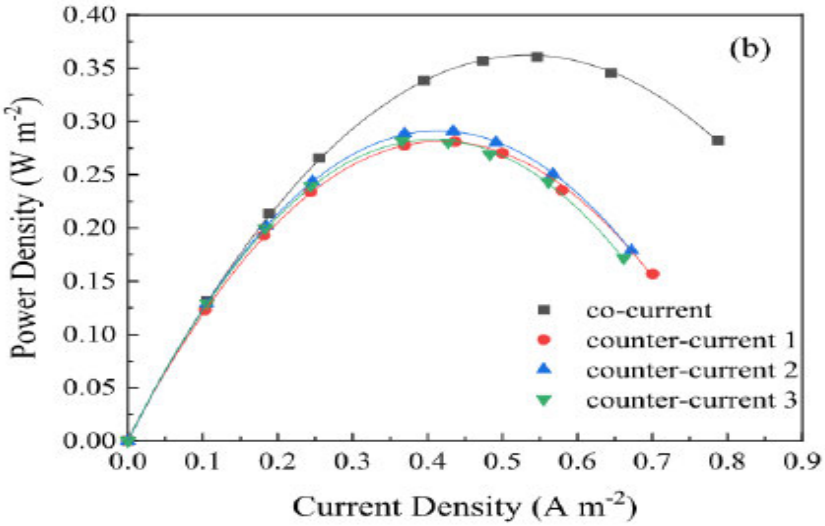

Figure 2- 16: Graph depicting the co-current to counterflow design comparison in obtaining power density (Adapted from Cui *et al.* (2022)).

2.17.2. Electrode Systems for RED

Veerman *et al.* (2010) investigated a suitable electrode system for RED and reported that special stable metal electrodes, graphite electrodes, other reversible redox couples, capacitive electrodes, and electrolytes with carbon particles should be considered to improve the electrode system. The study compared the electrode systems used by other researchers with regard to safety, health, environment, technical feasibility, and economics, as shown in Figure 3-7.

Anode	Anolyte+ Bulk	Repeating unit	Catholyte + Bulk	Cathode	Electrode reactions
Cu	$CuSO_4$	S = R ≠ Na^+ Cl^-	$CuSO_4$	Cu	cath: $Cu^{2+} + 2e \Longrightarrow Cu$ anode: $Cu \Longrightarrow Cu^{2+} + 2e$
Metal	Sea	S = R ≠ Na^+ Cl^-	Sea	Metal	cath: $2H_2O + 2e \Longrightarrow H_2 + 2OH^-$ anode: $2Cl^- \Longrightarrow Cl_2 + 2e$
AgCl	Sea	S = R ≠ Na^+ Cl^-	NaCl	AgCl	cath: $AgCl + e \Longrightarrow Ag + Cl$ anode: $Ag + Cl^- \Longrightarrow AgCl + e$
Zn	$ZnCl_2$	S = R ≠ Na^+ Cl^-	$ZnCl_2$	Metal	cath: $Zn^{2+} + 2e \Longrightarrow Zn$ anode: $Zn \Longrightarrow Zn^{2+} + 2e$
Ti/Ru	$Fe(CN)_6^{3+}$/ $Fe(CN)_6^{4-}$ NaCl	S = R = Cl^- Na^+	$Fe(CN)_6^{3+}$/ $Fe(CN)_6^{4-}$ NaCl	Ti/Ru	cath: $Fe(CN)_6^{3-} + e \Longrightarrow Fe(CN)_6^{4-}$ anode: $Fe(CN)64 \Longrightarrow Fe(CN)_6^{3-} + e$

Figure 2- 17: Comparison of different electrode systems for RED (Adapted from Veerman *et al.* (2010)).

According to their findings, the highest ranking was attained by systems with the $[Fe(CN)_6]^{4-}$/$Fe(CN)_6]^{3}$ (Ferrocyanide) couple. Based on the literature, many researchers have conducted laboratory-scale experiments with $[Fe(CN)_6]^{4-}$/$Fe(CN)_6]^{3}$ owing to the fast charge-transfer rate. Consequently, $[Fe(CN)_6]^{4-}$/$Fe(CN)_6]^{3}$ is used in this study. Due to its high stability and favourable processing circumstances, as noted by numerous researchers.

2.17.1. Fouling of the membrane

Membrane fouling is a process by which the particles, colloidal particles, or solute macromolecules are deposited or adsorbed onto the membrane pores or onto a membrane surface by physical and chemical interactions or mechanical action, which results in smaller or blocked membrane pores (Lin *et al.* 2013; Liu *et al.* 2019; Li *et al.* 2020). Fouling may occur in four mechanisms, as illustrated in Figure 2-18. Fouling can be classified into the following types.

Biofouling

It is defined as the undesirable accumulation of microorganisms at a phase transition interface solid–liquid, gas–liquid or liquid–liquid), which may occur by deposition, growth, and metabolism of bacteria cells or flocs on the membranes (Guo, Ngo and Li 2012; Vanysacker *et al.* 2014; AlSawaftah *et al.* 2022).

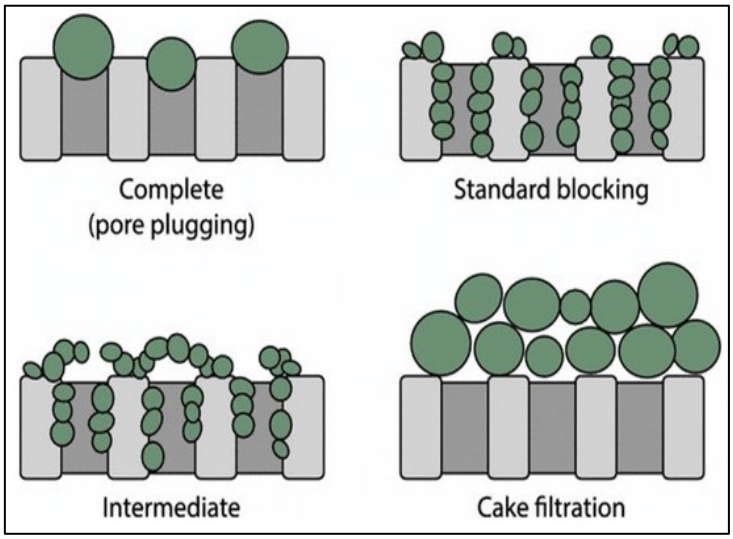

Figure 2- 18: Fouling mechanism (Adapted from Zulkefli *et al.* (2021)).

Colloidal fouling

It refers to materials that are tens of nanometres up to about one micron. Typical colloids include clays, silica, iron and aluminium hydroxides, and organic debris. Colloidal fouling in a membrane system is caused by the convective deposition of colloids on the membrane surface (Ng and Elimelech 2004; Ning and Troyer 2007; Dickhout *et al.* 2017).

Organic fouling

Organic fouling is caused by the accumulation and deposition of relatively dense natural organic materials. When these compounds accumulate over time, they cause opposition to permeate flow (Costa *et al.* 2006; Amy 2008; Kim *et al.* 2014; Lin *et al.* 2014).

Inorganic fouling

Inorganic fouling, also known as scaling, is the deposition of inorganic compounds (salts)on the membrane surface or inside the membrane pores. These salts are hydroxides, sulphates, carbonates, calcium, magnesium, iron, ortho-phosphates, silicic acids, and silica. Salts form supersaturated solutions and eventually precipitate out of the solution and onto the surface of the membrane (AlSawaftah *et al.* 2021). Membrane fouling can be reduced by pre-treating the feed. This will significantly improve the effectiveness of membrane filtration; nevertheless, cleaning methods are consistently applied (Koh *et al.* 2014; Chen *et al.* 2021; Du *et al.* 2023).

2.17.1. Pre-treatment strategies

Wastewater pre-treatment removes contaminants or reclaims valuable metals and chemicals from industrial wastewater before discharge to meet regulatory requirements. Pre-treatment processes play vital roles in mitigating membrane fouling and achieving efficient energy use (Zulkefli *et al.* 2021). RED is less prone to fouling than typical pressure-driven membrane processes. Hence, proper pre-treatment in wastewater seawater is required to guarantee the RED system operates effectively. The kind of pre-treatment method depends on the nature of the wastewater to be treated. Therefore, selecting a pre-treatment strategy for the impaired water is critical (Vanoppen *et al.* 2019).

These methods, which provide additional value to the RED process, might help compensate for the barriers currently limiting the commercialisation of RED technology.

2.18. Optimisation of the Process

Optimisation aims to achieve the best performance under the given circumstances. Process optimisation minimises the production process's cost and the variability of quality characteristics to maximise the output product in a chemical process (Carter *et al.* 2016).

2.18.1. Design of Experiments (DOE)

Design of experiments (DOE) is a set of multivariate mathematical-statistical techniques that seek to investigate the behaviour of a system by combining the levels that the variables that affect it can assume (Cerqueira *et al.* 2021).

2.18.2. Response surface methodology (RSM)

RSM initiated from the design of the experiment (DOE) is used to determine the significant variables that affect an experiment. RMS is the process optimisation whereby a series of experimental design, analysis, and optimisation techniques were invented in 1951 by Box and Wilson, intending to improve products and industrial processes, optimising the unknown and noisy functions employing more straightforward approximately functions that are valid over a small region using designed experiments (Del Castillo 2007; Rodrigues and Iemma 2014). RMS is beneficial when many factors affect a particular process's production, yield, or percent removal (RSM *et al.* 2015).

RMS is frequently employed to design experiments, and it has several advantages over the Taguchi method of design, as experiments are conducted as per the experimental design, and the responses, such as output, are recorded. Analysis of variance is employed to identify the factors that significantly influence the response (Chelladurai *et al.* 2021). RSM effectively removes bias in an experiment, isolating noise within the experiment from its improvements (Sibiya *et al.* 2022). (Bezerra *et al.* 2008) highlighted that prior to applying the RSM methodology, selecting an experimental design that will define which experiments should be executed in the experimental region being studied is necessary.

2.18.3. Historical Data Design (HDD)

Historical design is utilised when prior knowledge or historical data is available about the variables and their levels (Widyaningsih *et al.* 2018; Ekpotu *et al.* 2020).

Chapter Summary

The world is currently experiencing a water scarcity crisis due to increasing demands on fresh water and increased volumes of industrial wastewater. Thus, coal-based industries release large quantities of wastewater that threaten the freshwater ecosystem. This challenge drives people to initiate and develop more sustainable techniques for wastewater management. The desalination process can improve freshwater salinisation as this decreases the amount of salt in the freshwater. Nevertheless, desalination sustainability is questioned due to energy consumption, environmental impact, and the potential for overreliance on technology. This drawback remains the challenge.

High energy consumption by desalination can contribute to high operation costs due to non-renewable energy sources. However, RED technology can promote renewable energy while banning fossil fuel-based energy sources, as the literature reports. As a result, energy costs can be saved, and RED can significantly contribute to reducing environmental impact in coal-based industries' desalination plants. This study aims to address the feasibility of RED as a viable technology that can desalinate while generating power. There is no extensive investigation on simultaneous power generation and desalination. Studies that look at both power generation and removal efficiency are needed to address the knowledge gaps, especially on desalination by RED technology.

CHAPTER 3 -THERMODYNAMICS FUNDAMENTAL

Chapter overview

The chapter's objective is to understand the fundamental thermodynamics of reverse electrodialysis clearly. Equations developed by many researchers have been discussed in detail. Fundamentals of electro-membrane that provide a better understanding of the process of chemicals involved in transport phenomena through the membrane (IEMs) are also discussed. It implements the Free Gibbs Energy theoretical method to better comprehend how RED stacks produce energy, which involves mixing two salt solutions with various salt concentrations to produce electricity energy.

3.1. Gibbs Free Energy of Mixing

A paper by (Jia *et al.* 2014) reported that the portion of a system's energy available for use is reflected by its Gibbs energy. The total amount of energy available from mixing 1 m^3 of a concentrated and 1 m^3 of a diluted salt solution can be determined from the chemical potential difference of the system after mixing, subtracted by the chemical potential of the system before mixing. The equation describing the Gibbs free energy is as follows: (Jia *et al.* 2014)

$$\Delta G_{mix} = \Delta G_b - (\Delta G_c + \Delta G_d) \tag{3-1}$$

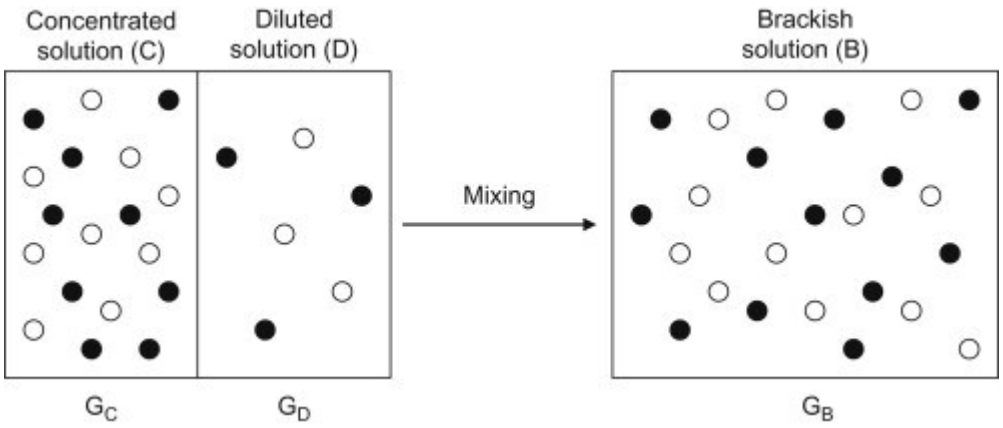

Figure 3- 1 : Mixing of concentrated and dilute solution to brackish solution (Adapted from Jia *et al.* (2014))

where subscripts b, c, d, and d represent the brackish, concentrated and dilute solution resulting from the mixing. The link with the entropy of mixing $\Delta_{mix}S$ can be obtained by expressing Eq.

(3-2) in the following way: (Bazhin 2015)

$$\Delta_{mix}G = (n_c + n_d)T\Delta_{mix}S_b - (-n_cT\Delta_{mix}S_c - n_dT\Delta_{mix}S_d) \tag{3-2}$$

where n is the number of particles (mol); T is the temperature (K); and $\Delta_{mix}S$ is the molar entropy of mixing (J·(mol·K)$^{-1}$) that can be expressed as: (Bazhin 2015)

$$\Delta_{mix}S = -R\sum_i x_i \ln x_i \tag{3-3}$$

where R is the universal gas constant (8.314 J·(mol·K)$^{-1}$); is the molar fraction of component x_i (in the case of ocean and fresh water, i it is mostly NaCl and H2O). Using these calculations, it is feasible to determine the potential energy that might be collected from any river mouth. According to (Schaetzle and Buisman 2015), when using RED, mixing 1 m^3 of seawater at 0.5 mol·L^{-1} of NaCl with 1 m^3 of river water at 0.01 mol·L $^{-1}$ of NaCl at a temperature of 293 K leads to a theoretical maximum amount of extractable energy of 1.4 MJ.

3.2. Theory aspect of Reverse Electrodialysis

Electromotive force, internal resistance, and delivered power are considered key parameters of RED cells. The voltage across a 100% selective membrane can be calculated if pure NaCl solutions of 1 and 30 g/L at 298 K are used, giving values of 0.080 V for a CEM and 0.078 V for an AEM, or together E_{cell} = 0.158 V for a cell. The power efficiency (η_P) is the fraction of total power that is delivered to an external power consumer with resistance Ru: (Veerman and Vermaas 2016).

$$\eta_p = \frac{I^2R_u}{I^2R_i + I^2R_u} = \frac{R_u}{R_i + R_u} \tag{3-4}$$

At maximal power output (Ru = Ri), the power efficiency is below 50%. A higher efficiency can be achieved (by taking Ru > Ri) at the cost of a decreased power output. The power density P_d of a RED system is defined as the external power per membrane area (W/m^2) and is maximal under the condition of Ru = Ri: (Veerman and Vermaas 2016).

$$P_d = \frac{P_u}{2A} = \frac{I^2R_u}{2A} = \left(\frac{E_{Cell}}{R_i + R_u}\right)^2 \frac{R_u}{2A} \tag{3-5}$$

$$= \frac{E^2{}_{cell}}{8AR_i} = \frac{E_{cell}{}^2}{8A\left(R_{AEM} + R_{CEM} + R_{river} + R_{sea}\right)} \tag{3-6}$$

where A stands for the active cell area and 2A for the total membrane area (AEM and CEM) in a cell. R_{AEM}, R_{CEM}, $R_{river,}$ and R_{sea} are the resistances of the AEM, CEM, river water compartment, and seawater compartment, respectively.

3.3. Main parameter of a RED Process

One of the main parameters in a reverse electrodialysis process is typically the Open Circuit Voltage which is also called total electromotive force. The total electromotive force harvested in the RED stack, is the sum of the Nernst potential over each cell, whereby OCV is mainly dependent on the membrane perm selectivity, the concentration gradient, and the valence of the transported ions (Ju *et al.* 2020).OCV can be obtained by the following equation: (Ju *et al.* 2020).

$$OCV = \frac{NRT}{F} * \left(\frac{\alpha_{CEM}}{Z_{ct}} In \frac{Y_{c,ct} c_c}{Y_{d,ct} c_d} + \frac{\alpha_{AEM}}{Z_{an}} In \frac{Y_{c,an} C_c}{Y_{d,an} C_d} \right) \tag{3-7}$$

$$OCV = \alpha * \frac{N_m RT}{zF} \left(In \frac{C_H \gamma_H}{C_L \gamma_L} \right) \tag{3-8}$$

OCV is multiplied with the apparent membrane permselectivity (α) to rectify the nonideal behaviour of the IEMs. α is the ratio of membrane voltage to the theoretical voltage**.** N is the number of membrane pairs (cell pairs), α is the permselectivity of the ion exchange membrane, subscripts ‘an’ and ‘ct’ donate ‘anion’ and ‘cation’, respectively. (Strathmann 2004; Ju *et al.* 2020). Z is the valence of the ionic species, F is the Faraday constant (96.485 ˚C mol^{-1}), C is the salt concentration (mol L^{-1}), and γ is the activity coefficient of the salt. The subscripts H and L refer to HCC and LCC, respectively. Potential differences over each pair of membranes must be totalled to obtain the system’s whole potential.

Electrical resistance can be calculated from Ohm’s law: (Tedesco, Scalici et al. 2016)

$$V = (OCV - Rstack \times I) \tag{3-9}$$

where R_{stack} is the resistance of the stack. The output power (P) is given by: (Tedesco, Scalici et al. 2016)

$$P = (V \times I) \tag{3-10}$$

The power density per cell pair can be given by: (Tedesco, Scalici et al. 2016)

$$P_{\mathrm{d}} = \frac{P}{NA} \tag{3-11}$$

where N is the number of cell pairs, and A is the area of one cell pair.

For an ideal RED stack, the maximum power density P_{dmax} (W/m^2: Watt per m^2 of total membrane area) is obtained when the load resistance equals the internal stack resistance (R_L=R_i). Considering that the sum of E across all cells equals OCV, and indicating with A (m^2) the active membrane area, Eq. (3-12) is adapted to calculate the maximum power density P_{dmax} (W/m^2) as follows: (Othman, Kabay et al. 2022)

$$P_{d\max} = \frac{OCV^2}{4AR_i} \tag{3-12}$$

where R_i (R_{stack}) is the total electrical area resistance per stack (Ω cm^2). The sum of three different sections, i.e., cell resistance, change of concentration in the bulk solution, and the boundary layer, gives the total resistance of the system, as shown in Equation 3-13: (Othman, Kabay et al. 2022)

$$R_i = R_{ohmic} + R_{\Delta C} + R_{BL} \tag{3-13}$$

According to (Daniilidis *et al.* 2014), R_{ohmic} is the ohmic area resistance per cell (Ω cm^2), $R_{\Delta C}$ and R_{BL} are the areas of resistance when concentration changes in bulk solution and boundary layer, respectively. The R_i and R_{ohmic} values can be obtained from the experiment using voltage produced, electrical current, and Ohm's law. Meanwhile, the nonohmic resistances ($R_{\Delta C}$ and R_{BL}) are the reduced electromotive forces (EMFs) when the salinity gradient over the membrane decreases. From the output voltage: (Othman, Kabay et al. 2022)

$$R_i = \frac{(OCV - V)}{I} \tag{3-14}$$

Generally, some electrical energy is consumed by pumping the feeds into the RED stack and circulating the electrode rinse solution. Therefore, the net output power P_{dnet} is calculated by subtracting the power dissipated over the pumps (hydrodynamic loss) P_h from the gross power density P_d: (Simões 2023)

$$P_{dnet} = P_{d-}p_h \tag{3-15}$$

The hydrodynamic loss P_h can be obtained from the theoretical pumping power required to recirculate the solutions through HCC and LCC, which depends on the pressure drop along the compartment Δp (Pa) and the volumetric feed flow rate Q (m^3/s) normalised by the total cell pair area of the stack (N.A). Therefore, Eq. (3-16) is written as follows: (Simões 2023)

$$P_{dnet} = P_d - \frac{\Delta P_{HCC}Q_{HCC}+\Delta P_{LCC}Q_{LCC}}{N.A} \tag{3-16}$$

Flow velocity can be estimated as: (Vermaas, Guler et al. 2012)

$$v = \frac{Q}{\delta w \varepsilon} \tag{3-17}$$

where Q is the volumetric flow rate (m^3/s) in a single channel, δ the spacer thickness (m), w the compartment width (m) and ε the spacer porosity.

3.4. Permeation flux measurements

The amount of permeate produced during membrane separation is referred to as permeate flux and is measured in units of time. Mass permeate was collected and weighed in each run after reaching stable operation. The mass of a solution is equivalent to the volume of the solution (lL = 1,000.00 g). Permeation flux was calculated using the following equation: (Ezugbe 2021).

$$J_w = \left(\frac{V_p}{A*t}\right) \tag{3-18}$$

Where J_w is the water flux (L/m^2min); Vp is the permeate-volume (L); A is the effective membrane area (m^2) of the membrane, and t is the time (min) taken for the experiment.

CHAPTER 4 – EXPERIMENTAL METHODOLOGY

Chapter Overview

This chapter describes the experimental approach used to achieve the study's goal. The synthesis procedure and the standard analytical methods used are described. Detailed explanations have been provided for all experimental procedures. RED stack equipment was used for experimental measurements. This study used synthesised wastewater to simulate colliery mine and coal power plant wastewater. Deionised water was used to mimic the sampling point before discharge to the river, assuming no NaCl would be present. A three-part investigation was conducted in this study. First, the study explored experimentally the influence of the chosen parameters. M Tedesco is the investigation method used here, well documented in the literature. In part two of the investigation, RSM was used to determine the combined influence of parameters, develop empirical models, and determine optimal conditions. In the last step, we examined the effects of divalent ions in the coal that were not considered in the first two steps.

4.1. Materials

4.1.1. Purity of materials

Material purity margins (above 98%) were acceptable in this study, and no further purification was required. The materials used in this study are listed in section 4.2.1. Deionised (DI) water with a conductivity of 1.5 μS was used in all measurements. The DI was supplied by the Mangosuthu University of Technology's (MUT) research laboratory situated in the Chemical Engineering department.

Table 4- 1: Suppliers and quoted purity of all Organic salts used in this study.

Compound	Quoted Purity (wt.%)	Supplier†
$K_3Fe(CN)_6$	≥ 99.0	United Scientific SA
$K_4Fe(CN)_6$	≥ 99.0	United Scientific SA
Na_2SO_4	≥ 99.0	United Scientific SA
$CaCl_2$	≥ 98.0	United Scientific SA
NaCl	≥ 99.9	United Scientific SA

† Supplier quoted purity

All the chemicals and reagents used for the research study are listed in Table 4 -1. These chemicals, purchased from local suppliers, were utilised to synthesise the wastewater and

electrode rinse solution. Deionised water and Ultra-pure NaCl were used to prepare the feed solutions. The aqueous electrode rinse solution contained 0.1 M $K_3Fe(CN)_6$, 0.1 M $K_4Fe(CN)_6$, and 2.5 M NaCl as supporting electrolyte was utilised.

4.2. Experimental set-up

Figure 4-1 shows the equipment set-up used to determine salt removal percentage and power density. This set-up is similar to those used by other researchers (Tedesco *et al.* 2015).

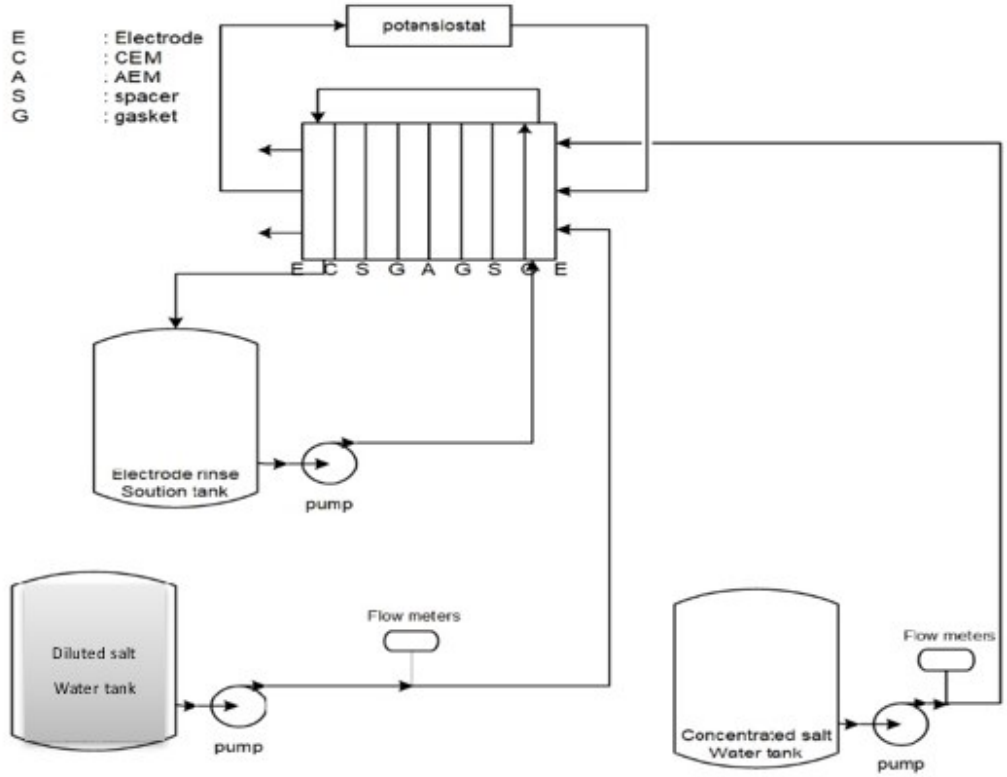

Figure 4- 1: Simplified scheme of the experimental apparatus.

4.2.1. Description of the experimental set-up apparatuses

The experimental apparatus comprised of:

RED stack

RED stack was used to generate electrical power and treat wastewater from the salinity difference between synthesised wastewater and deionised water. In desalination, the focus is on using this salinity gradient to produce permeate water rather than electricity. However, RED technology powers its processes, hence decarbonising the desalination plants. A RED stack (as shown in Figure 4-2) equipped with 60 pairs of cells was used for the experimental

measurements (supplied by Beijing Jingo, China). In each RES stack, 120 µm polyamide woven spacers and Fujifilm ion-exchange membranes supplied by Beijing Jingo (China) were used. Two electrodes with an oxide coating of Ru-Ir are mounted at the ends of RED stack compartments. Table 4-2 summarises membrane properties.

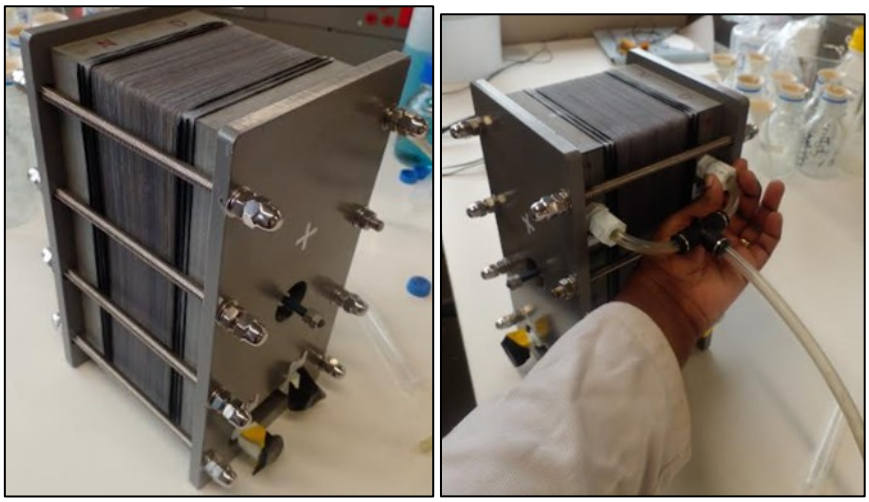

Figure 4- 2 : Assembled RED stacks with (right) and without (left) connection of rinse solution lines.

Table 4- 2: Properties of the IEMs employed in the experiments.

Membrane	**Thickness (µm)**	**Permselectivity (NaCl) (%)**	**Area resistance (Ω cm^2)**	**Water permeation (ml/bar.m^2.hr)**
AEM 80045-01	120	65	~1.8	4.96
CEM 80050-04	120	90	~2.5	4.72

Pump

A self-priming pump (supplied by Apex Scientific, SA) with flow rate controllers was used to pump DI water from two buckets with 10 L capacity to the RED stack unit. Flow rates used in this study ranged from 896 mL/min to 1550 mL/min. A peristaltic pump set at 50% flow rate (supplied by Apex Scientific, SA) was used to pump ERS.

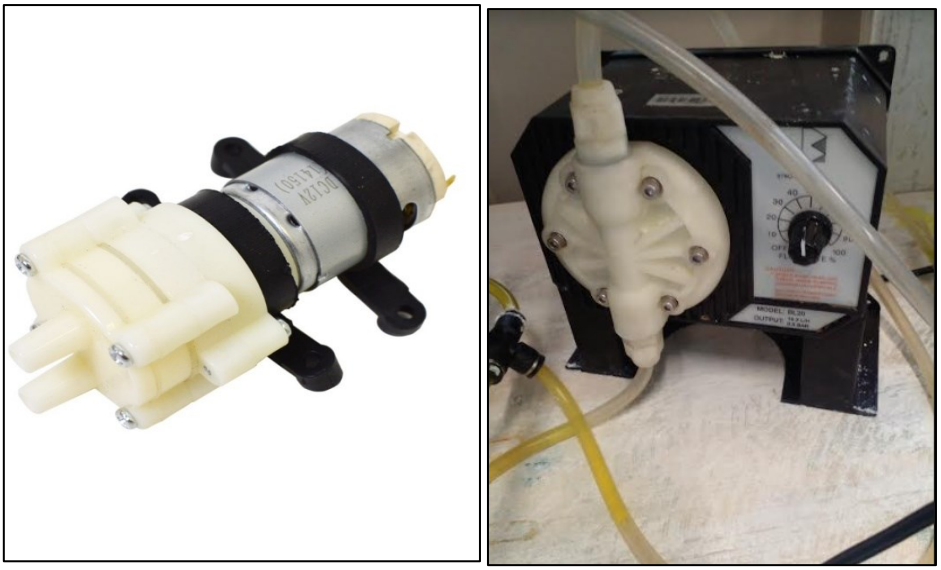

Figure 4- 3: Self-primary water pump (Left) and peristaltic pump (Right) for ERS.

Conductivity meter

The Conductivity Meter (Figure 4-4) and Benchtop Multiparameter Model A215 (supplied by Fisher Scientific, UK) were used to measure salt removal from NaCl. Preparation of synthetic solutions and ERS solution were first heated on a UC152 Hot plate stirrer (supplied by Stuart, SA) at 200 rpm to the required temperature and stored in sample bottles. Afterwards, conductivity measurements were recorded, and the samples were fed buckets. The conductivity of drawn solutions was also measured after heating with a thermostated circulating water bath, as illustrated in Figure 4-4. Calculations of salt removal efficiency/percentage were carried out using equation (4-5). A buffer solution of 12.88 *m*S/cm (supplied by United Scientific SA) was used to calibrate the conductivity meter.

$$R_{removal} = \left(\frac{Z_A - Z_B}{Z_A}\right)100\% \qquad (4\text{-}5)$$

where Z_A and Z_B represent the initial and final conductivity, and R is the percentage removal.

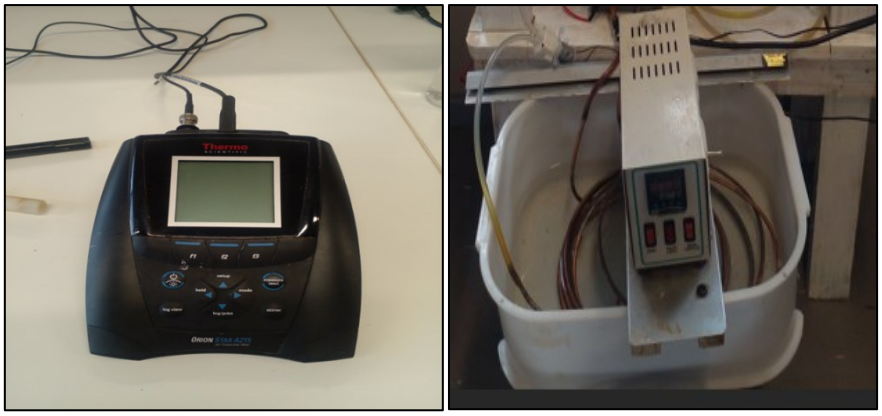

Figure 4- 4: A Conductivity meter and thermostated water bath.

Temperature sensor

The conductivity meter described above was also used to measure the system's temperature since it included a thermostat probe. The instruments were able to measure temperature while measuring the conductivity of samples. A thermostated circulating water bath measured temperatures of 30 to 40 °C. With lower temperature (below room temperature), air conditioning was utilised and monitored continuously until a stable temperature of 20℃ was reached. Natural light was blocked from entering the room, and the samples were stored away from light to prevent deviations.

Flow sensor

The measurements of solutions flowrate were carried out with a flow sensor (supplied by Apex Scientific, SA) as demonstrated in Figure 4-5. The flow rates were set at range of 896ml/L to 1550ml/L.

Figure 4- 5: Flow sensor

Electrical measurements (Fluke)

A Fluke multimeter, Model 15B+ Compact Digital supplied (supplied by Voltex, SA), was used to measure voltages during experiments, which were then used to calculate power density. In this regard, data was recorded when the system had reached a steady state. The power density was calculated as follows from Ohm's law:

$$P = VI \tag{4-1}$$

$$P = \frac{V^2}{R} \tag{4-2}$$

where V, I and R denotes voltage, current and external resistance. The power density of the membrane is given by:

$$P_d = \frac{P}{A} \tag{4-3}$$

where A denotes the membrane area.

Similarly, the open circuit voltages (OCVs) were measured using the same device. Circuits with OCV have no load connected to them, as shown in Figure 4-6 (orange circle). Data was collected while the wire was disconnected from the external load. When the steady state was reached, data was then recorded.

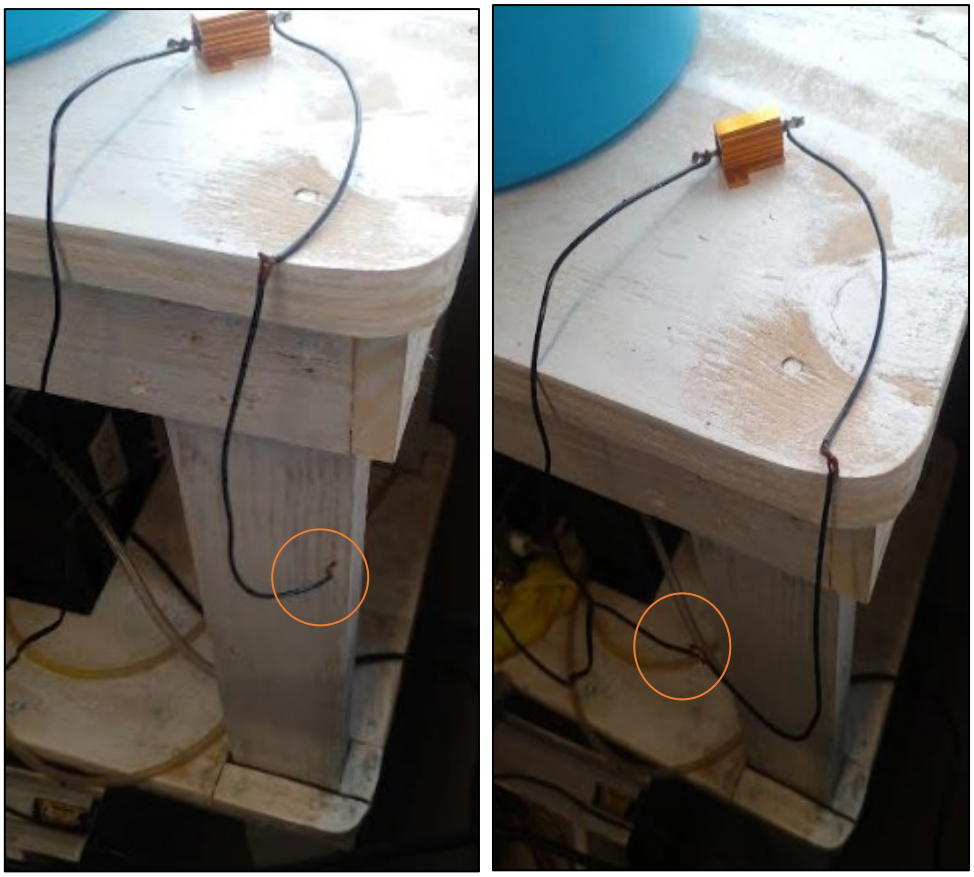

Figure 4- 6: Open Circuit (left) and Closed circuit (right) voltage.

Stirring heating plate

Mixing and heating of the synthesized solutions and ERS solution was carried out with Stuart UC152 Hot plate stirrer (supplied by Stuart, SA). Stirring heating plate was set at 200 rpm to the required temperature for solutions and at room temperature for ERS.

Figure 4- 7: Stuart UC152 Hot plate stirrer

Analytical weighing balance/or scale

Measurements of sample (salts) weights was carried out by Analytical weighing scale (supplied by Scaletec, SA) presented in Figure (4-8).

Figure 4- 8: Analytical weighing balance/or scale

4.2.2. Experimental measurements

- After the preparation of experimental set-up as presented in Figure 4.2.3, two solutions (deionized and artificial wastewater) were filled in the buckets to the 5L mark.
- Bucket valves were fully opened.
- Dilute and concentration solutions were pumped to the RED with self-primary water pump connected to flow sensor that control the flow.
- Temperature water bath was installed in between the piping system of the inlet streams to heat up the solutions at a desired temperature.
- The electrode rinse solution (ERS) was pumped to the stack from 1L bottle using peristaltic pump.
- During the operation, ERS solution was covered with aluminium foil to prevent decomposition of redox couple due to light exposure.
- Multimeter was connected to the RED stack for voltage and open circuit voltage measurements.
- Power measurements were performed under the constant external load of 10Ω, which was connected a stack as shown in Figure 4-6.
- **C**onductivity measurements were taken immediately after each run using conductivity meter.

NB: This procedure was used for investigating the effect of process variables, Optimization (18 runs) and investigating the effect of divalent ions.

4.2.3. Preparation of experimental set-up prior to measurements

Preparation of the experimental set-up is required before conducting experiments. To prepare, the RED stacks should be cleaned, and the electrode rinse lines, adjacent lines, and valves should be leak tested. The samples used in the measurements also needed to be prepared. Thus, the following details the preparation procedures.

Cleaning the RED stacks

Feed buckets were filled with 10L DI water before each experimental measurement. The valves were fully opened, and pumps were turned on to clean the RED stack. The process was repeated for three cycles to eliminate possible impurities in a piping system and membrane before conducting a new experiment.

Leak testing and RED stacks equilibration

Leakage tests were conducted before each experimental run to verify that the RED stack was assembled and the piping lines were connected correctly. During this test, DI water was circulated in the low and ERS channels while the inlet valve for the high channel was closed, but its outlet was left open. DI water was distributed in the high channel and the ERS channel to determine low channel leakage while the inlet valve and outlet valve of the high channel were closed. As shown in equation (4-4) below, leakage percentages are calculated from the volume (V) leak from the high compartment divided by test duration (minutes) and flow rate (Q = 896 mL/min). A sample calculation is provided in the appendix section (Appendix C).

$$Leakage\ \% = \left(\frac{V_{mL\ leakage}}{t*Q}\right)\times 100 \tag{4-4}$$

After that, solutions containing 1M NaCl were used in the high compartment, while deionised water was used in the low compartment to equilibrate the membrane with NaCl solution. The NaCl solution was circulated for 5 minutes to ensure that it was evenly distributed throughout all membrane compartments.

Sample preparation

Calcium chloride (Ca_2Cl), potassium ferricyanide ($K_4Fe\ (CN)_6$), and potassium ferrocyanide ($K_3Fe\ (CN)_6$) were used in the ERSs made with DI water (ELGA PURELAB Option-Q water deioniser, UK). The weights of salts and DI water in the preparation of ERS were measured using an analytical weighing balance (supplied by Kern, SA) with a standard uncertainty of 0.0001. Three types of ERSs were used in this study: two highly concentrated ones that mimic coal mining and coal power plant wastewater and a lower concentrated one that mimics river water. ERSs were synthesised in the lab to represent coal mining and power plant wastewater with high NaCl concentrations before being discharged into the environment. Further, another ERS was prepared to assess the impact of divalent ions, such as sodium sulphate and calcium chloride, on coal mining and power plant wastewater. DI water was used to prepare synthetic wastewater, and NaCl was added in the required quantities. For all experiments, all ERSs were stirred for 10 minutes and rested for 20 minutes to ensure that the salts were fully dissolved. A suitable salt mass was added to 1 L of DI water to prepare synthetic wastewater with concentrations ranging from 1 to 2 mol/L (M). Figures 4-9 show that the samples were kept away from natural light and covered with aluminium foil to prevent degradation.

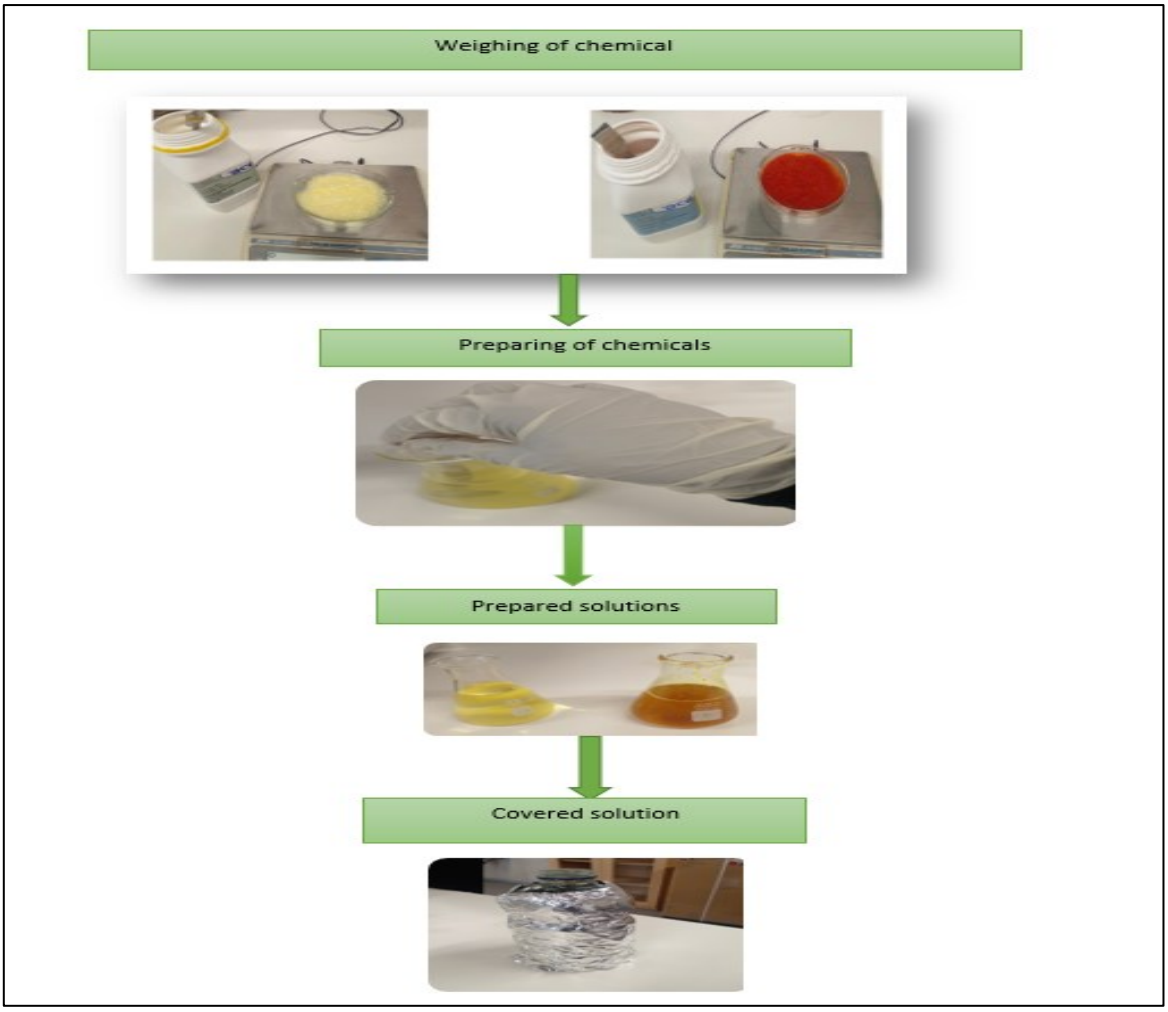

Figure 4- 9: The procedure used to prepare ERSs.

It was necessary to treat synthetic wastewater prior to each experimental run to avoid fouling the membranes. A filter cloth was used to filter dirt wastewater solution, as shown in Figure 4-10, until the concentration of the solution was acceptable.

Figure 4- 10: Dirt-synthesised wastewater (left) and filtered wastewater (right).

4.3. Sample characterisation

In order to assess desalination efficiency, each cation (Na^+ and Ca^{2+}) was measured by inductively coupled plasma Optical emission spectroscopy (ICP-OES). A cellulose nitrate membrane filter (Whatman, 0.22 µm) was used to filter the sample. The test result was assured by (UKZN-PMB School of Chemistry). The instrument's conditions and results are presented in Figures F-1 and Figure F-2 (Appendix), respectively. A multi-element standard ICP grade from spectroscopic solutions, as shown in Figures 4-11 below, was used.

Figure 4- 11: Picture of Multi-element standard ICP grade provided by (UKZN-PMB School of Chemistry.

4.4. Influence on (high concentration, temperature and flowrate)

The first phase of the experiments was carried out at the lab to ascertain whether the process variables effectively improved the RED stack's performance. A reference test was defined (as shown in Table 4-4) where artificial feed solution equal to coal mining and power wastewater (2M NaCl), a flow velocity of 896 mL/min, and a temperature of 20°C were fixed. The dependencies on the main operating parameters (feed concentration, temperature, flow rates) were investigated by changing one parameter per time.

Table 4- 3: Conditions selected for the reference test.

Influence measurements	Changing variables	Reference test value
Concentration	1 – 2 mol/L NaCl	Temperature = 20°C Flow rate = 896mL/min
Temperature	20 – 40 °C	Flowrate = 896mL/min High concentration = 2mol/L NaCl
Flow rate	896 – 1550mL/min	High concentration = 2mol/L NaCl Temperature = 20°C

ERS			
Pumping Efficiency	**Temperature**	**Conductivity**	**pH**
50%	25.4°C	89.1mS/cm	10.61

4.5.Experimental design, Modelling and Optimisation with RSM

Figure 4-12 shows the flowchart presenting the methodology for designing experiments, developing empirical models, and optimising process parameters for the investigated systems.

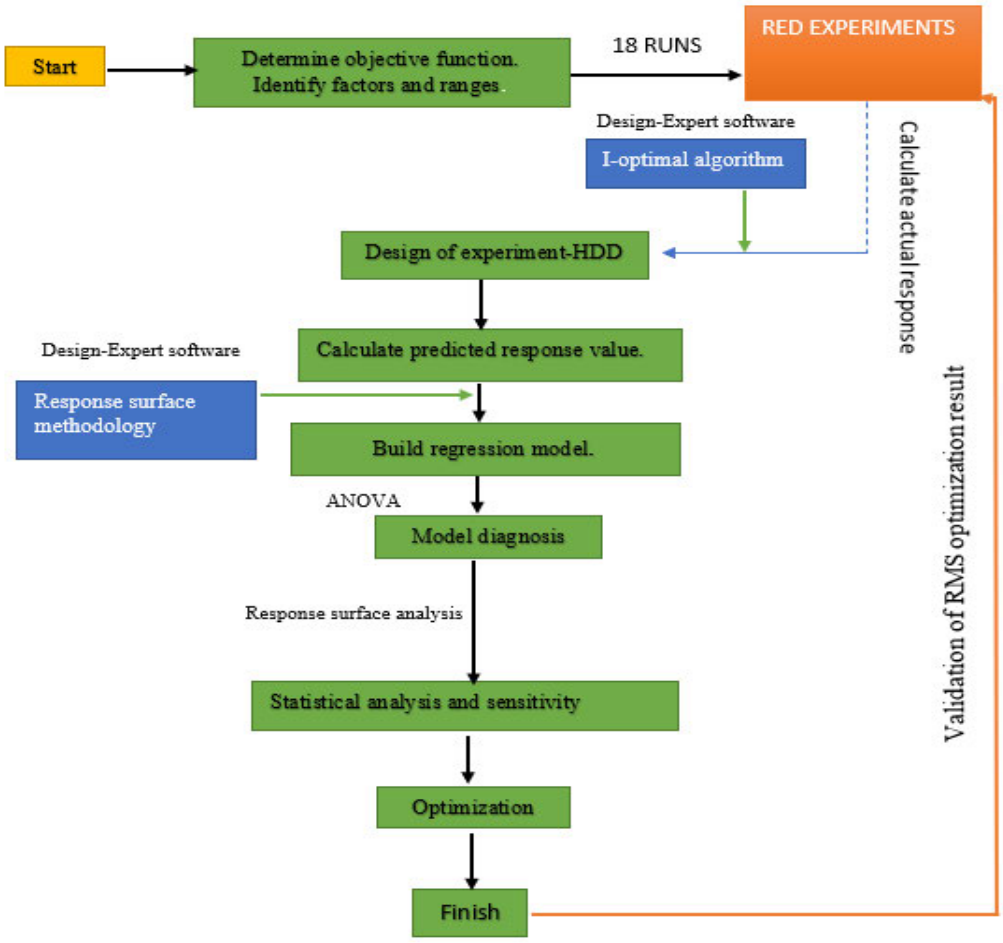

Figure 4- 12: Flow chart of a framework for RSM optimisation of the RED process.

4.5.1. Design of Experiments (DOE)

The experiments were designed using RSM-incorporated Stat-Ease Design-Expert software version 11 (Stat-Ease Inc., Minneapolis, MN, USA) to reduce the number of experiments and the amount of time spent on them. This study used a full factorial design (FFD) of RSM to design experiments (DOEs) of the wastewater treatment and power production process. Three process parameters investigated were NaCl concentration (mol/L), flow rate (mL/min), and temperature (°C). The selected process parameters were converted into dimensionless codified data in three levels: low (-1), medium (0), and high (+1), as shown in Table 4-4.

Table 4- 4: Coded and actual levels of the process parameters for the design of the HDD experiment.

Process parameters	Factors	Coded levels		
		-1	0	+1
NaCl concentration (M)	A	1	1.5	2
Flow rate (mL/min)	B	896	1369	1550
Temperature (°C)	C	20	30	40

The number of experimental runs reported in Table 4- 5 was determined by equation (4-5), (Leong *et al.* 2017).

$$y = \beta_0 + \sum_n^k \beta_i x_i + \sum_n^k \beta x_{ii}^2 + \sum_n^k \beta_{ij} x_i x_j + \varepsilon \quad (4\text{-}5)$$

Where y is the response (dependent variable, β_o is the constant coefficient, β_i, β_{ii}, β_{ij} are the regression coefficients for linear, quadratic and interaction terms, respectively, whereas x_i and x_j are independent variables, while ε is the error. A total of 18 experimental runs were designed in the RSM, as shown in Table 4- 6. To reduce unforeseen variability in the expected responses, experiments were conducted randomly.

Table 4- 7: Experimental plan determined by DOE.

Run order	Process parameters		
	NaCl Concentration (M)	Flowrate (mL/min)	Temperature (°C)
1	1.0	896	20
2	1.0	1369	20
3	1.0	1550	20
4	1.5	896	20
5	1.5	1369	20
6	1.5	1550	20
7	2.0	896	20
8	2.0	1369	20
9	2.0	1550	20
10	1.0	896	40
11	1.0	1369	40
12	1.0	1550	40
13	1.5	896	40
14	1.5	1369	40
15	1.5	1550	40
16	2.0	896	40
17	2.0	1369	40
18	2.0	1550	40

4.5.2. Empirical Modelling

Experimental process parameters and responses were inserted through the historical data design option. The responses were power density (Y_1) and NaCl removal (Y_2). The subsequent power density and NaCl removal were modelled using 2FI expressions in equations 4-6 and 4-7 as suggested by the model.

The equation for power density

$$Y_1 = 1.57930 - 1.47325A + 0.002395B + 0.141472C - 0.001378AB + 0.145126AC - 0.000129BC \quad (4\text{-}6)$$

The equation for salt removal percentage

$$Y_2 = -3.12940 + 14.48209 + 0.014178B + 0.214078C - 0.014218AB - 0.091045AC + 0.000024BC \quad (4\text{-}7)$$

Here, the NaCl concentration is shown as A, the solution feed flow rate as B, and the system temperature as C. The RED stack performance (power density and NaCl removal) was estimated by fitting the experimental results into empirical 2FI models as presented below:

The equation for salt removal

$$= 13.23 - 2.64A - 1.94B + 1.07C - 2.15AB - 0.4552AC + 0.0735BC \quad (4\text{-}8)$$

Equation power density

$$= 5.90 + 0.6146A - 1.07B + 2.04C - 0.2081AB + 0.7256AC - 0.39BC \quad (4\text{-}9)$$

Here, the NaCl concentration is shown as A, the solution feed flow rate as B, and the system temperature as °C.

4.6.Optimisation Framework

Figure 4-13 shows the set-up for this process. The experiment was conducted in a co-flow mode. The operating conditions for this process were high concentration of 1 to 2 mol/L, temperature of 20℃ to 40℃ and flowrate of 896 ml/min to 1550ml/min.18 runs generated by RMS, were needed to be optimized, as this helps to improve efficiency of the RED, economic viability, and overall performance of the process. Through optimization, the performance of the reverse electrodialysis system can be enhanced. Following, present the sensitivity of each investigated parameter with regards to process cost, maintenance, utility and energy cost.

High concentration

High concentrations of ions in the solutions may cause the ion-selective membranes to scale and foul hence regular maintenance may be necessary to clean or replace the membranes resulting in increasing cost. High concentrations may impact water quality, and the system may need additional processes to handle the discharge solutions appropriately; and this might add to the utility requirements of the overall system.

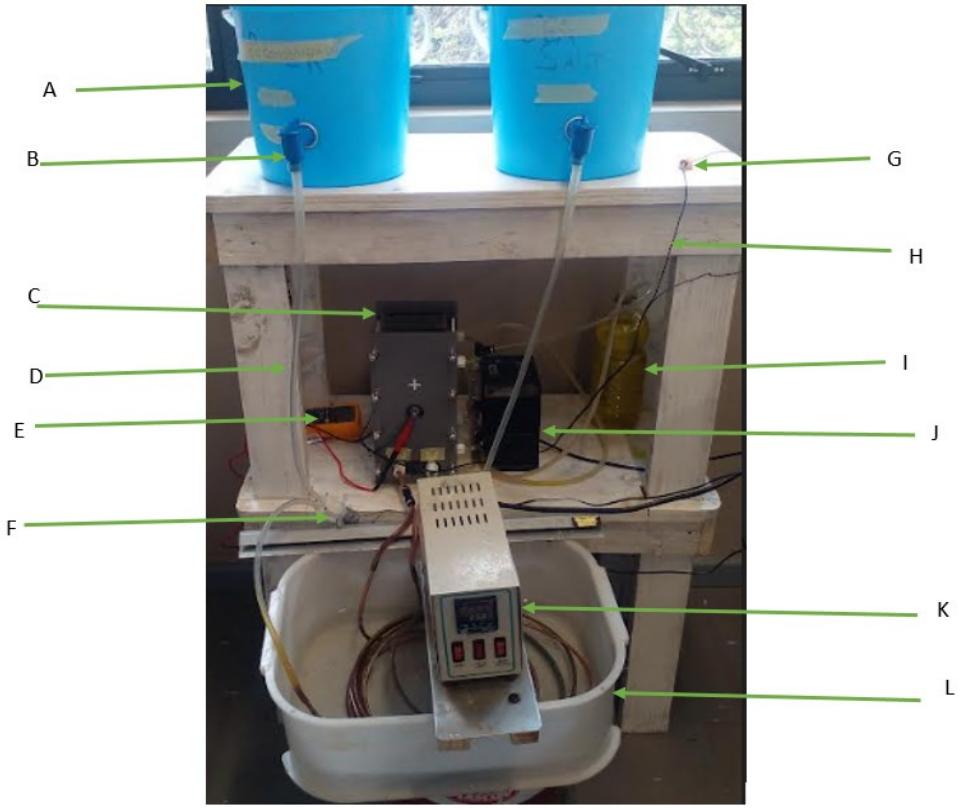

Figure 4- 13: RED experimental set-up used in the study.

A-Solutions bucket; B-Bucket valve; C-RED stack; D-Connecting tube; E-Multimeter; F-solutions pump; G-Resistor; H-Electric wire; I -ERS bottle J- ERS peristaltic pump; K-Temperature controller.

Temperature

Temperature changes may affect salts' solubility, perhaps leading to scaling issues within the stack. Higher temperatures generally have a favourable effect on ion mobility and electrochemical processes, increasing power output. However, high temperatures can improve power production efficiency; they may also lead to increased energy consumption for temperature control and cooling. Therefore, it is best to select an optimal operating temperature.

Flowrate

Higher flow rates require more energy to pump the solutions through the system, resulting in high energy consumption and increasing water usage. Proper water management becomes vital to maintain the salinity gradient between the solutions. This also impacts the RED system's capital costs as pumps, pipes, and membranes may need to be sized differently based on the desired flow rate. Therefore, it is crucial to optimise the process variables to balance increased power output and removal efficiency with the associated pumping energy costs, maintenance, and utility.

CHAPTER 5 - RESULTS AND DISCUSSION

Chapter overview

This chapter presents research findings. The results from the operation of the RED stack, which was utilised to evaluate its performance and ability to desalinate and harvest power from synthesised coal mining and power plant wastewater, are presented in this study. Appendix B shows the raw data and a sample of calculations for all performance-monitoring variables discussed in the following sections. The first phase of the experimental runs was focused on the effect of the main operating variables (concentration, flow rate, and temperature of the feed compartment) on the process performance, testing the RED unit of 110 mm x 270 m, 60 cell pairs with two different sets of membranes. The investigated ranges were selected according to the method recommended by Tedesco *et al.* (2015a) in order to fit the expected operative conditions of the RED stack test rig. Afterwards, an RSM was used to identify the best operating conditions and determine salt removal percentage and power output model equations. Finally, the impact of divalent ions was investigated using acquired optimum conditions.

5.1. Influence of investigated parameters

Several parameters can significantly influence the performance of reverse electrodialysis (RED) systems. The first experiments were performed using a synthetic solution. Results collected during the experimental runs are presented in sections 5.1.1 to 5.1.3. One factor was varied to investigate the effect on each variable while the other two factors were kept constant following conditions selected for the reference test, as presented in Table 4-5.

5.1.1. High Concentration

Figure 5-1 demonstrates the influence of high concentration on power density, salt removal percentage and OCV.

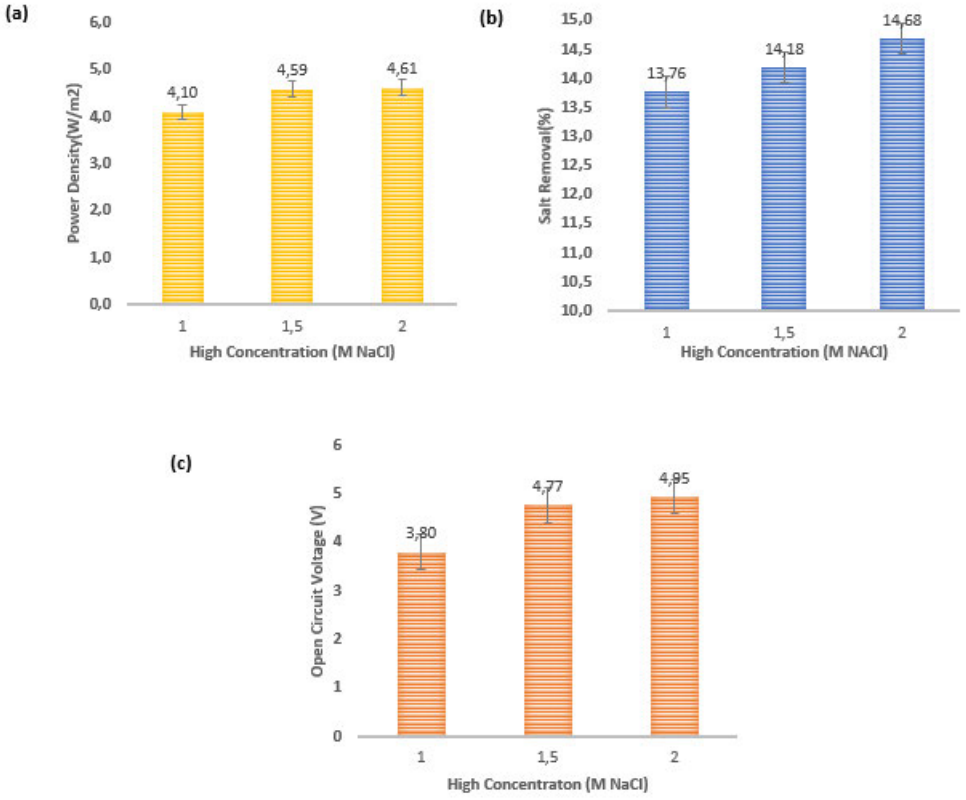

Figure 5-1: High concentration influence process performance. Symbols “a, b and c” denote the power density, salt removal percentage, and OCV.

It can be seen that the trends for power density, OCV, and salt removal increase with increasing concentrations ranging from 1 mol/L to 2 mol/L. Several studies indicated that increasing the concentration of a solution can also lead to a reduction of stack resistance, hence increasing the power output. In this regard, by utilising 1mol/L to 2mol/L, an increase ranged from 4.10 to 4.61, 13.76 to 14.18 and 3.80 to 4.95, which relates to power density, salt removal percentage, and OCV, respectively, registered. This indicates that increasing the conductivity of the solution positively affects the RED performance. However, not much enhancement of all responses was observed when increasing the high concentration from 1.5mol/L to 2mol/L.This could be the selection of the dilute stream used in this study, which tends to play a huge role regarding the salinity ratio between the high concentration and dilute stream, as Zoungrana and Çakmakci (2021) reported that the salinity ratio between HC and LC should be over 25-fold for effectual power output.

On the other hand, this study used thicker IEM; however, RED favours thinner IEM since they reduce the electrical resistance of the compartment, hence increasing the output power, which also results in increasing the salt removal efficiency. In such case, the thicker membrane used and the selection of dilute had negatively affected the power and removability obtained, as a slight increase was observed when the process variable was varied.

5.1.2. Temperature

The temperature has a significant impact on the transport properties of the membrane and solution. In other studies, in which a similar method was employed, an increasing power density from 20 to 40°C was observed. Though their data referred to different experimental conditions, feed concentration and feed velocity were not similar to this study. As shown in Figure 5-2a, power density increased from 4.95 to 10.75 W/m^2.

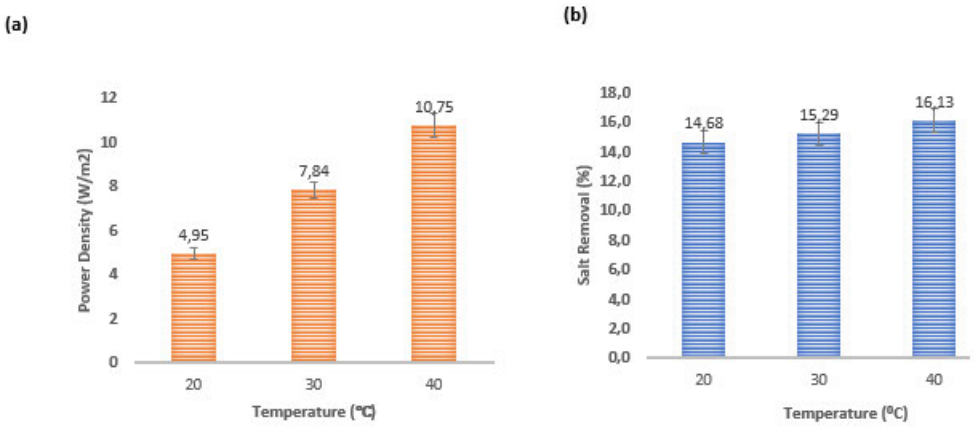

Figure 5-2: Influence of temperature on process performance (a) power density and (b) salt removal percentage.

This explains that higher feed temperature increases the ion separation rate due to the solution's ion mobility and electrical resistance. On the other hand, Figure 5-2b shows an 8.99% increase in salt removal efficiency, indicating that the rise in feed temperature has positive effects. This validates that a high temperature can increase the efficiency of desalination.

5.1.3. Flow rate

Flow velocity is described as the average fluid velocity inside a single spacer-filled channel, and it can directly affect the ion transport rate (Gurreri *et al.* 2014). Figure 5-3a shows a decreasing power density as the flow rate decelerates. This explained that the reduction of flow rate has minimised the residence time of ions in the RED stack. Therefore, it leads to insufficient time for the fluid to pass across the membrane and leave the stack before being removed from the dilute stream to the concentrated stream.

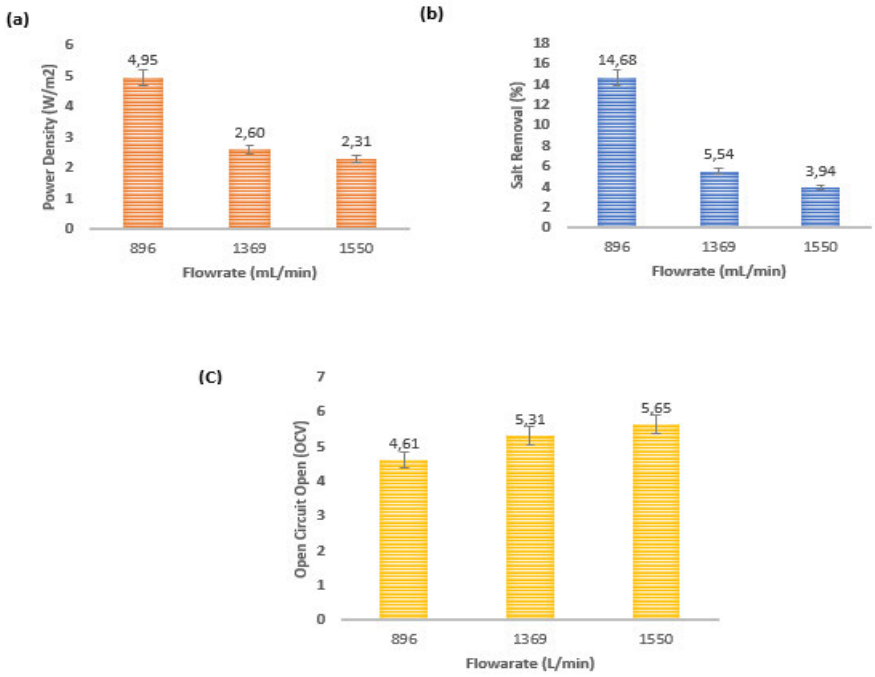

Figure 5-3: Influence of flow rate on process performance. Symbols "a, b and c" denote the power density, salt removal percentage, and OCV.

Generally, increasing the flow rate of solution also increases OCV, as observed. Surprisingly, decreasing power density from 4.95 to 2.31W/$m^{2,}$ as shown in the figure above, could be caused by the non-ratio of high and low solutions Therefore, this elucidates the drops observed in power outputs at high concentrations because of the ratio in salinity. It is worth noting that a further decrease in solution flow rate leads to increased stack resistance, hence reducing the power output despite the high concentration used.

On the other hand, a notable drastic reduction in salt removal percentage was observed, as shown in Figures 5-3b. This indicates that varying flow rates from 1369 to 1550 mL/min,

respectively, could significantly affect the power output of the RED system.

Many authors have investigated the effect of increasing flow rate, whether it has a positive, negative, or no impact on ion removal rate. However, inconsistent results were presented mainly due to the difference in the types of membranes used, stack cell design, and other operational parameters.

5.1.4. Permeate Flux under Different Conditions

In the context of reverse electrodialysis (RED), "permeate flux" describes the rate at which ions move through a membrane in the direction opposite to the normal flow of ions during the electrochemical process. Therefore, the permeate produced during membrane separation is measured in time units. In this study, mass permeate was collected and weighed in each run after reaching stable operation. The mass of a solution is equivalent to the volume of the solution (lL = 1,000.00 g).

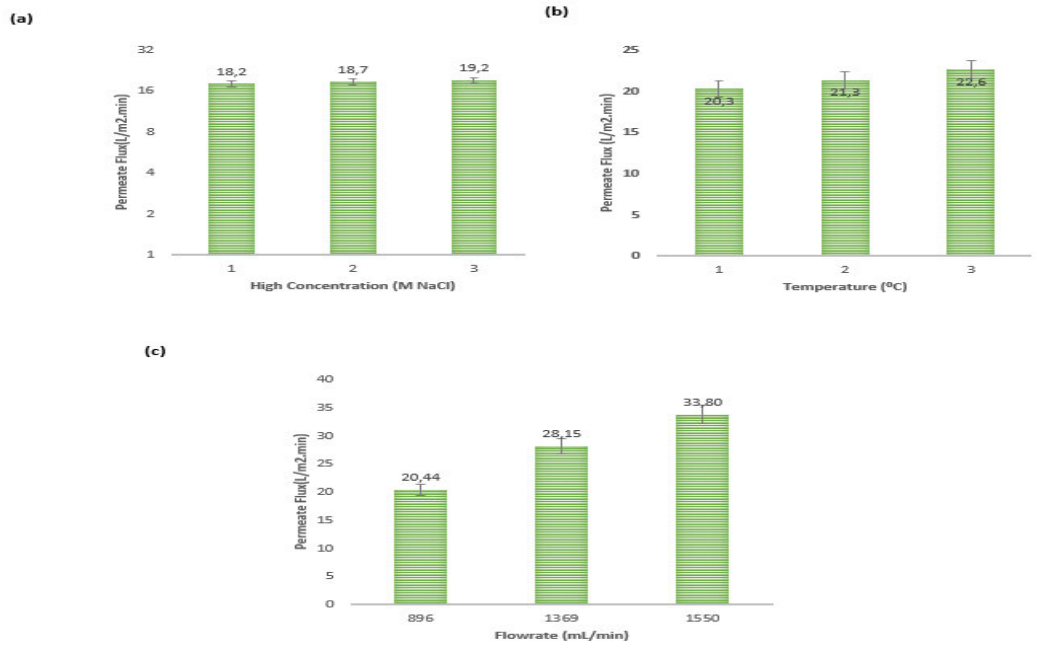

Figure 5-4: Effect of different high concentrations (a), varying temperatures (b) and varying feed flow rates (c) on permeate flux.

Figure 5-4a indicates the influence of the increasing high concentration from 1 to 2 mol/L NaCl on the permeate flux at a constant temperature of 20 °C and a flow rate of 896mL/min. Figure 5-4b shows the effect of consecutively increasing the operating temperatures from 20 to 40°C

on the permeate flux at constant flow rate and feed solution concentration of 896ml/min and 2mol/L, respectively. Subsequently, Figure 5-4c demonstrates the influence of accelerating solution flow rate from 896 to 1550 mL/min on permeate flux at a constant temperature of 20°C and a high concentration of 2 mol/L NaCl. Results show that higher permeate flux is also acquired as high concentration, temperature, and flow rate increase. However, results indicate that concentration is less sensitive to permeate flux, as the observation signifies an increase of 5.49% from low to high. The concentration has shown limited alteration in the permeate flux. Results also revealed an increase of permeate flux to 11.33% with temperature. In addition, the flow rate increment from 896 to 1550mL/min has caused an increase in the permeate flux to 65.36%, concluding that permeate flux on the RED stack is mainly dominated by flow rate.

5.6. Optimisation of input parameters.

The optimisation aims to find the optimal combination of the high concentration, solutions flow rate, and temperatures to maximise the power production and salt removal percentage. A design expert (historical data design) tool was used for optimisation. Investigated parameters such as flow rate have not been tested and reported by other authors. Therefore, experimental runs (18), as shown in Table 5-3, were conducted, and after that, factors and response results were exported to the tool for further RMS analysis, as illustrated by Table 5-3. Model fitness is demonstrated by coefficient of determination (R^2), adjusted R^2, standard deviation (SD), coefficient of variance (CV), and adequate precision (AP) (Sibiya *et al.* 2022). As shown in Table 5-2, Fisher's *F*-values and associated *p*-values with a 95% confidence level with a 99% population were employed to determine the relevance of the model equations for each output parameter.

Table 5- 1: Point prediction table by DOE

Response	Predicted Mean	Predicted Median	Observed	Std Dev	SE Mean	95% CI low for Mean	95% CI high for Mean	95% TI low for 99% Pop	95% TI high for 99% Pop
Salt removal (%)	13.2294	13.2294		1.78285	0.434961	12.272	14.1867	5.32724	21.1315
Power density (W/m^2)	5.89518	5.89518		0.596486	0.145525	5.57489	6.21548	3.25137	8.539

5.6.1. Model fitting

Table 5- 2: The HHD design matrix for desalination and power production technique displays the experimental and predicted results.

Run	FACTORS			RESPONSES			
				Response 1	Response 2	Response 1	Response 2
	High Concentration (Molar NaCl)	Flowrate(mL/min)	Temperature(°C)	Salt Removal (%) Actual	Salt Removal (%) Predicted	Power Density (W/m^2) Actual	Power Density (W/m^2) Predicted
1	1	896	20	13.76	14.21	3.80	4.43
2	1	1369	20	13.54	14.43	3.58	3.69
3	1	1550	20	13.12	14.51	3.45	3.41
4	1.5	896	20	14.18	14.17	4.77	4.53
5	1.5	1369	20	13.61	11.02	4.49	3.46
6	1.5	1550	20	12.67	9.82	3.21	3.06
7	2	896	20	14.68	14.14	4.95	4.63
8	2	1369	20	5.54	7.62	2.60	3.24
9	2	1550	20	3.94	5.13	2.31	2.70
10	1	896	40	18.18	17.11	8.49	7.85
11	1	1369	40	17.87	17.55	5.66	5.89
12	1	1550	40	16.51	17.72	5.19	5.14
13	1.5	896	40	14.29	16.16	9.27	9.40
14	1.5	1369	40	14.04	13.24	6.34	7.11
15	1.5	1550	40	12.85	12.12	6.23	6.24
16	2	896	40	16.13	15.21	10.75	10.95
17	2	1369	40	7.39	8.93	8.23	8.33
18	2	1550	40	7.31	6.52	8.10	7.33

The regression analysis was conducted on the responses to determine the coefficients of the model terms. The historical data design of the factors and responses in this study is shown in Table 5.2.

5.6.2. Analysis of variance

The Analysis of variance (ANOVA) is frequently used to summarise the significance of the regression model and test for significance on individual model coefficients. The statistical fitness and the appropriateness of the regression models generated, which were set at a 95% confidence interval, were determined by utilising ANOVA, as shown in Tables 5-3 and 5-4. The f-value determines the response variation and can be verified by the regression equation. On the other hand, P-values were utilised to ensure each coefficient's significance, which in turn might show the interaction patterns between variables (Widyaningsih *et al.* 2018; Sibiya *et al.* 2022). A significant model can be seen if the p-values are less than 0.05, whereas an insignificant model can be determined by p-values greater than 0.001(Bezerra *et al.* 2008; Danmaliki *et al*. 2017; Chelladurai *et al.* 2021).

Table 5- 3: ANOVA of 2FI regression model for salt removal percentage

Source	Sum of Squares	df	Mean Square	F-value	p-value	
Model	246.44	6	41.07	12.92	0.0002	significant
A-High Concentration	78.14	1	78.14	24.58	0.0004	
B-Flowrate	56.38	1	56.38	17.74	0.0015	
C-Temperature	19.12	1	19.12	6.01	0.0321	
AB	46.11	1	46.11	14.51	0.0029	
AC	2.49	1	2.49	0.7824	0.3953	
BC	0.0811	1	0.0811	0.0255	0.8760	
Residual	34.96	11	3.18			
Cor Total	281.40	17				

R^2	Adjusted R^2	Predicted R^2	Adeq Precision	Std. Dev.	Mean	C.V. %	PRESS
0.8758	0.8080	0.6949	11.3262	1.78	12.76	13.98	85.87

Table 5- 4: ANOVA of 2FI regression model for power density

Source	Sum of Squares	df	Mean Square	F-value	p-value	
Model	98.47	6	16.41	46.13	< 0.0001	significant
A-High Concentration	4.23	1	4.23	11.89	0.0054	
B-Flowrate	17.21	1	17.21	48.38	< 0.0001	
C-Temperature	70.23	1	70.23	197.39	< 0.0001	
AB	0.4333	1	0.4333	1.22	0.2933	
AC	6.32	1	6.32	17.76	0.0015	
BC	2.28	1	2.28	6.41	0.0278	
Residual	3.91	11	0.3558			
Cor Total	102.38	17				

R^2	Adjusted R^2	Predicted R^2	Adeq Precision	Std. Dev.	Mean	C.V. %	PRESS
0.9618	0.9409	0.8704	22.1686	0.5965	5.63	10.59	13.27

A discrepancy of 0.11 and 0.0705 (salt removal efficiency and power density), respectively, between the adjusted R^2 and predicted $R^{2,}$ which is less than 0.2, demonstrate that the suggested models are good for variation between adjusted and predicted(Noordin *et al.* 2004; Amini *et al.* 2008; Ghafari *et al.* 2009; Ighose *et al.* 2017). However, it can be notable that prediction R^2 values for the regression models for salt removal and power density, which are 0.6949 and 0.8704, respectively, show that the two models can not accurately predict. Consequently, the generated model did not carry 12,42% and 3,82 % of the overall variable for salt removal and power density.

5.6.3. Validation of the model

From Tables 5-5 and 5-6, it is worth noting that factors from Model 1(A, B, C, and AB) and Module 2 (A, B, C, AB, AC, and BC) with regard to P-value were significant. Nevertheless, AC and BC were insignificant, implying that the high concentration integrated with solution temperature and flow rate integrated with solution temperature did not affect the salt removal in the solution. The models gave 95 % confidence and 5 % significance levels.

Both models indicated an F-value (Fisher variation ratio) less than 0.02 and 0.01% (Model 1 and 2), respectively, which occurred due to noise. The Models F-value of 12.92 and 46.13 implies the model is significant, as shown in Tables 5-3 and 5-4. A ratio greater than 4 is desirable. In this case, the ratio 11.326 and 22.169 for modules 1 and 2, respectively, indicates that precision is adequate .2FI models are advisable, as suggested by the model. Nevertheless, this study does not recommend this model for historical data because of the low regressions of the models.

5.6.4. Verification of Model Adequacy

Figures 5-5 (a and b) present predicted and actual salt removal efficiency and power density interaction. The adequacy of the regression model was also ascertained between the predicted and actual values plot, as shown in the figures below. The actual value represents the measured result for each experimental run, while the predicted value is evaluated from the independent variables in the regression model. It can be seen from the two figures below, that a good agreement represented by diagnosed plots in both graphs implies good compatibility to establish a relationship between an independent and a dependent for desalination as well as power production (Widyaningsih *et al.* 2018; Sibiya *et al.* 2022; Yaro *et al.* 2022). R^2 for power density and salt removal percentage were 0.8758 and 0.968 , respectively. However, the

predicted R^2 value is not close to the R^2 adjusted value on both responses, indicating that historical data is not recommended in this study.

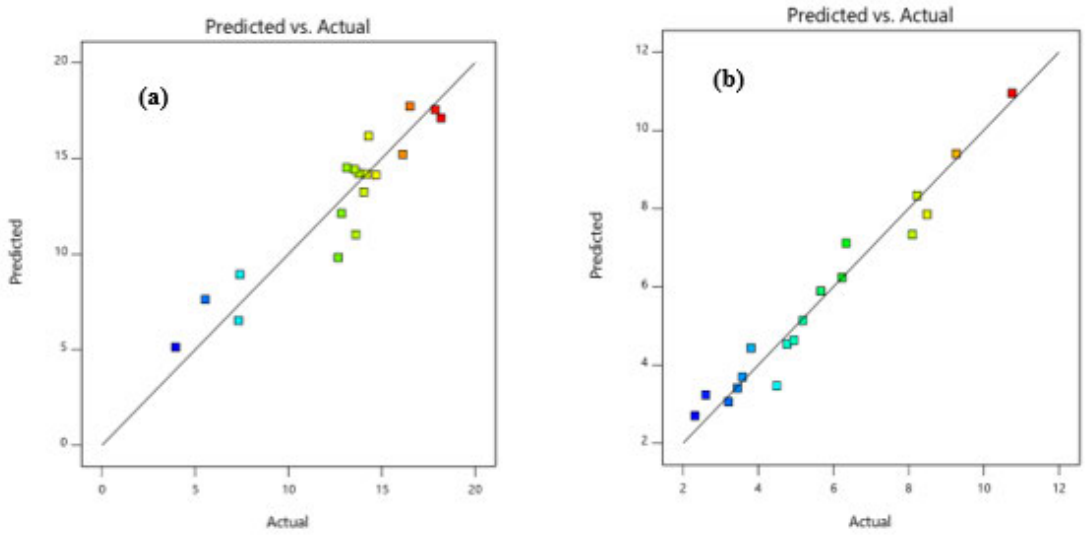

Figure 5-5: Parity plot showing the experimental distribution against the predicted values. Symbols "a and b" denote the salt removal percentage and power density.

Figures 5-6 (a and b) demonstrate the studentised residual versus predicted values for salt removal efficiency and power density**,** respectively. This shows that the variance of the original observations and all the response values, distributed plot, are constant (Salahi *et al.* 2013; Garlapati and Roy 2017). Scattered plots and non-S shape curves presented by both graphs indicate that no actual data transformation is necessary and also aided in determining the model's suitability. Furthermore, the model cannot be enhanced any further by changing the responses. Moreover, the residual limits are ± 3.94 (see Appendix D for calculation). In both graphs, there were no points that were outliers, i.e., outside the residual limits. This means that all observations fit well by the model. There is also no need for response transformation, as there are no outliers in either graph.

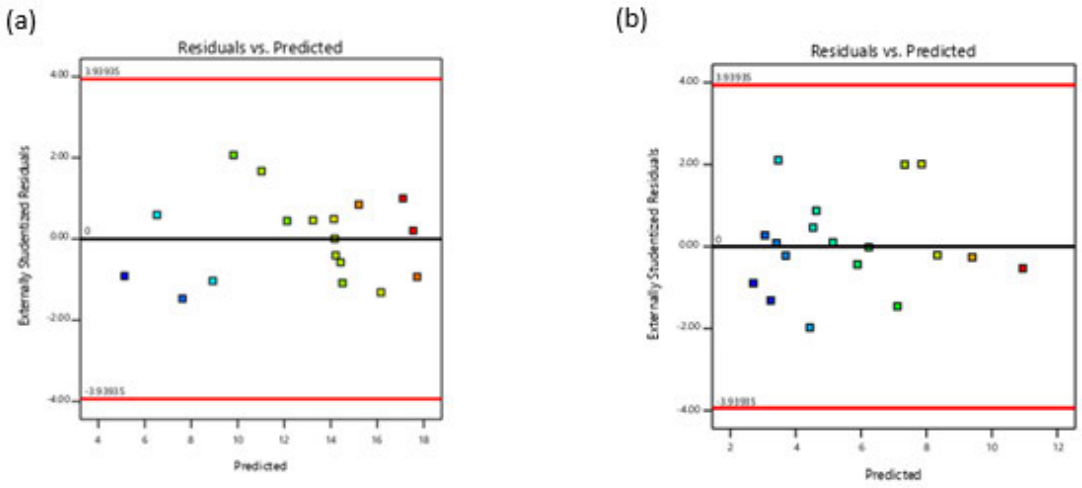

Figure 5-6: Externally studentised residual against predicted. Symbols "a and b" denote the salt removal percentage and power density.

5.6.4.1. Cube graphs

Figure 5-7 (a and b) depicts the maximum desalination and power generated concerning the RED area at a point (A and B-C) located at the top left and bottom right of both graphs, respectively, where response values are 17.6748% and 10.9493 W/m^2 was predicted, which correspond to increasing levels high concentration, flowrate and temperature of solutions (Coman and Bahrim 2011; Kamble *et al.* 2019). In conclusion, according to the figures below, temperature is considered the most significant parameter in both graphs. The effectiveness of removing salt and the power density has dramatically increased as the temperature rises.

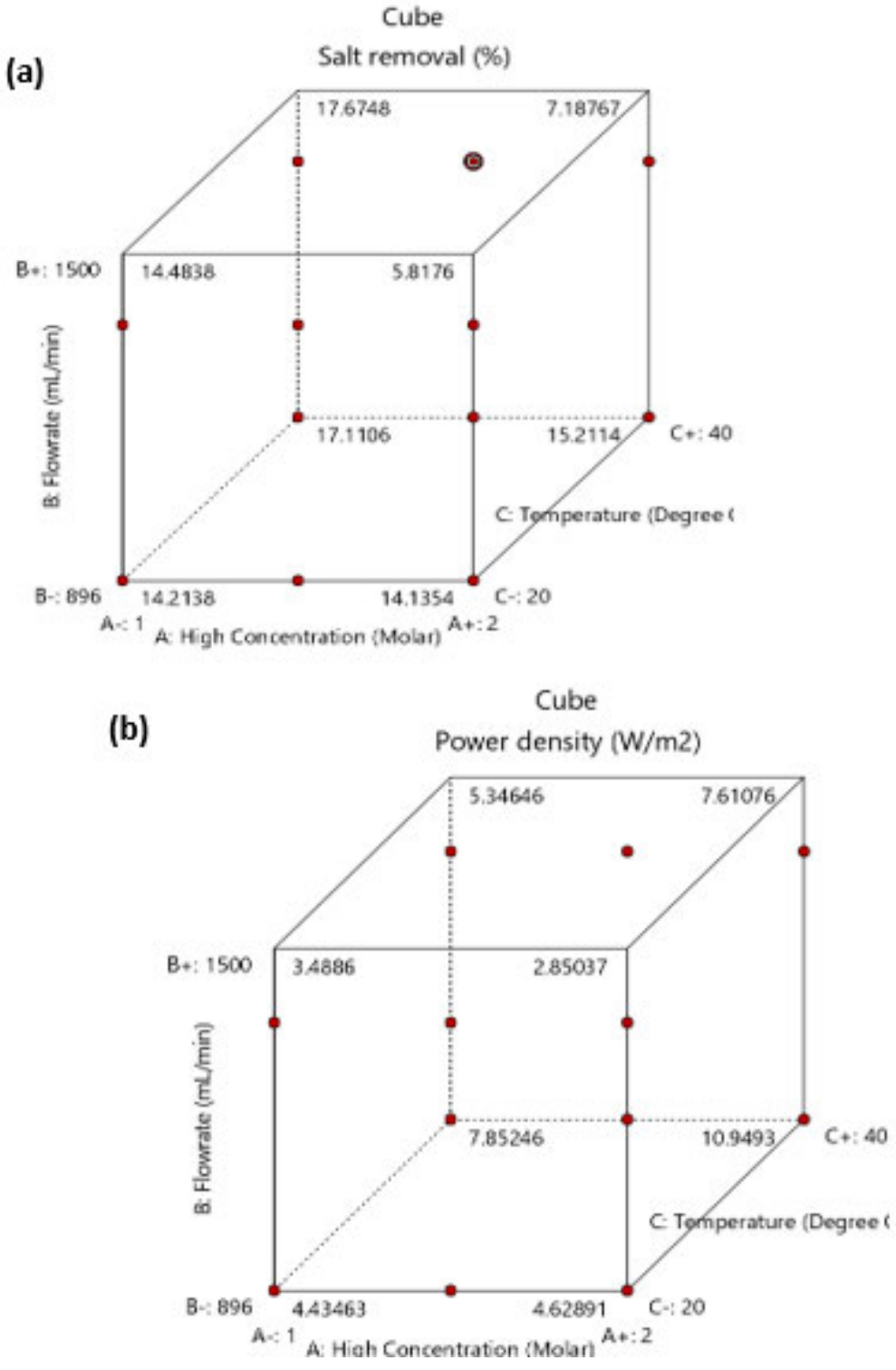

Figure 5-7: Cubes graphs. Symbols “a and b” denote the salt removal percentage and power density.

5.6.4.2. Three-dimensional and contour plots.

The three-dimensional (3D) plots show the behaviour of the salt removal efficiency and power density of the RED stack from the interaction of high concentration (NaCl), temperature, and flow rate of the solutions. As shown in Figures 5-8a and 5-9a, the response surface plots are graphical or visual representations of the relationship between two independent variables and a response. The response is represented on the z-axis, while the two independent variables are plotted on the x and y axes (Hiew *et al.* 2019). Similar to the counter graphs illustrated by Figures 5-8b and 5-9b, two independent variables are plotted on the x and y axes.

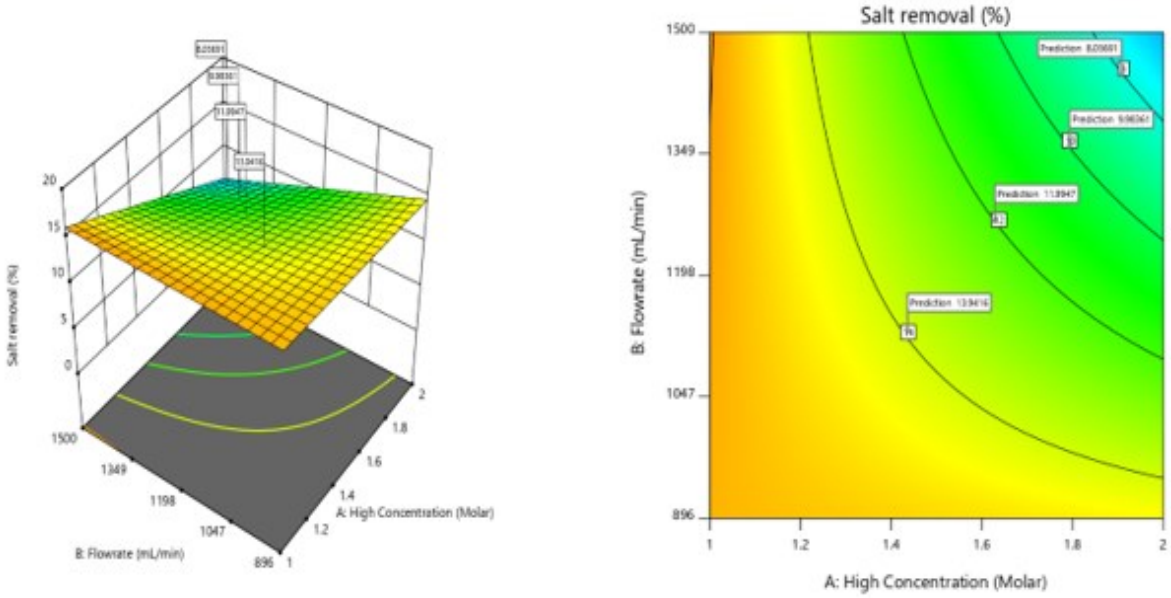

Figure 5-8: Response surface plots showing cross-factor interactions for salt removal percentage. 3D plot (left) and contour plot (right).

Figure 5-8a shows a change in salt removability (drop), notable as the solution concentrations increase from 1mol/L to 2mol/L NaCl at a higher flow rate of 1500mL/min. This concludes that flow rate has much influence on desalination. The interactive influence of high concentration and feed flow rate on power density is depicted by 3D contour plots in Figure 5-9a. The transition from high to low concerning flow rates in Figure 5-9a is represented by the change from green to dark green. They are indicating that the flow rate is sensitive to power production.

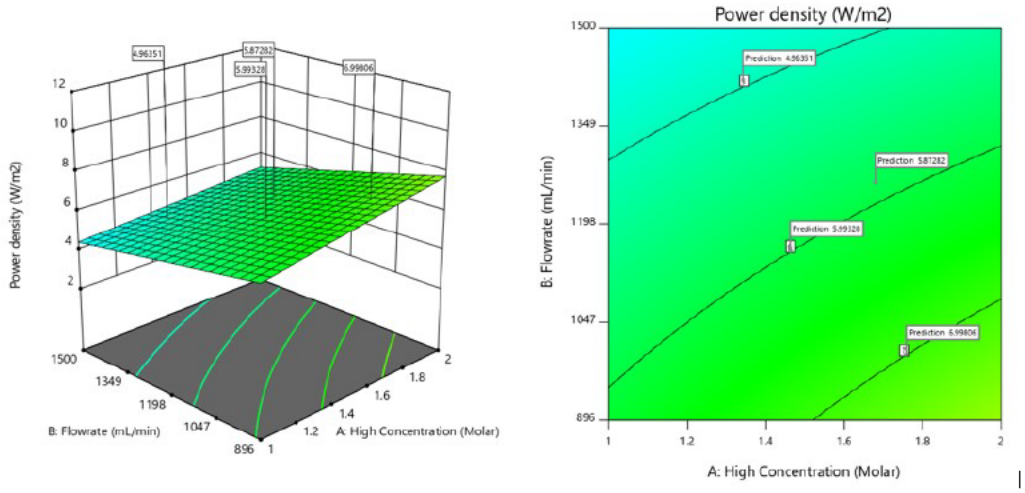

Figure 5-9: Response surface plots showing cross-factor interactions for power density; 3D plot (left) and contour plot (right).

5.6.4.3. Perturbation graphs

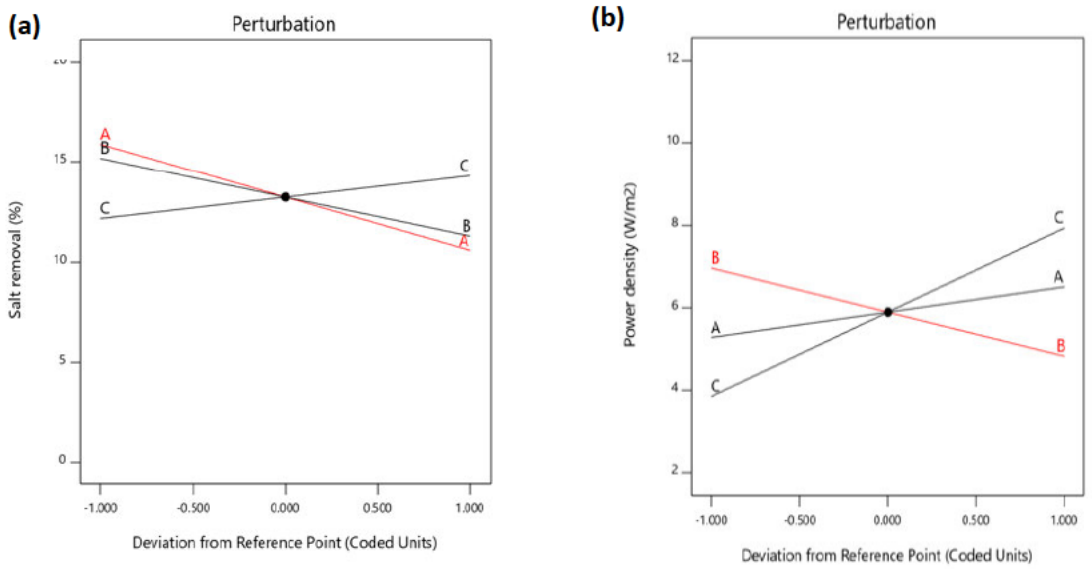

Figure 5-10: Perturbation graph for three factors involved in desalination and power production. Symbols "a and b" denote the salt removal percentage and power density.

Perturbation graphs help evaluate every factor's impact on a particular point using space design (Wu *et al.* 2010; Noshad *et al.* 2012; Liu *et al.* 2018; Aggarwal *et al.* 2020). The responses (salt removal efficiency and power density) are represented graphically by altering one component while keeping the others constant (Coman and Bahrim 2011; Noshad *et al.* 2012; Vijayan,

Ranjithkumar and Shanmugarajan 2018; Kazemian *et al.* 2021). For model 1, represented by Figure 5-10a, it's been discovered that a high concentration impacts the desalination process (straight line A) followed by the flow rate of the solution (straight line B). Conversely, for model 2, represented by Figure 5-10b. Flow rate, followed by high concentration, affects the power density. The rest of the DOE parameters are shown in Appendix D.

5.6.5. Optimisation of desalination technique

Regarding the optimisation process, a numerical approach on Design Expert was employed to optimise three process operating conditions. Table 5-5 demonstrates the details of the conditions of optimisation, where all input variables (high concentration, temperature, and flow rate) were within range. The response variables (salt removal % and power density) were maximised to target 95% confidence predicted levels. Figure 5-11 shows that ideal operating conditions and desirability were achieved. 89.4% desirability was acquired (After achieving 100 conditional solutions) at 1.93 mol/L (NaCl), 896 mL/min, and 40°C. This yielded a salt removal efficiency of 15.33% and a power density of 10.75 W/m^2. Based on the proposed solutions presented in Table 5-6, the first option was selected for verification to show the repeatability and applicability of the design models at a 95% confidence level. Therefore, as shown in section 5.6.6, triplicated experimental runs were used to evaluate the models' validity under optimal conditions (see Figures 5-12 and 5-13).

Table 5- 5: Conditions for optimising desalination and power production process variables.

Independent actors	Goal	Lower Limit	Upper Limit
A: High Concentration (Molar)	Within the range	1	2
B: Flowrate (ml/min)	Within the range	896	1500
C: Temperature (°C)	Within the range	20	40
Salt removal (%)	Maximise	3.94366	18.1818
Power density (W/m^2)	Maximise	2.31394	10.7521

5.6.1. Solutions

The design expert Software iterated over the range of factors and found the maximum salt removal percentage and power density. There are 60 possible solutions. Thus, the one suggested by the software is the selected one, as shown in the Table (5-6) below.

Table 5- 6: HDD optimisation solutions

Number	High Concentration	Flowrate	Temperature	Salt removal	Power density	Desirability	
1	**1.936**	**896.003**	**40.000**	**15.332**	**10.752**	**0.894**	**Selected**
2	1.940	896.000	39.958	15.322	10.752	0.894	
3	1.940	896.479	39.971	15.318	10.752	0.894	
4	1.950	896.001	39.994	15.306	10.793	0.893	
5	1.949	896.003	39.875	15.301	10.752	0.893	
6	1.956	896.001	40.000	15.294	10.814	0.893	
7	1.953	896.076	39.830	15.289	10.752	0.893	
8	1.960	896.001	39.765	15.274	10.752	0.892	
9	1.943	899.688	39.997	15.273	10.752	0.892	
10	1.909	896.001	40.000	15.385	10.667	0.892	
11	1.968	896.180	39.687	15.252	10.752	0.891	
12	1.975	896.005	39.618	15.238	10.752	0.891	
13	1.992	896.093	40.000	15.226	10.923	0.890	
14	1.986	896.001	39.507	15.210	10.752	0.890	

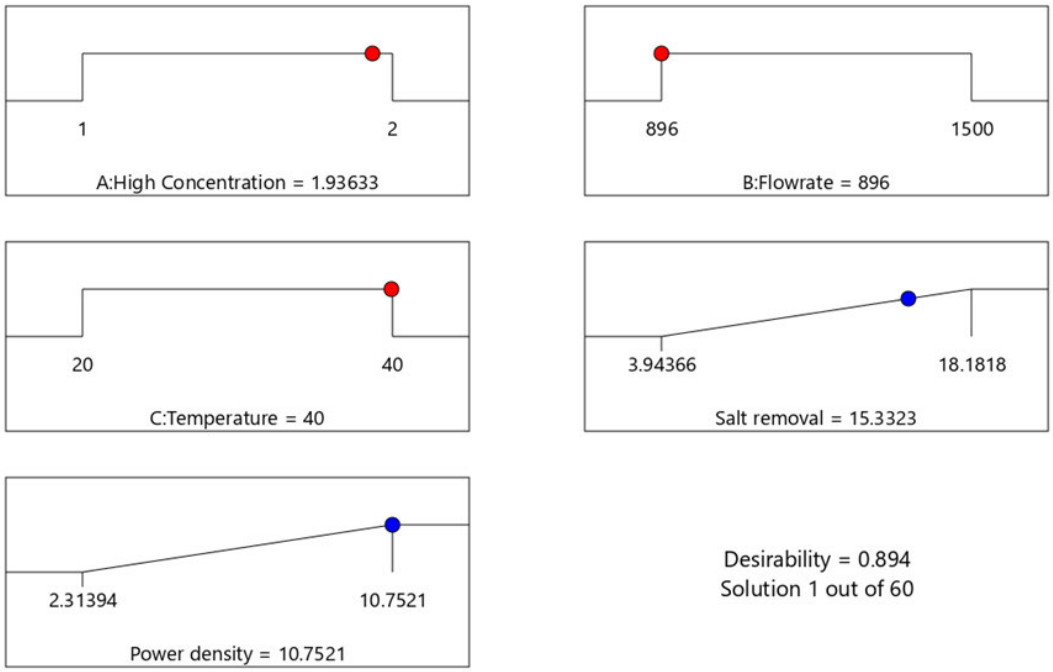

Figure 5-11: Ramp plot displaying the optimised conditions of desalination and power production process variables at the desirability of 89.4 %.

5.6.2. Validation of the RSM optimisation results

Based on the results mentioned earlier, further analysis was validated to see the accuracy of the suggested models under the identified optimal operating conditions. The Figures below show the results of the confirmatory runs. A wide variation of 4.2% is observed in salt removal efficiency. Interestingly, a little deviation of less than 1% for power density is observed in Figure 5-13, and this indicates that the models can appropriately capture the link between experimental and predicted results. Hence, the models showed acceptable ability to predict and improve the desalination-energy production performance of the RED stack. However, this model cannot be recommended for optimising HDD data due to low regressions.

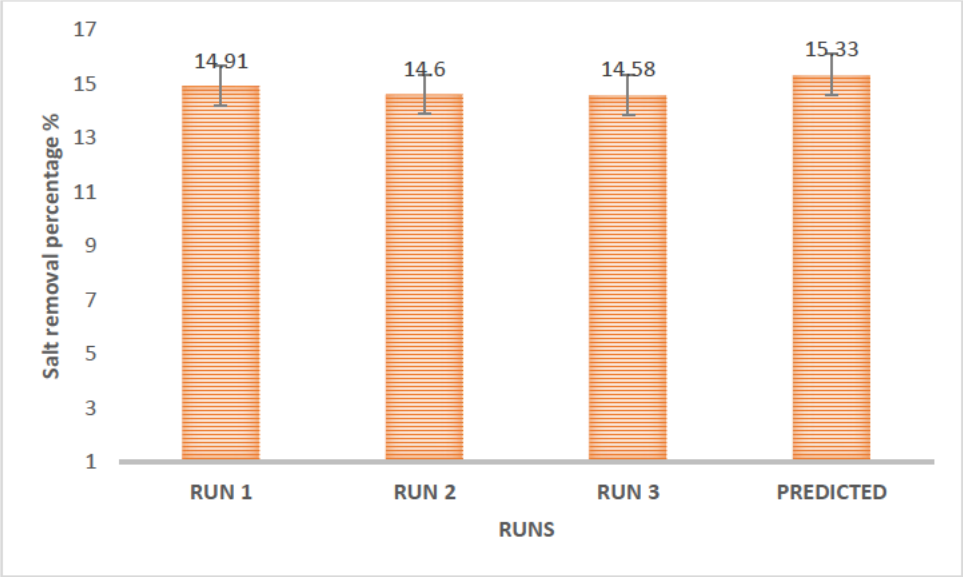

Figure 5-12: Comparing the RSM predicted response value to the experimented response of salt removal at temp 40°C, the flow rate of 896mL/min, and a high concentration of 1.93 mol/L NaCl.

Figure 5-13: Comparing the RSM predicted response value to the experimented response of power density at temp 40°C, flow rate of 896mL/min, and high concentration of 1.93 mol/L NaCl.

5.7. Effect of divalent ions

Wastewater from coal mining and coal power plants contains other ions rather than Na^+ and Cl^- (SO_4^{-2}, K^+, Mg^{2+}, Ca^{2+}), which may still influence performance. Therefore, from the RSM study, the optimum operational conditions for the RED process acquired were utilised in investigating the influences of divalent ions (Na_2SO_4 and $CaCl_2$) with the ionic formulas, respectively:

$$Na_2^{+1}SO_4^{-2}$$

$$[Ca]^{2+}\,2[Cl]^{-1}$$

Sodium sulphate and calcium chloride were used as divalent ions for this study, in which four experiments were examined and conclusions were drawn, employing these optimum conditions. The table presents the ion concentration in the feed solution.

Table 5- 7: Ion concentration in the feed solution

TEST 1	
100% NaCl	0% $CaCl_2$
100% NaCl	25% $CaCl_2$
100% NaCl	75% $CaCl_2$
TEST 2	
100% NaCl	0% Na_2SO_4
75% NaCl	25% Na_2SO_4
25% NaCl	75% Na_2SO_4

This section investigates the negative effects of divalent cations in RED, as shown in Figures 5-14 and 5-15 (a, b, c, and d), respectively. All the parameters were kept constant (optimum values). Prior research has demonstrated that the presence of divalent ions leads to a decrease in RED power densities (Rijnaarts *et al.* 2017; Moreno *et al.* 2018; Gómez-Coma *et al.* 2019), and no work has been reported on salt removal percentage. Thus, the goal of this study is to examine both responses. Figures 5-14 and 5-15 (a, b, c, and d) present the effect of $CaCl_2$ and Na_2SO_4 results.

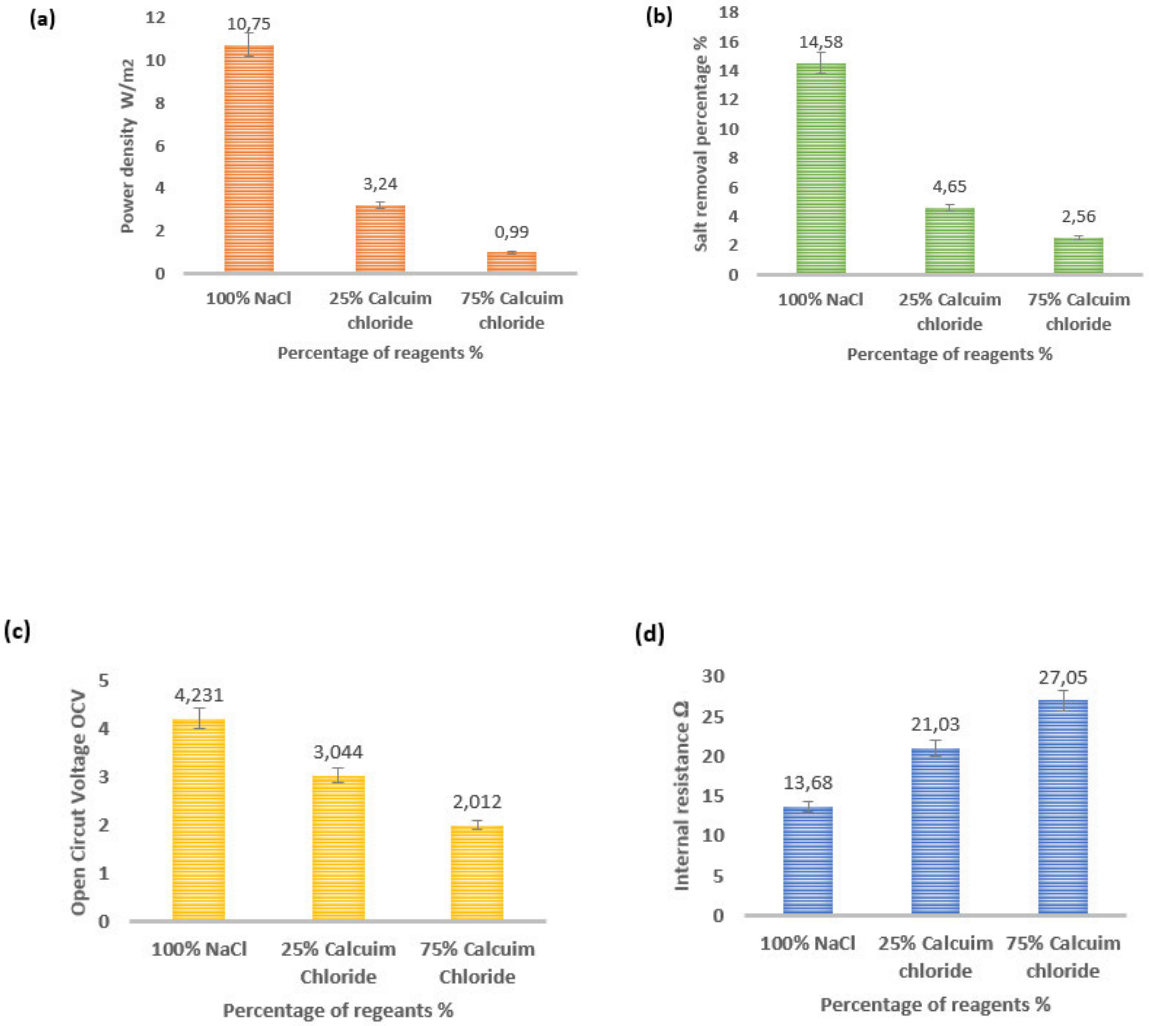

Figure 5-14: Depicts the effect of divalent cation on the performance of the RED stack. Symbols "a, b, c and d" denote the salt removal percentage, power density, OCV and internal resistance.

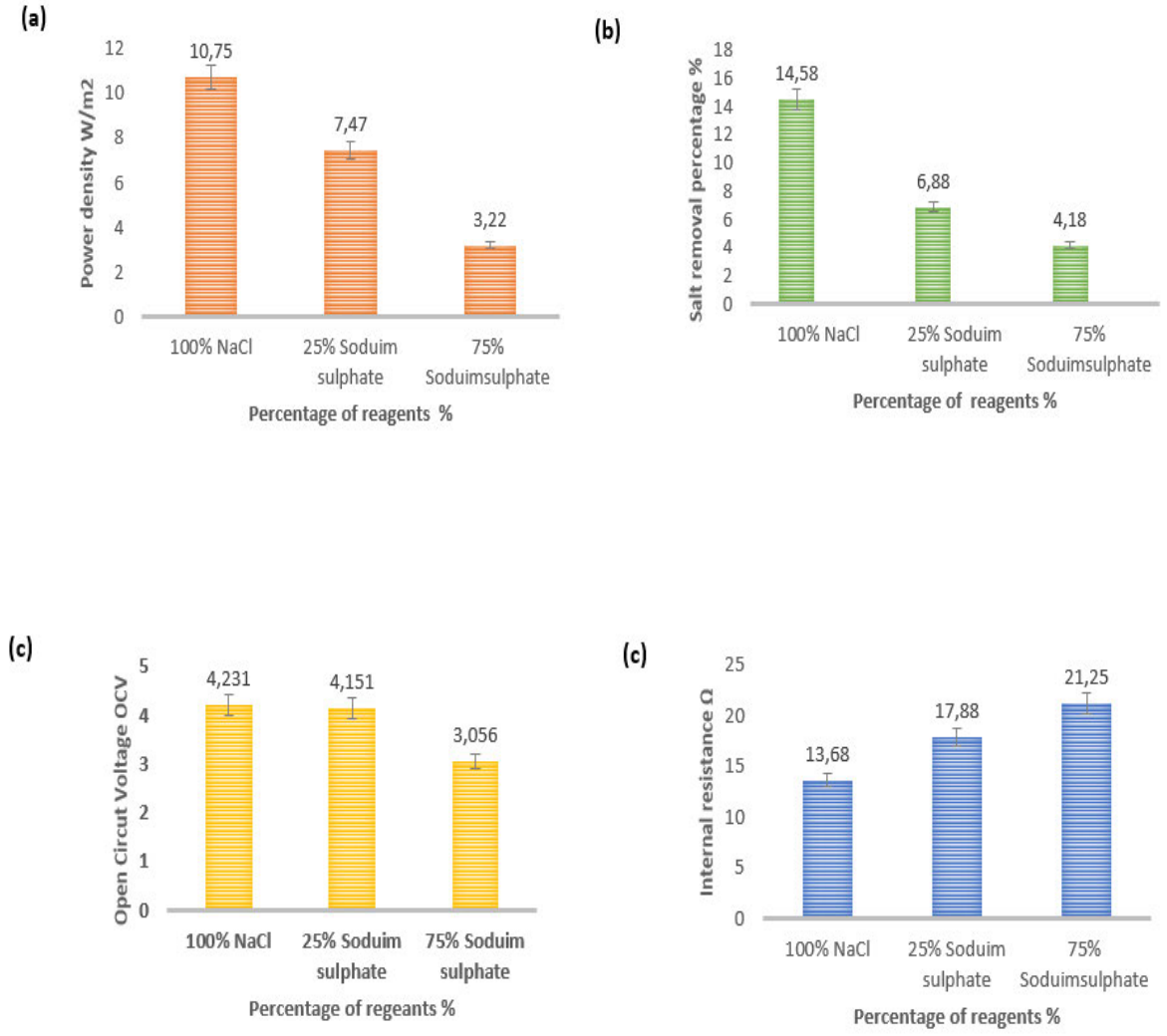

Figure 5-15: Depicts the effect of divalent anion on the performance of the RED stack. Symbols "a, b, c and b" denote the salt removal percentage, power density, OCV and internal resistance.

For Figures 5-14(c) and 5-15(c), OCV decreased after introducing divalent ions to a basis solution. Hence, a negligible effect on the OCV of anion (25% Na_2SO_4) from 4.231 to 4.151 is observed, and a considerable effect on the OCV of cation (25% $CaCl_2$) from 4.231 to 3.044 is notable. However, adding a 75% percentage of divalent ions to 100% NaCl has reduced OCV drastically, as presented in both graphs. This proves that adding divalent salts influences the concentrations of Na+ and Cl− and, therefore, the membrane voltage.

Stack resistances, as shown in Figures 5-14(d) and 5-15(d), a significant increment of 98.45% and 99%, respectively, were observed in both graphs, as more divalent was added to pure NaCl solution. A decrease in OCV and increased stack resistance have considerably decreased power density and salt removal percentage. Power density and salt removal percentage are significantly reduced by adding 75% to a pure solution, as presented in Figures 5-14 (a and b) and 5-15 (a and b). This indicates that adding divalent ions causes uphill transportation, hence increasing membrane resistance and affecting the performance of the RED stack.

The results indicate that divalent ions decrease membrane permselectivity and membrane potential while altering the ion concentrations within the membrane to increase the electrical resistance of the membrane.

This study shows that RED power densities and salt removal percentage can be improved by selecting an ion exchange membrane suitable for the divalent ion composition of the feed streams.

CHAPTER 6-CONCLUSIONS AND RECOMMENDATIONS

Chapter overview

This chapter presents the research study's significant conclusions and local decisions about the optimization of desalination as well as power generation from coal mining and colliers' wastewater using reverse electrodialysis.

The main achievements of the research activities presented can be summarised as follows:

> ***Experimental investigation on a laboratory scale***. The finding revealed that flow rate is one of the factors that negatively influence the performance, as a reduction in both salt removal percentage and power density were registered under used conditions (process parameter); however, flowrate was more sensitive to permeate flux than other responses as 65.36% increase was observed when the flow rate of the solutions was investigated. Based on the findings, the results acquired are in agreement with the findings from (Vermaas 2014), which concludes by validating that "The utilization of river water has a notable disadvantage: the low conductivity of the solution causes high electric resistance within the unit, limiting the output power achievable. In this case, deionized, which represents the point of the river with less or no NaCl, was used as a dilute. In particular, the diluted (deionized) has been found to have a greater impact on process performance. Therefore, it can be concluded that using (110x270 mm^2, 60 cell pairs) has led to significant outcomes for characterising the process conditions, as this study shows feasibility in applying RED in coal mining and colliers: however, a careful selection of process conditions; membranes properties should be considered as it can lead to a better performance of the RED technology since desalination efficiency in this study shows a very low salt removability of 15.33% at optimum conditions.

***Development of model equations for optimization*.** Utilizing the historical data obtained from the lab. The model was able to forecast the behaviour of the process utilizing synthesized concentrations under conditions unexplored before. 2FI model highlighted that predicted and actual were in good agreement, which indicates a model significant. However, due to low regressions for power density and salt removal, it can be concluded that the developed empirical cannot be used to make predictions. Therefore, optimizing experimental results using historical data design is not recommended.

Analysis of ions influencing the RED performance. The addition of divalent ions to pure NaCl solutions was evaluated. Thus, power density and salt removal percentage reduction were registered even at a lower percentage. This demonstrates unequivocally that divalent ions have a significant impact on RED performance. Therefore, intensive pre-treatment is required when using real solutions.

In summary, all objectives were met in this study. The novelty in this study lies in simultaneously demonstrating energy production and desalination of artificial coal mining and collier wastewater. Based on these results, this study significantly contributes to coal-based desalination plants in SA. This project has never been implemented in Southern Africa; hence, it is best to recommend the following.

Recommendation

Despite the milestones attained in this study, there is still more work to be done in the future. Thus, the following factors can be considered for future research:

- Utilizing South African coal mining and collieries, real wastewater should be considered for future studies since artificial solutions might overcome some drawbacks of real effluent, e.g., the requirement of intensive pre-treatment techniques to prevent fouling.
- Consideration should be given to the best selection of dilute streams.
- RED stack performance can be enhanced by carefully selecting membrane properties.
- Research using similar experimental data should be conducted to develop models that produce reliable and accurate predictions.

REFERENCES

Abidin, M. N. Z., Nasef, M. M. and Veerman, J. 2022. Towards the development of new generation of ion exchange membranes for reverse electrodialysis: A review. *Desalination*, 537: 115854.

Aggarwal, V., Singh, J., Sharma, S., Sharma, A., Singh, G. and Parshad, J. 2020. Empirical modeling of machining parameters during WEDM of inconel 690 using response surface methodology. In: Proceedings of *AIP Conference Proceedings*. AIP Publishing,

Al-Amshawee, S., Yunus, M. Y. B. M., Azoddein, A. A. M., Hassell, D. G., Dakhil, I. H. and Hasan, H. A. 2020. Electrodialysis desalination for water and wastewater: A review. *Chemical Engineering Journal*, 380: 122231.

Al-Hotmani, O. M. A., Al-Obaidi, M. A. A., John, Y. M., Patel, R. and Mujtaba, I. M. 2020. Scope and Limitations of the Mathematical Models Developed for the Forward Feed Multi-Effect Distillation Process—A Review. *Processes*, 8 (9): 1174.

Al-Shammiri, M. and Safar, M. 1999. Multi-effect distillation plants: state of the art. *Desalination*, 126 (1-3): 45-59.

Ali, A., Tufa, R. A., Macedonio, F., Curcio, E. and Drioli, E. 2018. Membrane technology in renewable-energy-driven desalination. *Renewable and Sustainable Energy Reviews*, 81: 1-21.

AlSawaftah, N., Abuwatfa, W., Darwish, N. and Husseini, G. A. 2022. A review on membrane biofouling: Prediction, characterization, and mitigation. *Membranes*, 12 (12): 1271.

Altıok, E., Kaya, T. Z., Güler, E., Kabay, N. and Bryjak, M. 2021. Performance of reverse electrodialysis system for salinity gradient energy generation by using a commercial ion exchange membrane pair with homogeneous bulk structure. *Water*, 13 (6): 814.

Alvarez-Silva, O., Osorio, A. F. and Winter, C. 2016. Practical global salinity gradient energy potential. *Renewable and Sustainable Energy Reviews*, 60: 1387-1395.

Amini, M., Younesi, H., Bahramifar, N., Lorestani, A. A. Z., Ghorbani, F., Daneshi, A. and Sharifzadeh, M. 2008. Application of response surface methodology for optimization of lead biosorption in an aqueous solution by Aspergillus niger. *Journal of hazardous materials*, 154 (1-3): 694-702.

Amy, G. 2008. Fundamental understanding of organic matter fouling of membranes.

Desalination, 231 (1-3): 44-51.

Anis, S. F., Hashaikeh, R. and Hilal, N. 2019. Microfiltration membrane processes: A review of research trends over the past decade. *Journal of Water Process Engineering*, 32: 100941.

Annandale, J., Beletse, Y., De Jager, P., Jovanovic, N., Steyn, J., Benadé, N., Lorentz, S., Hodgson, F., Usher, B. and Vermeulen, D. 2007. Predicting the environmental impact and sustainability of irrigation with coal mine water. *Water Research Commission Report*, Article ID(1149/01): 07.

Ariono, D., Prabandari, D., Wulandari, R. and Wenten, I. 2017. Preparation and characterization of polysulfone/PEG heterogeneous ion exchange membrane for reverse electrodialysis (RED). In: Proceedings of *journal of physics: conference series*. IOP Publishing, 012075.

Arnott, S. E., Celis-Salgado, M. P., Valleau, R. E., DeSellas, A. M., Paterson, A. M., Yan, N. D., Smol, J. P. and Rusak, J. A. 2020. Road salt impacts freshwater zooplankton at concentrations below current water quality guidelines. *Environmental Science & Technology*, 54 (15): 9398-9407.

Asadollahi, M., Bastani, D. and Musavi, S. A. 2017. Enhancement of surface properties and performance of reverse osmosis membranes after surface modification: a review. *Desalination*, 420: 330-383.

Avci, A. H., Sarkar, P., Tufa, R. A., Messana, D., Argurio, P., Fontananova, E., Di Profio, G. and Curcio, E. 2016. Effect of Mg2+ ions on energy generation by Reverse Electrodialysis. *Journal of Membrane Science*, 520: 499-506.

Avci, A. H., Tufa, R. A., Fontananova, E., Di Profio, G. and Curcio, E. 2018. Reverse Electrodialysis for energy production from natural river water and seawater. *Energy*, 165: 512-521.

Aydar, A. Y. 2018. Utilization of response surface methodology in optimization of extraction of plant materials. *Statistical approaches with emphasis on design of experiments applied to chemical processes*, Article ID: 157-169.

Bahuguna, A., Singh, S., Bahuguna, A., Sharma, S. and Dadarwal, B. K. 2021. Physical method of Wastewater treatment-A review. *J. Res. Environ. Earth Sci*, 7: 2348-2532.

Bazhin, N. M. (2015). "Gibbs energy role in fresh and salt water mixing." Desalination 365: 343-346.

Belmer, N., Tippler, C., Davies, P. J. and Wright, I. A. 2014. Impact of a coal mine waste discharge on water quality and aquatic ecosystems in the Blue Mountains World Heritage Area. In: Proceedings of *Proceedings of the 7th Australian Stream Management Conference, Townsville, Queensland*. 385-391.

Benjamin, M. M. and Lawler, D. F. 2013. *Water quality engineering: physical/chemical treatment processes*. John Wiley & Sons.

Benneker, A. M., Rijnaarts, T., Lammertink, R. G. and Wood, J. A. 2018. Effect of temperature gradients in (reverse) electrodialysis in the Ohmic regime. *Journal of membrane science*, 548: 421-428.

Besha, A. T., Tsehaye, M. T., Aili, D., Zhang, W. and Tufa, R. A. 2019. Design of monovalent ion selective membranes for reducing the impacts of multivalent ions in reverse electrodialysis. *Membranes*, 10 (1): 7.

Bezerra, M. A., Santelli, R. E., Oliveira, E. P., Villar, L. S. and Escaleira, L. A. 2008. Response surface methodology (RSM) as a tool for optimization in analytical chemistry. *Talanta*, 76 (5): 965-977.

Brauns, E. 2009. Salinity gradient power by reverse electrodialysis: effect of model parameters on electrical power output. *Desalination*, 237 (1-3): 378-391.

Broggi, M. L. 2013. Water desalination and purification using sustainable energy technologies. Article IDThe University of Tennessee at Chattanooga.

Brover, S., Lester, Y., Brenner, A. and Sahar-Hadar, E. 2022. Optimization of ultrafiltration as pre-treatment for seawater RO desalination. *Desalination*, 524: 115478.

Bruce, P. G., Hardgrave, M. T. and Vincent, C. A. 1992. The determination of transference numbers in solid polymer electrolytes using the Hittorf method. *Solid State Ionics*, 53: 1087-1094.

Castillo, A. M., Sharpe, D. M., Ghalambor, C. K. and De León, L. F. 2018. Exploring the effects of salinization on trophic diversity in freshwater ecosystems: a quantitative review. *Hydrobiologia*, 807: 1-17.

Cerqueira, U. M. F. M., Bezerra, M. A., Ferreira, S. L. C., de Jesus Araújo, R., da Silva, B. N.

and Novaes, C. G. 2021. Doehlert design in the optimization of procedures aiming food analysis–a review. *Food Chemistry*, 364: 130429.

Chelladurai, S. J. S., Murugan, K., Ray, A. P., Upadhyaya, M., Narasimharaj, V. and Gnanasekaran, S. 2021. Optimization of process parameters using response surface methodology: A review. *Materials Today: Proceedings*, 37: 1301-1304.

Chen, Y., Li, H., Pang, W., Zhou, B., Li, T., Zhang, J. and Dong, B. 2021. Pilot Study on the Combination of Different Pre-Treatments with Nanofiltration for Efficiently Restraining Membrane Fouling While Providing High-Quality Drinking Water. *Membranes*, 11 (6): 380.

Cipollina, A., Micale, G., Tamburini, A., Tedesco, M., Gurreri, L., Veerman, J. and Grasman, S. 2016. Reverse electrodialysis: applications. In: *Sustainable energy from salinity gradients*. Elsevier, 135-180.

Cogho, V. 2012. Optimum Coal Mine: striving towards a'zero effluent'mine. *Journal of the Southern African Institute of Mining and Metallurgy*, 112 (2): 119-126.

Coman, G. and Bahrim, G. 2011. Optimization of xylanase production by Streptomyces sp. P12-137 using response surface methodology and central composite design. *Annals of microbiology*, 61: 773-779.

Cosgrove, W. J. and Loucks, D. P. 2015. Water management: Current and future challenges and research directions. *Water Resources Research*, 51 (6): 4823-4839.

Costa, A. R., de Pinho, M. N. and Elimelech, M. 2006. Mechanisms of colloidal natural organic matter fouling in ultrafiltration. *Journal of Membrane Science*, 281 (1-2): 716-725.

Crini, G. and Lichtfouse, E. 2018. Wastewater treatment: an overview. *Green adsorbents for pollutant removal: fundamentals and design*, Article ID: 1-21.

Cui, W.-Z., Ji, Z.-Y., Tumba, K., Zhang, Z.-D., Wang, J., Zhang, Z.-X., Liu, J., Zhao, Y.-Y. and Yuan, J.-S. 2022. Response of salinity gradient power generation to inflow mode and temperature difference by reverse electrodialysis. *Journal of Environmental Management*, 303: 114124.

Curto, D., Franzitta, V. and Guercio, A. 2021. A review of the water desalination technologies. *Applied Sciences*, 11 (2): 670.

D'Angelo, A., Tedesco, M., Cipollina, A., Galia, A., Micale, G. and Scialdone, O. 2017. Reverse electrodialysis performed at pilot plant scale: Evaluation of redox processes and simultaneous generation of electric energy and treatment of wastewater. *Water research*, 125: 123-131.

Danaeifar, M., Ocheje, O. M. and Mazlomi, M. A. 2023. Exploitation of renewable energy sources for water desalination using biological tools. *Environmental Science and Pollution Research*, 30 (12): 32193-32213.

Daniilidis, A., Vermaas, D. A., Herber, R. and Nijmeijer, K. 2014. Experimentally obtainable energy from mixing river water, seawater or brines with reverse electrodialysis. *Renewable energy*, 64: 123-131.

Danmaliki, G. I., Saleh, T. A. and Shamsuddeen, A. A. 2017. Response surface methodology optimization of adsorptive desulfurization on nickel/activated carbon. *Chemical Engineering Journal*, 313: 993-1003.

Darre, N. C. and Toor, G. S. 2018. Desalination of water: a review. *Current Pollution Reports*, 4: 104-111.

de Pinho, M. N. and Minhalma, M. 2019. Introduction in membrane technologies. In: *Separation of Functional Molecules in Food by Membrane Technology*. Elsevier, 1-29.

Del Castillo, E. 2007. *Process optimization: a statistical approach*. Springer Science & Business Media.

Dickhout, J. M., Moreno, J., Biesheuvel, P., Boels, L., Lammertink, R. and De Vos, W. 2017. Produced water treatment by membranes: A review from a colloidal perspective. *Journal of colloid and interface science*, 487: 523-534.

Długołęcki, P., Dąbrowska, J., Nijmeijer, K. and Wessling, M. 2010. Ion conductive spacers for increased power generation in reverse electrodialysis. *Journal of Membrane Science*, 347 (1-2): 101-107.

Do Thi, H. T., Pasztor, T., Fozer, D., Manenti, F. and Toth, A. J. 2021. Comparison of desalination technologies using renewable energy sources with life cycle, PESTLE, and multi-criteria decision analyses. *Water*, 13 (21): 3023.

Dolan, S. L. and Heath, G. A. 2012. Life cycle greenhouse gas emissions of utility-scale wind power: systematic review and harmonization. *Journal of Industrial Ecology*, 16: S136-S154.

Drioli, E. and Giorno, L. 2018. *Encyclopedia of membranes*. Springer.

Du Plessis, A. and du Plessis, A. 2019. Current and future water scarcity and stress. *Water as an inescapable risk: current global water availability, quality and risks with a specific focus on South Africa*, Article ID: 13-25.

Du, X., Zhi, X., Li, B., Wang, Z., Luo, Y. and Qu, F. 2023. Boron doped diamond electro-oxidation coupled with ultrafiltration for Microcystis aeruginosa and Microcystins removal in offshore environment: The significance of in-situ generation of chloramine and membrane fouling mitigation. *Separation and Purification Technology*, 306: 122579.

El-Ghonemy, A. 2018. Performance test of a sea water multi-stage flash distillation plant: Case study. *Alexandria engineering journal*, 57 (4): 2401-2413.

Elsaid, K., Sayed, E. T., Abdelkareem, M. A., Mahmoud, M. S., Ramadan, M. and Olabi, A. 2020. Environmental impact of emerging desalination technologies: A preliminary evaluation. *Journal of Environmental Chemical Engineering*, 8 (5): 104099.

Emami, Y., Mehrangiz, S., Etemadi, A., Mostafazadeh, A. and Darvishi, S. 2013. A brief review about salinity gradient energy. *Int. J. Smart Grid Clean Energy*, 2 (2): 295-300.

Ezugbe, E. O. (2021). Desalination of a local oil refinery effluent to meet discharge limits.

Farquharson, D., Jaramillo, P., Schivley, G., Klima, K., Carlson, D. and Samaras, C. 2017. Beyond global warming potential: a comparative application of climate impact metrics for the life cycle assessment of coal and natural gas based electricity. *Journal of Industrial Ecology*, 21 (4): 857-873.

Feria-Díaz, J. J., López-Méndez, M. C., Rodríguez-Miranda, J. P., Sandoval-Herazo, L. C. and Correa-Mahecha, F. 2021. Commercial thermal technologies for desalination of water from renewable energies: A state of the art review. *Processes*, 9 (2): 262.

Fontananova, E., Zhang, W., Nicotera, I., Simari, C., van Baak, W., Di Profio, G., Curcio, E. and Drioli, E. 2014. Probing membrane and interface properties in concentrated electrolyte solutions. *Journal of Membrane Science*, 459: 177-189.

G'ofurovich, H. O., Abdurashidovich, U. A., O'g'li, I. J. R. And Ravshanovich, S. F. 2020. Prospects for the industrial use of coal in the world and its process of reproducing. *Prospects*, 6 (5).

Gao, H., Li, J., Fu, R., Wang, L., Wang, H., Pan, T. and Kong, X. 2023. The effect of flow modes on the capture of the energy between concentrated brine and seawater by reverse electrodialysis. *Energy Conversion and Management*, 292: 117357.

Garlapati, V. K. and Roy, L. 2017. Utilization of response surface methodology for modeling and optimization of tablet compression process. Article ID.

Gebreeyessus, G. D. 2019. Status of hybrid membrane–ion-exchange systems for desalination: a comprehensive review. *Applied Water Science*, 9 (5): 135.

Geise, G. M., Cassady, H. J., Paul, D. R., Logan, B. E. and Hickner, M. A. 2014. Specific ion effects on membrane potential and the permselectivity of ion exchange membranes. *Physical Chemistry Chemical Physics*, 16 (39): 21673-21681.

Ghafari, S., Aziz, H. A., Isa, M. H. and Zinatizadeh, A. A. 2009. Application of response surface methodology (RSM) to optimize coagulation–flocculation treatment of leachate using poly-aluminum chloride (PAC) and alum. *Journal of hazardous materials*, 163 (2-3): 650-656.

Goh, P. and Ismail, A. 2018. Flat-sheet membrane for power generation and desalination based on salinity gradient. In: *Membrane-Based Salinity Gradient Processes for Water Treatment and Power Generation*. Elsevier, 155-174.

Gombert, P., Sracek, O., Koukouzas, N., Gzyl, G., Valladares, S. T., Fraczek, R., Klinger, C., Bauerek, A., Areces, J. E. A. and Chamberlain, S. 2019. An overview of priority pollutants in selected coal mine discharges in Europe. *Mine Water and the Environment*, 38 (1): 16-23.

Gómez-Coma, L., Ortiz-Martínez, V. M., Carmona, J., Palacio, L., Prádanos, P., Fallanza, M., Ortiz, A., Ibañez, R. and Ortiz, I. 2019. Modeling the influence of divalent ions on membrane resistance and electric power in reverse electrodialysis. *Journal of Membrane Science*, 592: 117385.

Gude, V. G. 2017. Desalination and water reuse to address global water scarcity. *Reviews in Environmental Science and Bio/Technology*, 16 (4): 591-609.

Guler, E. and Nijmeijer, K. 2018. Reverse electrodialysis for salinity gradient power generation: Challenges and future perspectives. *Journal of Membrane Science and Research*, 4 (3): 108-110.

Guo, W., Ngo, H.-H. and Li, J. 2012. A mini-review on membrane fouling. *Bioresource technology*, 122: 27-34.

Guo, Z.-Y., Ji, Z.-Y., Zhang, Y.-G., Yang, F.-J., Liu, J., Zhao, Y.-Y. and Yuan, J.-S. 2018. Effect of ions (K+, Mg2+, Ca2+ and SO42−) and temperature on energy generation performance of reverse electrodialysis stack. *Electrochimica Acta*, 290: 282-290.

Gupta, V. K., Ali, I., Saleh, T. A., Nayak, A. and Agarwal, S. 2012. Chemical treatment technologies for waste-water recycling—an overview. *Rsc Advances*, 2 (16): 6380-6388.

Gurreri, L., Battaglia, G., Tamburini, A., Cipollina, A., Micale, G. and Ciofalo, M. 2017. Multi-physical modelling of reverse electrodialysis. *Desalination*, 423: 52-64.

Gurreri, L., Tamburini, A., Cipollina, A., Micale, G. and Ciofalo, M. 2014. CFD prediction of concentration polarization phenomena in spacer-filled channels for reverse electrodialysis. *Journal of membrane science*, 468: 133-148.

Halkos, G. and Zisiadou, A. 2023. Energy Crisis Risk Mitigation through Nuclear Power and RES as Alternative Solutions towards Self-Sufficiency. *Journal of Risk and Financial Management*, 16 (1): 45.

Hamanaka, A., Su, F.-q., Itakura, K.-i., Takahashi, K., Kodama, J.-i. and Deguchi, G. 2021. Experimental study on evaluation of underground coal gasification with a horizontal hole using two different coals. *Fuel*, 305: 121556.

Hamed, O. A. 2020. Thermal Desalination: Performance and Challenges. *Corrosion and Fouling Control in Desalination Industry*, Article ID: 29-47.

Hancox, P. J. and Götz, A. E. 2014. South Africa's coalfields—A 2014 perspective. *International Journal of Coal Geology*, 132: 170-254.

Hareesh, K. 2015. Water Quality Analysis in Coal Washeries. Article ID.

Härtel, A., Janssen, M., Samin, S. and van Roij, R. 2015. Fundamental measure theory for the electric double layer: implications for blue-energy harvesting and water desalination. *Journal of Physics: Condensed Matter*, 27 (19): 194129.

He, L., Xia, Y., Li, C., Jiang, A., Zhao, Y. and Xie, F. 2022. Simulation and Operational Optimization of RO Based Desalination for Coal-Fired Power Plants' Wastewater. *Membranes*, 12 (5): 478.

Helfer, F. and Lemckert, C. 2015. The power of salinity gradients: An Australian example. *Renewable and Sustainable Energy Reviews*, 50: 1-16.

Hiew, B. Y. Z., Lee, L. Y., Lai, K. C., Gan, S., Thangalazhy-Gopakumar, S., Pan, G.-T. and Yang, T. C.-K. 2019. Adsorptive decontamination of diclofenac by three-dimensional graphene-based adsorbent: response surface methodology, adsorption equilibrium, kinetic and thermodynamic studies. *Environmental research*, 168: 241-253.

Hong, J. G., Zhang, B., Glabman, S., Uzal, N., Dou, X., Zhang, H., Wei, X. and Chen, Y. 2015. Potential ion exchange membranes and system performance in reverse electrodialysis for power generation: A review. *Journal of Membrane Science*, 486: 71-88.

Hossain, M. Z. 2015. Water: The most precious resource of our life. *Global Journal of Advanced Research*, 2 (9): 1-11.

Iakovleva, E. and Sillanpää, M. 2013. The use of low-cost adsorbents for wastewater purification in mining industries. *Environmental Science and Pollution Research*, 20: 7878-7899.

Ighose, B. O., Adeleke, I. A., Damos, M., Junaid, H. A., Okpalaeke, K. E. and Betiku, E. 2017. Optimization of biodiesel production from Thevetia peruviana seed oil by adaptive neuro-fuzzy inference system coupled with genetic algorithm and response surface methodology. *Energy conversion and Management*, 132: 231-240.

Iglesias, M. C.-A. 2020. A review of recent advances and future challenges in freshwater salinization. *Limnetica*, 39 (1): 185-211.

Ismail, F., Khulbe, K. C. and Matsuura, T. 2018. *Reverse osmosis*. Elsevier.

Jaberi, M. and Ghassemi, A. 2015. Optimization of Electrode Design For Electrodialysis Reversal. *Desalination & Water Purification Research and Development Program*, Article ID.

Jagur-Grodzinski, J. and Kramer, R. 1986. Novel process for direct conversion of free energy of mixing into electric power. *Industrial & Engineering Chemistry Process Design and Development*, 25 (2): 443-449.

Januddi, M. A.-F. M. S., Zulkifli, I. S. and Yajid, M. A. M. 2023. Experimental Investigation and Optimization of Process Parameters of As-Sprayed Aerogel-Soda Lime Glass/NiCoCrAlYTa Coating with Historical Data Design Response Surface Methodology (RSM). In.

Jhariya, D., Khan, R. and Thakur, G. 2016. Impact of mining activity on water resource: an overview study. *Proceedings of the Recent Practices and Innovations in Mining Industry, Raipur, India*, Article ID: 19-20.

Jia, Z., Wang, B., Song, S. and Fan, Y. 2014. Blue energy: Current technologies for sustainable power generation from water salinity gradient. *Renewable and Sustainable Energy Reviews*, 31: 91-100.

Jones, A. and Finley, W. 2003. Recent development in salinity gradient power. *Oceans 2003. Celebrating the Past... Teaming Toward the Future (IEEE Cat. No. 03CH37492)*, 4: 2284-2287.

Joo, S. H. and Tansel, B. 2015. Novel technologies for reverse osmosis concentrate treatment: A review. *Journal of Environmental Management*, 150: 322-335.

Ju, J., Choi, Y., Lee, S., Kim, H. and Jung, N. 2020. Effect of design and operating parameters on power generation in reverse electrodialysis (RED): experimental analysis and modeling. *Desalination And Water Treatment*, 191: 29-39.

Kamal, Q. A. 2012. Energy crisis management. *New Horizons*, 6 (1): 26.

Kamble, P. P., Suryawanshi, S. S., Jadhav, J. P. and Attar, Y. C. 2019. Enhanced inulinase production by Fusarium solani JALPK from invasive weed using response surface methodology. *Journal of microbiological methods*, 159: 99-111.

Kamcev, J., Sujanani, R., Jang, E.-S., Yan, N., Moe, N., Paul, D. R. and Freeman, B. D. 2018. Salt concentration dependence of ionic conductivity in ion exchange membranes. *Journal of Membrane Science*, 547: 123-133.

Kang, K. C., Linga, P., Park, K.-n., Choi, S.-J. and Lee, J. D. 2014. Seawater desalination by gas hydrate process and removal characteristics of dissolved ions (Na+, K+, Mg2+, Ca2+, B3+, Cl−, SO42−). *Desalination*, 353: 84-90.

Karagiannis, I. C. and Soldatos, P. G. 2008. Water desalination cost literature: review and assessment. *Desalination*, 223 (1-3): 448-456.

Karimi, L. and Ghassemi, A. 2016. Effects of operating conditions on ion removal from brackish water using a pilot-scale electrodialysis reversal system. *Desalination and Water Treatment*, 57 (19): 8657-8669.

Kaushal, S. S., Likens, G. E., Pace, M. L., Haq, S., Wood, K. L., Galella, J. G., Morel, C., Doody, T. R., Wessel, B. and Kortelainen, P. 2019. Novel ‘chemical cocktails' in inland waters are a consequence of the freshwater salinization syndrome. *Philosophical Transactions of the Royal Society B*, 374 (1764): 20180017.

Kaushal, S. S., Likens, G. E., Pace, M. L., Reimer, J. E., Maas, C. M., Galella, J. G., Utz, R. M., Duan, S., Kryger, J. R. and Yaculak, A. M. 2021. Freshwater salinization syndrome: From emerging global problem to managing risks. *Biogeochemistry*, 154: 255-292.

Kazemian, A., Khatibi, M. and Ma, T. 2021. Performance prediction and optimization of a photovoltaic thermal system integrated with phase change material using response surface method. *Journal of Cleaner Production*, 290: 125748.

Kelly, A. E., Ou, H. D., Withers, R. and Dötsch, V. 2002. Low-conductivity buffers for high-sensitivity NMR measurements. *Journal of the American Chemical Society*, 124 (40): 12013-12019.

Kesari, K. K., Verma, H. N. and Behari, J. 2011. Physical methods in wastewater treatment. *International Journal of Environmental Technology and Management*, 14 (1-4): 43-66.

Khan, Q., Maraqa, M. A. and Mohamed, A.-M. O. 2021. Inland desalination: Techniques, brine management, and environmental concerns. *Pollution Assessment for Sustainable Practices in Applied Sciences and Engineering*, Article ID: 871-918.

Khennas, S. 2012. Understanding the political economy and key drivers of energy access in addressing national energy access priorities and policies: African Perspective. *Energy Policy*, 47: 21-26.

Kim, H.-K., Lee, M.-S., Lee, S.-Y., Choi, Y.-W., Jeong, N.-J. and Kim, C.-S. 2015. High power density of reverse electrodialysis with pore-filling ion exchange membranes and a high-open-area spacer. *Journal of Materials Chemistry A*, 3 (31): 16302-16306.

Kim, H., Kim, J., Cho, J. and Hong, J. 2003. Optimization and characterization of UV-curable adhesives for optical communications by response surface methodology. *Polymer Testing*, 22 (8): 899-906.

Kim, Y., Elimelech, M., Shon, H. K. and Hong, S. 2014. Combined organic and colloidal fouling in forward osmosis: Fouling reversibility and the role of applied pressure. *Journal of Membrane Science*, 460: 206-212.

Kingsbury, R. and Coronell, O. 2021. Modeling and validation of concentration dependence of ion exchange membrane permselectivity: Significance of convection and Manning's counter-ion condensation theory. *Journal of Membrane Science*, 620: 118411.

Koh, L. L. A., Nguyen, H. T. H., Chandrapala, J., Zisu, B., Ashokkumar, M. and Kentish, S. E. 2014. The use of ultrasonic feed pre-treatment to reduce membrane fouling in whey ultrafiltration. *Journal of membrane science*, 453: 230-239.

Konovšek, D., Nadvežnik, J. and Medved, M. 2017. An overview of world history of underground coal gasification. In: Proceedings of *AIP Conference Proceedings*. AIP Publishing,

Kotelo, L. O. 2013. Characterising the acid mine drainage potential of fine coal wastes. Article IDUniversity of Cape Town.

Křivčík, J., Neděla, D., Hadrava, J. and Brožová, L. 2015. Increasing selectivity of a heterogeneous ion-exchange membrane. *Desalination and Water Treatment*, 56 (12): 3160-3166.

Kucera, J. 2023. *Reverse osmosis*. John Wiley & Sons.

Kurz, T., Donaghue, N., Rapley, M. and Walker, I. 2005. The ways that people talk about natural resources: Discursive strategies as barriers to environmentally sustainable practices. *British journal of social psychology*, 44 (4): 603-620.

Larchet, C., Dammak, L., Auclair, B., Parchikov, S. and Nikonenko, V. 2004. A simplified procedure for ion-exchange membrane characterisation. *New Journal of Chemistry*, 28 (10): 1260-1267.

Lebepe, C. 2022. Investigation of environmental impacts of disposing coal slurry and discard in mined out pits with the focus on groundwater pollution. Article ID.

Li, C., Sun, W., Lu, Z., Ao, X. and Li, S. 2020. Ceramic nanocomposite membranes and membrane fouling: A review. *Water Research*, 175: 115674.

Li, X., Jin, X., Zhao, N., Angelidaki, I. and Zhang, Y. 2017. Novel bio-electro-Fenton technology for azo dye wastewater treatment using microbial reverse-electrodialysis electrolysis cell. *Bioresource technology*, 228: 322-329.

Lin, H., Peng, W., Zhang, M., Chen, J., Hong, H. and Zhang, Y. 2013. A review on anaerobic membrane bioreactors: applications, membrane fouling and future perspectives. *Desalination*, 314: 169-188.

Lin, T., Shen, B., Chen, W. and Zhang, X. 2014. Interaction mechanisms associated with organic colloid fouling of ultrafiltration membrane in a drinking water treatment system. *Desalination*, 332 (1): 100-108.

Liu, L., Luo, X.-B., Ding, L. and Luo, S.-L. 2019. Application of nanotechnology in the removal of heavy metal from water. In: *Nanomaterials for the removal of pollutants and resource reutilization*. Elsevier, 83-147.

Liu, Y., Zhang, J., Pang, Z. and Wu, W. 2018. Investigation into the influence of laser energy input on selective laser melted thin-walled parts by response surface method. *Optics and Lasers in Engineering*, 103: 34-45.

Luo, T., Abdu, S. and Wessling, M. 2018. Selectivity of ion exchange membranes: A review. *Journal of membrane science*, 555: 429-454.

Mabiletsa, M. and du Plessis, W. 2001. The impact of environmental legislation on mining in South Africa. *South African Journal of Environmental Law and Policy*, 8 (2): 185-213.

Mabrouk, A. N. and Fath, H. E. 2015. Technoeconomic study of a novel integrated thermal MSF–MED desalination technology. *Desalination*, 371: 115-125.

Madondo, N. I. 2017. Optimization of anaerobic co-digestion of sewage sludge using bio-chemical substrates. Article IDDurban University of Technology.

Madzivire, G. 2009. Removal of sulphates from South African mine water using coal fly ash. Article IDUniversity of the Western Cape.

Mahlase, B. 2021. The use of constructed wetlands to ameliorate discharge water from coal mines in the Witbank Coalfield. Article ID.

Maiti, D., Ansari, I., Rather, M. A. and Deepa, A. 2019. Comprehensive review on wastewater discharged from the coal-related industries–characteristics and treatment strategies. *Water Science and Technology*, 79 (11): 2023-2035.

Majdi, H., Esfahani, J. A. and Mohebbi, M. 2019. Optimization of convective drying by response surface methodology. *Computers and electronics in Agriculture*, 156: 574-584.

Manmai, N., Unpaprom, Y. and Ramaraj, R. 2021. Bioethanol production from sunflower stalk: application of chemical and biological pretreatments by response surface methodology (RSM). *Biomass Conversion and Biorefinery*, 11: 1759-1773.

Marais, E. A., Silvern, R. F., Vodonos, A., Dupin, E., Bockarie, A. S., Mickley, L. J. and Schwartz, J. 2019. Air quality and health impact of future fossil fuel use for electricity generation and transport in Africa. *Environmental science & technology*, 53 (22): 13524-13534.

McCleskey, R. B., Nordstrom, D. K. and Ryan, J. N. 2012. Comparison of electrical conductivity calculation methods for natural waters. *Limnology and Oceanography: Methods*, 10 (11): 952-967.

McGranahan, G. 2002. *Demand-side water strategies and the urban poor*. IIED.

Mehdizadeh, S., Kakihana, Y., Abo, T., Yuan, Q. and Higa, M. 2021. Power generation performance of a pilot-scale reverse electrodialysis using monovalent selective ion-exchange membranes. *Membranes*, 11 (1): 27.

Mehdizadeh, S., Yasukawa, M., Abo, T., Kuno, M., Noguchi, Y. and Higa, M. 2019a. The effect of feed solution temperature on the power output performance of a pilot-scale reverse electrodialysis (RED) system with different intermediate distance. *Membranes*, 9 (6): 73.

Mehdizadeh, S., Yasukawa, M., Kuno, M., Kawabata, Y. and Higa, M. 2019b. Evaluation of energy harvesting from discharged solutions in a salt production plant by reverse electrodialysis (RED). *Desalination*, 467: 95-102.

Mehdizadeh, S., Yasukawa, M., Suzuki, T. and Higa, M. 2020. Reverse electrodialysis for power generation using seawater/municipal wastewater: Effect of coagulation pretreatment. *Desalination*, 481: 114356.

Micari, M., Giacalone, F., Cipollina, A., Micale, G. and Tamburini, A. 2022. Reverse electrodialysis heat engine (REDHE). In: *Salinity Gradient Heat Engines*. Elsevier, 127-162.

Mishra, R. K. 2023. Fresh water availability and its global challenge. *British Journal of Multidisciplinary and Advanced Studies*, 4 (3): 1-78.

Moothi, K., Iyuke, S. E., Meyyappan, M. and Falcon, R. 2012. Coal as a carbon source for carbon nanotube synthesis. *Carbon*, 50 (8): 2679-2690.

Moreno, J., Díez, V., Saakes, M. and Nijmeijer, K. 2018. Mitigation of the effects of multivalent ion transport in reverse electrodialysis. *Journal of membrane science*, 550: 155-162.

Mtsweni, S. 2016. Performance of a horizontal roughing filtration system for the pretreatment of greywater. Article ID.

Nasrollahi, M., Motevali, A., Banakar, A. and Montazeri, M. 2023. Comparison of environmental impact on various desalination technologies. *Desalination*, 547: 116253.

Natarajan, U., Periyanan, P. and Yang, S. 2011. Multiple-response optimization for micro-endmilling process using response surface methodology. *The International Journal of Advanced Manufacturing Technology*, 56: 177-185.

Ng, H. Y. and Elimelech, M. 2004. Influence of colloidal fouling on rejection of trace organic contaminants by reverse osmosis. *Journal of membrane science*, 244 (1-2): 215-226.

Ning, R. Y. and Troyer, T. L. 2007. Colloidal fouling of RO membranes following MF/UF in the reclamation of municipal wastewater. *Desalination*, 208 (1-3): 232-237.

Noordin, M. Y., Venkatesh, V., Sharif, S., Elting, S. and Abdullah, A. 2004. Application of response surface methodology in describing the performance of coated carbide tools when turning AISI 1045 steel. *Journal of materials processing technology*, 145 (1): 46-58.

Noshad, M., Mohebbi, M., Shahidi, F. and Ali Mortazavi, S. 2012. Multi-objective optimization of osmotic–ultrasonic pretreatments and hot-air drying of quince using response surface methodology. *Food and Bioprocess Technology*, 5: 2098-2110.

Obotey Ezugbe, E. and Rathilal, S. 2020. Membrane technologies in wastewater treatment: a review. *Membranes*, 10 (5): 89.

Onu, M. A., Ayeleru, O. O., Oboirien, B. and Olubambi, P. A. 2023. Challenges of wastewater generation and management in sub-Saharan Africa: A Review. *Environmental Challenges*, Article ID: 100686.

Ortiz-Martínez, V. M., Gómez-Coma, L., Tristán, C., Pérez, G., Fallanza, M., Ortiz, A., Ibáñez, R. and Ortiz, I. 2020. A comprehensive study on the effects of operation variables on reverse electrodialysis performance. *Desalination*, 482: 114389.

Othman, N. H., Kabay, N. and Guler, E. 2022. Principles of reverse electrodialysis and development of integrated-based system for power generation and water treatment: A review. *Reviews in Chemical Engineering*, 38 (8): 921-958.

Palani, G., Arputhalatha, A., Kannan, K., Lakkaboyana, S. K., Hanafiah, M. M., Kumar, V. and Marella, R. K. 2021. Current trends in the application of nanomaterials for the removal of pollutants from industrial wastewater treatment—a review. *Molecules*, 26 (9): 2799.

Palit, S. 2020. Microfiltration, Ultrafiltration, and Other Membrane Separation Processes: A Critical Overview and a Vision for the Future. *Chemistry and Industrial Techniques for Chemical Engineers*, Article ID: 209-226.

Pan, L., Liu, P., Ma, L. and Li, Z. 2012. A supply chain based assessment of water issues in the coal industry in China. *Energy Policy*, 48: 93-102.

Pandey, S. R., Jegatheesan, V., Baskaran, K. and Shu, L. 2012. Fouling in reverse osmosis (RO) membrane in water recovery from secondary effluent: a review. *Reviews in Environmental Science and Bio/Technology*, 11: 125-145.

Papapetrou, M., Cipollina, A., La Commare, U., Micale, G., Zaragoza, G. and Kosmadakis, G. 2017. Assessment of methodologies and data used to calculate desalination costs. *Desalination*, 419: 8-19.

Pathak, H. 2020. Comparative Analysis of Desalination Technologies: A Review. *Journal of Indian Association for Environmental Management (JIAEM)*, 40 (3): 1-8.

Pintossi, D., Chen, C.-L., Saakes, M., Nijmeijer, K. and Borneman, Z. 2020. Influence of sulfate on anion exchange membranes in reverse electrodialysis. *NPJ Clean Water*, 3 (1): 29.

Polisi, M., Thopil, G. A. and Pouris, A. 2021. Quantification of the water footprint inventory in South African coal fuel cycle. *Journal of Cleaner Production*, 319: 128617.

Pondja, E. 2013. Treatment methods for water pollution from coal mining in Moatize (Mozambique). *TVVR 13/5008*, Article ID.

Prabudi, M., Nurtama, B. and Purnomo, E. H. 2018. Aplikasi response surface methodology (RSM) dengan historical data pada optimasi proses produksi burger. *Jurnal Mutu Pangan: Indonesian Journal of Food Quality*, 5 (2): 109-115.

Priya, A., Pachaiappan, R., Kumar, P. S., Jalil, A., Vo, D.-V. N. and Rajendran, S. 2021. The war using microbes: A sustainable approach for wastewater management. *Environmental Pollution*, 275: 116598.

Qasim, M., Badrelzaman, M., Darwish, N. N., Darwish, N. A. and Hilal, N. 2019. Reverse osmosis desalination: A state-of-the-art review. *Desalination*, 459: 59-104.

Rahman, M. M. 2023. Membranes for Osmotic Power Generation by Reverse Electrodialysis. *Membranes*, 13 (2): 164.

Raimi, M. O., Ayibatonbira, A. A., Anu, B., Odipe, O. E. and Deinkuro, N. S. 2019. 'Digging Deeper'Evidence on Water Crisis and Its Solution in Nigeria for Bayelsa State: A Study of Current Scenario. *Int J Hydro*, 3 (4): 244-257.

Ran, J., Wu, L., He, Y., Yang, Z., Wang, Y., Jiang, C., Ge, L., Bakangura, E. and Xu, T. 2017. Ion exchange membranes: New developments and applications. *Journal of Membrane Science*, 522: 267-291.

Rashed, M. N. 2013. Adsorption technique for the removal of organic pollutants from water and wastewater. *Organic pollutants-monitoring, risk and treatment*, 7: 167-194.

Reid, A. J., Carlson, A. K., Creed, I. F., Eliason, E. J., Gell, P. A., Johnson, P. T., Kidd, K. A., MacCormack, T. J., Olden, J. D. and Ormerod, S. J. 2019. Emerging threats and persistent conservation challenges for freshwater biodiversity. *Biological Reviews*, 94 (3): 849-873.

Renu, Agarwal, M. and Singh, K. 2017. Methodologies for removal of heavy metal ions from wastewater: an overview. *Interdisciplinary Environmental Review*, 18 (2): 124-142.

Rijnaarts, T., Huerta, E., van Baak, W. and Nijmeijer, K. 2017. Effect of divalent cations on RED performance and cation exchange membrane selection to enhance power densities. *Environmental science & technology*, 51 (21): 13028-13035.

Rodrigues, M. I. and Iemma, A. F. 2014. *Experimental design and process optimization*. Crc Press.

Ruppert Bulmer, E., Pela, K., Eberhard-Ruiz, A. and Montoya, J. 2021. Global perspective on coal jobs and managing labor transition out of coal. Article ID.

Sahu, O. and Chaudhari, P. 2013. Review on chemical treatment of industrial waste water. *Journal of Applied Sciences and Environmental Management*, 17 (2): 241-257.

SAICE. 2011. *SAICE Infrastructure Report Card for South Africa*: The South African Institution of Civil Engineering Midrand.

Sairinen, R., Tiainen, H. and Mononen, T. 2017. Talvivaara mine and water pollution: An analysis of mining conflict in Finland. *The Extractive Industries and Society*, 4 (3): 640-651.

Salahi, A., Noshadi, I., Badrnezhad, R., Kanjilal, B. and Mohammadi, T. 2013. Nano-porous membrane process for oily wastewater treatment: Optimization using response surface methodology. *Journal of Environmental Chemical Engineering*, 1 (3): 218-225.

Saleem, H., Abounahia, N. M., Siddiqui, H. R. and Zaidi, S. J. 2023. Qatar desalination research: An overview. *Desalination*, Article ID: 116802.

Samer, M. 2015. Biological and chemical wastewater treatment processes. *Wastewater treatment engineering*, 150: 212.

Sarp, S. and Hilal, N. 2018. *Membrane-based salinity gradient processes for water treatment and power generation*. Elsevier.

Sata, T. 2007. *Ion exchange membranes: preparation, characterization, modification and application*. Royal Society of chemistry.

Schulz, M., Soltani, A., Zheng, X. and Ernst, M. 2016. Effect of inorganic colloidal water constituents on combined low-pressure membrane fouling with natural organic matter (NOM). *Journal of Membrane Science*, 507: 154-164.

Schwarzenbach, R. P., Egli, T., Hofstetter, T. B., Von Gunten, U. and Wehrli, B. 2010. Global water pollution and human health. *Annual review of environment and resources*, 35: 109-136.

Shan, V., Singh, S. and Haritash, A. 2020. Water Crisis in the Asian countries: status and future trends. *Resilience, Response, and Risk in Water Systems: Shifting Management and Natural Forcings Paradigms*, Article ID: 173-194.

Shatat, M. and Riffat, S. B. 2014. Water desalination technologies utilizing conventional and renewable energy sources. *International Journal of Low-Carbon Technologies*, 9 (1): 1-19.

Sibiya, N. P., Amo-Duodu, G., Tetteh, E. K. and Rathilal, S. 2022. Model prediction of coagulation by magnetised rice starch for wastewater treatment using response surface methodology (RSM) with artificial neural network (ANN). *Scientific African*, 17: e01282.

Simões, C., Pintossi, D., Saakes, M. and Brilman, W. 2021. Optimizing multistage reverse electrodialysis for enhanced energy recovery from river water and seawater: Experimental and modeling investigation. *Advances in Applied Energy*, 2: 100023.

Simoes, C., Vital, B., Sleutels, T., Saakes, M. and Brilman, W. 2022. Scaled-up multistage reverse electrodialysis pilot study with natural waters. *Chemical Engineering Journal*, 450: 138412.

Simões, C. (2023). "Advances in reverse electrodialysis for renewable energy generation."

Singh, J., Yadav, P., Pal, A. K. and Mishra, V. 2020. Water pollutants: Origin and status. *Sensors in water pollutants monitoring: Role of material*, Article ID: 5-20.

Sivaiah, P. and Chakradhar, D. 2018. Analysis and modeling of cryogenic turning operation using response surface methodology. *Silicon*, 10: 2751-2768.

Skrzyniarz, M., Sajdak, M., Zajemska, M., Biniek-Poskart, A., Iwaszko, J. and Skibiński, A. 2023. Possibilities of RDF Pyrolysis Products Utilization in the Face of the Energy Crisis. *Energies*, 16 (18): 6695.

Smoot, G. 2022. What is the carbon footprint of hydropower energy? A life-cycle assessment. *impactful. ninja. https://impactful. ninja/the-carbon-footprint-of-hydropower/. Accessed*, 14.

Souri, M., Hoseinpour, V., Shakeri, A. and Ghaemi, N. 2018. Optimisation of green synthesis of MnO nanoparticles via utilising response surface methodology. *IET nanobiotechnology*, 12 (6): 822-827.

Srivastava, S. and Garg, R. 2017. Process parameter optimization of gas metal arc welding on IS: 2062 mild steel using response surface methodology. *Journal of Manufacturing Processes*, 25: 296-305.

Stages, L. C. 2012. Life cycle greenhouse gas emissions from solar photovoltaics. *J. Ind. Ecol*, Article ID.

Steyn, A. J. 2019. Geochemical investigation of union collery underground mine workings, Mpumalanga, South Africa. Article IDUniversity of the Free State.

Strathmann, H. 2004. *Ion-exchange membrane separation processes*. Elsevier.

Sukthomya, W. and Tannock, J. D. 2005. Taguchi experimental design for manufacturing process optimisation using historical data and a neural network process model. *International Journal of Quality & Reliability Management*, 22 (5): 485-502.

Suppes, R. and Heuss-Aßbichler, S. 2021. Resource potential of mine wastes: A conventional and sustainable perspective on a case study tailings mining project. *Journal of Cleaner Production*, 297: 126446.

Tanaka, Y. 2015. *Ion exchange membranes: fundamentals and applications*. Elsevier.

Tansel, B. 2012. Significance of thermodynamic and physical characteristics on permeation of ions during membrane separation: Hydrated radius, hydration free energy and viscous effects. *Separation and purification technology*, 86: 119-126.

Tedesco, M., Brauns, E., Cipollina, A., Micale, G., Modica, P., Russo, G. and Helsen, J. 2015a. Reverse electrodialysis with saline waters and concentrated brines: A laboratory investigation towards technology scale-up. *Journal of Membrane Science*, 492: 9-20.

Tedesco, M., Cipollina, A., Tamburini, A., Bogle, I. D. L. and Micale, G. 2015b. A simulation tool for analysis and design of reverse electrodialysis using concentrated brines. *Chemical Engineering Research and Design*, 93: 441-456.

Tedesco, M., Cipollina, A., Tamburini, A. and Micale, G. 2017. Towards 1 kW power production in a reverse electrodialysis pilot plant with saline waters and concentrated brines. *Journal of Membrane Science*, 522: 226-236.

Tedesco, M., Cipollina, A., Tamburini, A., van Baak, W. and Micale, G. 2012. Modelling the Reverse ElectroDialysis process with seawater and concentrated brines. *Desalination and Water Treatment*, 49 (1-3): 404-424.

Tedesco, M., Hamelers, H. and Biesheuvel, P. 2017. Nernst-Planck transport theory for (reverse) electrodialysis: II. Effect of water transport through ion-exchange membranes. *Journal of Membrane Science*, 531: 172-182.

Tedesco, M., Mazzola, P., Tamburini, A., Micale, G., Bogle, I. D. L., Papapetrou, M. and Cipollina, A. 2015c. Analysis and simulation of scale-up potentials in reverse electrodialysis. *Desalination and Water Treatment*, 55 (12): 3391-3403.

Tedesco, M., Scalici, C., Vaccari, D., Cipollina, A., Tamburini, A. and Micale, G. 2016. Performance of the first reverse electrodialysis pilot plant for power production from saline waters and concentrated brines. *Journal of Membrane Science*, 500: 33-45.

Tetteh, E. K., Obotey Ezugbe, E., Rathilal, S. and Asante-Sackey, D. 2020. Removal of COD and SO42− from oil refinery wastewater using a photo-catalytic system—comparing tio2 and zeolite efficiencies. *Water*, 12 (1): 214.

Thimmaraju, M., Sreepada, D., Babu, G. S., Dasari, B. K., Velpula, S. K. and Vallepu, N. 2018. Desalination of water. *Desalination and water treatment*, Article ID: 333-347.

Thiruvenkatachari, R., Younes, M. and Su, S. 2011. Coal mine site investigation of wastewater quality in Australia. *Desalination and Water Treatment*, 32 (1-3): 357-364.

Ting, M. B. and Byrne, R. 2020. Eskom and the rise of renewables: Regime-resistance, crisis and the strategy of incumbency in South Africa's electricity system. *Energy Research & Social Science*, 60: 101333.

Tong, X., Zhang, B. and Chen, Y. 2016. Fouling resistant nanocomposite cation exchange membrane with enhanced power generation for reverse electrodialysis. *Journal of Membrane Science*, 516: 162-171.

Tran, N. H., Chen, H., Reinhard, M., Mao, F. and Gin, K. Y.-H. 2016. Occurrence and removal of multiple classes of antibiotics and antimicrobial agents in biological wastewater treatment processes. *Water Research*, 104: 461-472.

Tristán, C., Fallanza, M., Ibáñez, R. and Ortiz, I. 2020a. Recovery of salinity gradient energy in desalination plants by reverse electrodialysis. *Desalination*, 496: 114699.

Tristán, C., Fallanza, M., Ibáñez, R. and Ortiz, I. 2020b. Reverse electrodialysis: Potential reduction in energy and emissions of desalination. *Applied Sciences*, 10 (20): 7317.

Tsalidis, G. A., Tourkodimitri, K. P., Mitko, K., Gzyl, G., Skalny, A., Posada, J. and Xevgenos, D. 2022. Assessing the environmental performance of a novel coal mine brine treatment technique: A case in Poland. *Journal of Cleaner Production*, 358: 131973.

Tufa, R. A., Pawlowski, S., Veerman, J., Bouzek, K., Fontananova, E., Di Profio, G., Velizarov, S., Crespo, J. G., Nijmeijer, K. and Curcio, E. 2018. Progress and prospects in

reverse electrodialysis for salinity gradient energy conversion and storage. *Applied energy*, 225: 290-331.

Tumba, K. Blue Energy from Southern African Water Bodies: State-of-the-art, Challenges and Opportunities. Article ID.

Ullah, I., Rasul, M. and Khan, M. 2013. An overview of solar thermal desalination technologies. In: Proceedings of *Proceedings of the 7th WSEAS International Conference on Renewable Energy Sources (RES'13), Kuala Lumpur, Malaysia*. 2-4.

Ullah, I. and Rasul, M. G. 2018. Recent developments in solar thermal desalination technologies: a review. *Energies*, 12 (1): 119.

Vanoppen, M., Van Vooren, T., Gutierrez, L., Roman, M., Croué, L. J., Verbeken, K., Philips, J. and Verliefde, A. 2019. Secondary treated domestic wastewater in reverse electrodialysis: What is the best pre-treatment? *Separation and Purification Technology*, 218: 25-42.

Vanysacker, L., Boerjan, B., Declerck, P. and Vankelecom, I. F. 2014. Biofouling ecology as a means to better understand membrane biofouling. *Applied microbiology and biotechnology*, 98: 8047-8072.

Vardhan, M. V., Sankaraiah, G., Yohan, M. and Rao, H. J. 2017. Optimization of Parameters in CNC milling of P20 steel using Response Surface methodology and Taguchi Method. *materials today: Proceedings*, 4 (8): 9163-9169.

Veerman, J. 2020. Reverse electrodialysis: Co-and counterflow optimization of multistage configurations for maximum energy efficiency. *Membranes*, 10 (9): 206.

Veerman, J., Saakes, M., Metz, S. J. and Harmsen, G. 2010. Reverse electrodialysis: evaluation of suitable electrode systems. *Journal of Applied Electrochemistry*, 40: 1461-1474.

Veerman, J. and D. Vermaas (2016). "Reverse electrodialysis: fundamentals." Sustainable energy from salinity gradients: 77-133.

Vermaas, D., Veerman, J., Yip, N., Elimelech, M., Saakes, M. and Nijmeijer, K. 2013a. ACS Sustainable Chem. *Eng*, 1: 1295-1302.

Vermaas, D. A. 2014. Energy generation from mixing salt water and fresh water: smart flow strategies for reverse electrodialysis. Article ID.

Vermaas, D. A., Veerman, J., Yip, N. Y., Elimelech, M., Saakes, M. and Nijmeijer, K. 2013b. High efficiency in energy generation from salinity gradients with reverse electrodialysis. *ACS sustainable chemistry & engineering*, 1 (10): 1295-1302.

Vijayan, K., Ranjithkumar, P. and Shanmugarajan, B. 2018. Comparison of response surface methodology and genetic algorithm in parameter optimization of laser welding process. *Applied Mathematics & Information Sciences*, 12 (1): 239-248.

Wagholikar, V. V., Zhuang, H., Moe, N. E., Barber, J., Ramanan, H. and Fuh, J. Y. 2020. Analysis of RED/dRED stack performance using a resistances in series model. *Desalination*, 496: 114505.

Wan, C. F. and Chung, T.-S. 2015. Osmotic power generation by pressure retarded osmosis using seawater brine as the draw solution and wastewater retentate as the feed. *Journal of Membrane Science*, 479: 148-158.

Wang, J., Wang, R., Zhu, Y. and Li, J. 2018. Life cycle assessment and environmental cost accounting of coal-fired power generation in China. *Energy Policy*, 115: 374-384.

Watson, V. J., Hatzell, M. and Logan, B. E. 2015. Hydrogen production from continuous flow, microbial reverse-electrodialysis electrolysis cells treating fermentation wastewater. *Bioresource technology*, 195: 51-56.

Weiner, A. M. and McGovern, R. K. 2015. A new reverse electrodialysis design strategy which significantly reduces the levelized cost of electricity. *Journal of Membrane Science*, 493: 605-614.

Wenten, I. G. 2016. Reverse osmosis applications: Prospect and challenges. *Desalination*, 391: 112-125.

Wick, G. L. 1978. Power from salinity gradients. *Energy*, 3 (1): 95-100.

Widyaningsih, T., Widjanarko, S., Waziiroh, E., Wijayanti, N. and Maslukhah, Y. 2018. Pilot plant scale extraction of black cincau (Mesona palustris BL) using historical-data response surface methodology. *International Food Research Journal*, 25 (2).

Wilson, S. T., Wang, H., Kabenge, M. and Qi, X. 2017. The mining sector of Liberia: Current practices and environmental challenges. *Environmental Science and Pollution Research*, 24: 18711-18720.

Wu, Y., Zhou, S., Qin, F., Ye, X. and Zheng, K. 2010. Modeling physical and oxidative removal properties of Fenton process for treatment of landfill leachate using response surface methodology (RSM). *Journal of hazardous materials*, 180 (1-3): 456-465.

Xiao, Y., De Araujo, C., Sze, C. C. and Stuckey, D. C. 2015. Toxicity measurement in biological wastewater treatment processes: a review. *Journal of Hazardous Materials*, 286: 15-29.

Yaro, N. S. A., Sutanto, M. H., Habib, N. Z., Napiah, M., Usman, A. and Muhammad, A. 2022. Comparison of Response Surface Methodology and Artificial Neural Network approach in predicting the performance and properties of palm oil clinker fine modified asphalt mixtures. *Construction and Building Materials*, 324: 126618.

Yip, N. Y., Vermaas, D. A., Nijmeijer, K. and Elimelech, M. 2014. Thermodynamic, energy efficiency, and power density analysis of reverse electrodialysis power generation with natural salinity gradients. *Environmental science & technology*, 48 (9): 4925-4936.

Zhang, B., Gao, H. and Chen, Y. 2015. Enhanced ionic conductivity and power generation using ion-exchange resin beads in a reverse-electrodialysis stack. *Environmental Science & Technology*, 49 (24): 14717-14724.

Zhang, S., Wang, H., He, X., Guo, S., Xia, Y., Zhou, Y., Liu, K. and Yang, S. 2020. Research progress, problems and prospects of mine water treatment technology and resource utilization in China. *Critical Reviews in Environmental Science and Technology*, 50 (4): 331-383.

Zhang, W., Zhou, Y., Hu, C. and Qu, J. 2021. Electricity generation from salinity gradient to remove chromium using reverse electrodialysis coupled with electrocoagulation. *Electrochimica Acta*, 379: 138153.

Zhang, X., Fan, L. and Roddick, F. A. 2015. Effect of feedwater pre-treatment using UV/H2O2 for mitigating the fouling of a ceramic MF membrane caused by soluble algal organic matter. *Journal of Membrane Science*, 493: 683-689.

Zhen, H., Xu-tao, Z. and Gui-qing, X. 2013. Product quality improvement through response surface methodology: A case study. In: Proceedings of *Diversity, Technology, and Innovation for Operational Competitiveness, Proceedings of the 2013 International Conference on Technology Innovation and Industrial Management, Phuket, Thailand*. 29-31.

Zheng, H. and Zheng, H. 2017. Solar desalination system combined with conventional technologies. *Solar Energy Desalination Technology*, Article ID: 537-622.

Zhou, Y., Zhao, K., Hu, C., Liu, H., Wang, Y. and Qu, J. 2018. Electrochemical oxidation of ammonia accompanied with electricity generation based on reverse electrodialysis. *Electrochimica Acta*, 269: 128-135.

Zoungrana, A. and Çakmakci, M. 2021. Optimization of the reverse electrodialysis power output through the ratio of the feed solutions salinity. *IET Renewable Power Generation*, 15 (4): 769-777.

Zulkefli, N. F., Alias, N. H., Jamaluddin, N. S., Abdullah, N., Abdul Manaf, S. F., Othman, N. H., Marpani, F., Mat-Shayuti, M. S. and Kusworo, T. D. 2021. Recent mitigation strategies on membrane fouling for oily wastewater treatment. *Membranes*, 12 (1): 26.

APPENDIX A-PROPERTIES

This appendix illustrates the properties of the ion exchange used in this study.

Table A- 1 Properties of the ion-exchange membranes.

Membrane	AEM	CEM	End membrane
Thickness (μm)	120	120	220
Ion exchange capacity (meq/g)	1.2	3	1.8
Resistance (Ω cm^2)	~ 1.8	~ 2.5	~ 4.5
Burst strength (kg cm^2)	4-5	4-5	15
Water content (wt%)	~ 14	~ 9	-
pH stability	0-9	0-11	1-13
Maximum temperature (°C)	60	50	50
Membrane type	Strong alkaline (ammonium)	Strongly acidic (sulfonic acid)	Strongly acidic (sulfonic acid)
Reinforcement	Polyester	Polyester	polyethylene

Note: The manufacturers provided all parameters.

APPENDIX B-SPECIFICATIONS

This appendix illustrates the general properties and specifications of the RED stack used in this study. The table used in the DOE sample of calculations is also included in this appendix.

Table B- 1: General properties and specifications of the RED stack used in the analysis.

Specification		**Value**
Effective membrane area (m^2)		0.0297
Membrane size (mm)		110×270
Processing length (mm)		80
Compartment width (mm)		160
Membrane spacing	Electrode-membrane (mm)	Ca.1
	Overcell (mm)	0.5
Spacer	Thickness (µm)	450
	Mesh orientation to flow direction	45º
	Porosity (%)	81
	Material	Silicon/polypropylene
Cell frame and tube material		Polypropylene
Pressure drops over cell		Max, 0.5 bar

Table B- 2: One-tailed/two tailed t-table

One-tailed / Two-tailed t-Table

Probability points of the t-distribution with df degrees of freedom

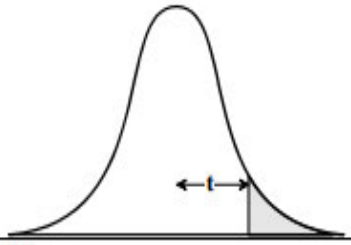

	tail area probability									
1-tail	**0.40**	**0.25**	**0.10**	**0.05**	**0.025**	**0.01**	**0.005**	**0.0025**	**0.001**	**0.0005**
2-tail	**0.80**	**0.50**	**0.20**	**0.10**	**0.050**	**0.02**	**0.010**	**0.0050**	**0.002**	**0.0010**
df=1	0.325	1.000	3.078	6.314	12.706	31.821	63.657	127.32	318.31	636.62
2	0.289	0.816	1.886	2.920	4.303	6.965	9.925	14.089	22.326	31.598
3	0.277	0.765	1.638	2.353	3.182	4.541	5.841	7.453	10.213	12.924
4	0.271	0.741	1.533	2.132	2.776	3.747	4.604	5.598	7.173	8.610
5	0.267	0.727	1.476	2.015	2.571	3.365	4.032	4.773	5.893	6.869
6	0.265	0.718	1.440	1.943	2.447	3.143	3.707	4.317	5.208	5.959
7	0.263	0.711	1.415	1.895	2.365	2.998	3.499	4.029	4.785	5.408
8	0.262	0.706	1.397	1.860	2.306	2.896	3.355	3.833	4.501	5.041
9	0.261	0.703	1.383	1.833	2.262	2.821	3.250	3.690	4.297	4.781
10	0.260	0.700	1.372	1.812	2.228	2.764	3.169	3.581	4.144	4.587
11	0.260	0.697	1.363	1.796	2.201	2.718	3.106	3.497	4.025	4.437
12	0.259	0.695	1.356	1.782	2.179	2.681	3.055	3.428	3.930	4.318
13	0.259	0.694	1.350	1.771	2.160	2.650	3.012	3.372	3.852	4.221
14	0.258	0.692	1.345	1.761	2.145	2.624	2.977	3.326	3.787	4.140
15	0.258	0.691	1.341	1.753	2.131	2.602	2.947	3.286	3.733	4.073
16	0.258	0.690	1.337	1.746	2.120	2.583	2.921	3.252	3.686	4.015
17	0.257	0.689	1.333	1.740	2.110	2.567	2.898	3.222	3.646	3.965
18	0.257	0.688	1.330	1.734	2.101	2.552	2.878	3.197	3.610	3.922
19	0.257	0.688	1.328	1.729	2.093	2.539	2.861	3.174	3.579	3.883
20	0.257	0.687	1.325	1.725	2.086	2.528	2.845	3.153	3.552	3.850
21	0.257	0.686	1.323	1.721	2.080	2.518	2.831	3.135	3.527	3.819
22	0.256	0.686	1.321	1.717	2.074	2.508	2.819	3.119	3.505	3.792
23	0.256	0.685	1.319	1.714	2.069	2.500	2.807	3.104	3.485	3.767
24	0.256	0.685	1.318	1.711	2.064	2.492	2.797	3.091	3.467	3.745
25	0.256	0.684	1.316	1.708	2.060	2.485	2.787	3.078	3.450	3.725
26	0.256	0.684	1.315	1.706	2.056	2.479	2.779	3.067	3.435	3.707
27	0.256	0.684	1.314	1.703	2.052	2.473	2.771	3.057	3.421	3.690
28	0.256	0.683	1.313	1.701	2.048	2.467	2.763	3.047	3.408	3.674
29	0.256	0.683	1.311	1.699	2.045	2.462	2.756	3.038	3.396	3.659
30	0.256	0.683	1.310	1.697	2.042	2.457	2.750	3.030	3.385	3.646
40	0.255	0.681	1.303	1.684	2.021	2.423	2.704	2.971	3.307	3.551
60	0.254	0.679	1.296	1.671	2.000	2.390	2.660	2.915	3.232	3.460
120	0.254	0.677	1.289	1.658	1.980	2.358	2.617	2.860	3.160	3.373
∞	0.253	0.674	1.282	1.645	1.960	2.326	2.576	2.807	3.090	3.291

Sourced from Handbook for experiment (2014)

Table B- 3: Percentage points of F-distribution

F-Table for 0.5%

Percentage points of the F-distribution:
upper 0.5% points

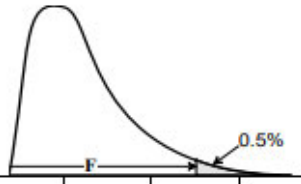

df_{num} / df_{den}	1	2	3	4	5	6	7	8	9	10	15	20
1	16210.7	19999.5	21614.7	22499.6	23055.8	23437.1	23714.6	23925.6	24091.0	24224.5	24630.2	24836.0
2	198.50	199.00	199.17	199.25	199.30	199.33	199.36	199.37	199.39	199.40	199.43	199.45
3	55.552	49.799	47.467	46.195	45.392	44.838	44.434	44.126	43.882	43.686	43.085	42.778
4	31.333	26.284	24.259	23.155	22.456	21.975	21.622	21.352	21.139	20.967	20.438	20.167
5	22.785	18.314	16.530	15.556	14.940	14.513	14.200	13.961	13.772	13.618	13.146	12.903
6	18.635	14.544	12.917	12.028	11.464	11.073	10.786	10.566	10.391	10.250	9.814	9.589
7	16.236	12.404	10.882	10.050	9.522	9.155	8.885	8.678	8.514	8.380	7.968	7.754
8	14.688	11.042	9.596	8.805	8.302	7.952	7.694	7.496	7.339	7.211	6.814	6.608
9	13.614	10.107	8.717	7.956	7.471	7.134	6.885	6.693	6.541	6.417	6.032	5.832
10	12.826	9.427	8.081	7.343	6.872	6.545	6.302	6.116	5.968	5.847	5.471	5.274
11	12.226	8.912	7.600	6.881	6.422	6.102	5.865	5.682	5.537	5.418	5.049	4.855
12	11.754	8.510	7.226	6.521	6.071	5.757	5.525	5.345	5.202	5.085	4.721	4.530
13	11.374	8.186	6.926	6.233	5.791	5.482	5.253	5.076	4.935	4.820	4.460	4.270
14	11.060	7.922	6.680	5.998	5.562	5.257	5.031	4.857	4.717	4.603	4.247	4.059
15	10.798	7.701	6.476	5.803	5.372	5.071	4.847	4.674	4.536	4.424	4.070	3.883
16	10.575	7.514	6.303	5.638	5.212	4.913	4.692	4.521	4.384	4.272	3.920	3.734
17	10.384	7.354	6.156	5.497	5.075	4.779	4.559	4.389	4.254	4.142	3.793	3.607
18	10.218	7.215	6.028	5.375	4.956	4.663	4.445	4.276	4.141	4.030	3.683	3.498
19	10.073	7.093	5.916	5.268	4.853	4.561	4.345	4.177	4.043	3.933	3.587	3.402
20	9.944	6.986	5.818	5.174	4.762	4.472	4.257	4.090	3.956	3.847	3.502	3.318
21	9.830	6.891	5.730	5.091	4.681	4.393	4.179	4.013	3.880	3.771	3.427	3.243
22	9.727	6.806	5.652	5.017	4.609	4.322	4.109	3.944	3.812	3.703	3.360	3.176
23	9.635	6.730	5.582	4.950	4.544	4.259	4.047	3.882	3.750	3.642	3.300	3.116
24	9.551	6.661	5.519	4.890	4.486	4.202	3.991	3.826	3.695	3.587	3.246	3.062
25	9.475	6.598	5.462	4.835	4.433	4.150	3.939	3.776	3.645	3.537	3.196	3.013
26	9.406	6.541	5.409	4.785	4.384	4.103	3.893	3.730	3.599	3.492	3.151	2.968
27	9.342	6.489	5.361	4.740	4.340	4.059	3.850	3.687	3.557	3.450	3.110	2.928
28	9.284	6.440	5.317	4.698	4.300	4.020	3.811	3.649	3.519	3.412	3.073	2.890
29	9.230	6.396	5.276	4.659	4.262	3.983	3.775	3.613	3.483	3.377	3.038	2.855
30	9.180	6.355	5.239	4.623	4.228	3.949	3.742	3.580	3.450	3.344	3.006	2.823
40	8.828	6.066	4.976	4.374	3.986	3.713	3.509	3.350	3.222	3.117	2.781	2.598
60	8.495	5.795	4.729	4.140	3.760	3.492	3.291	3.134	3.008	2.904	2.570	2.387
120	8.179	5.539	4.497	3.921	3.548	3.285	3.087	2.933	2.808	2.705	2.373	2.188
∞	7.880	5.299	4.280	3.715	3.350	3.091	2.897	2.745	2.621	2.519	2.187	2.000

Source from Handbook for experiment (2014)

Table B- 4: Reports results for salt removal percentage from DOE.

Run Order	Actual Value	Predicted Value	Residual	Leverage	Internally Studentized Residuals	Externally Studentized Residuals	Cook's Distance	Influence on Fitted Value DFFITS	Standard Order
1	13.76	14.21	-0.4501	0.639	-0.420	-0.404	0.045	-0.537	1
2	13.54	14.43	-0.8823	0.302	-0.592	-0.574	0.022	-0.378	2
3	13.12	14.51	-1.39	0.476	-1.077	-1.085	0.150	-1.034	3
4	14.18	14.17	0.0098	0.317	0.007	0.006	0.000	0.004	4
5	13.61	11.02	2.58	0.125	1.550	1.671	0.049	0.631	5
6	12.67	9.82	2.85	0.224	1.815	2.067	0.136	1.112	6
7	14.68	14.14	0.5454	0.639	0.509	0.491	0.065	0.653	7
8	5.54	7.62	-2.08	0.302	-1.398	-1.470	0.121	-0.967	8
9	3.94	5.13	-1.19	0.476	-0.918	-0.911	0.109	-0.868	9
10	18.18	17.11	1.07	0.639	1.000	1.000	0.252	1.329	10
11	17.87	17.55	0.3174	0.302	0.213	0.204	0.003	0.134	11
12	16.51	17.72	-1.21	0.476	-0.939	-0.934	0.114	-0.890	12
13	14.29	16.16	-1.88	0.317	-1.273	-1.315	0.108	-0.896	13
14	14.04	13.24	0.7977	0.125	0.478	0.461	0.005	0.174	14
15	12.85	12.12	0.7245	0.224	0.461	0.444	0.009	0.239	15
16	16.13	15.21	0.9199	0.639	0.858	0.847	0.186	1.127	16
17	7.39	8.93	-1.53	0.302	-1.030	-1.033	0.066	-0.679	17
18	7.31	6.52	0.7902	0.476	0.612	0.594	0.049	0.566	18

Table B- 5: Coefficients in Terms of Coded Factors for salt removal percentage

Factor	Coefficient Estimate	df	Standard Error	95% CI Low	95% CI High	VIF
Intercept	13.23	1	0.4350	12.27	14.19	
A-High Concentration	-2.64	1	0.5327	-3.81	-1.47	1.07
B-Flowrate	-1.94	1	0.4603	-2.95	-0.9254	1.0000
C-Temperature	1.07	1	0.4350	0.1094	2.02	1.07
AB	-2.15	1	0.5637	-3.39	-0.9062	1.07
AC	-0.4552	1	0.5147	-1.59	0.6775	1.0000
BC	0.0735	1	0.4603	-0.9395	1.09	1.07

Table B- 6: Reports results for power density from DOE.

Run Order	Actual Value	Predicted Value	Residual	Leverage	Internally Studentized Residuals	Externally Studentized Residuals	Cook's Distance	Influence on Fitted Value DFFITS	Standard Order
1	3.80	4.43	-0.6300	0.639	-1.757	-1.976	0.780	-2.627[(1)]	1
2	3.58	3.69	-0.1148	0.302	-0.230	-0.220	0.003	-0.145	2
3	3.45	3.41	0.0380	0.476	0.088	0.084	0.001	0.080	3
4	4.77	4.53	0.2362	0.317	0.479	0.462	0.015	0.315	4
5	4.49	3.46	1.03	0.125	1.840	2.109	0.069	0.797	5
6	3.21	3.06	0.1506	0.224	0.287	0.274	0.003	0.148	6
7	4.95	4.63	0.3170	0.639	0.884	0.875	0.197	1.163	7
8	2.60	3.24	-0.6346	0.302	-1.273	-1.315	0.100	-0.865	8
9	2.31	2.70	-0.3892	0.476	-0.901	-0.893	0.105	-0.851	9
10	8.49	7.85	0.6383	0.639	1.780	2.012	0.801	2.675[(1)]	10
11	5.66	5.89	-0.2260	0.302	-0.453	-0.436	0.013	-0.287	11
12	5.19	5.14	0.0464	0.476	0.108	0.103	0.002	0.098	12
13	9.27	9.40	-0.1339	0.317	-0.272	-0.260	0.005	-0.177	13
14	6.34	7.11	-0.7744	0.125	-1.388	-1.457	0.039	-0.551	14
15	6.23	6.24	-0.0091	0.224	-0.017	-0.017	0.000	-0.009	15
16	10.75	10.95	-0.1972	0.639	-0.550	-0.532	0.076	-0.707	16
17	8.23	8.33	-0.1094	0.302	-0.219	-0.210	0.003	-0.138	17
18	8.10	7.33	0.7653	0.476	1.772	1.999	0.407	1.905[(1)]	18

[(1)] Exceeds limits.

Table B- 7: Coefficients in Terms of Coded Factors for power density.

Factor	Coefficient Estimate	df	Standard Error	95% CI Low	95% CI High	VIF
Intercept	5.90	1	0.1455	5.57	6.22	
A-High Concentration	0.6146	1	0.1782	0.2224	1.01	1.07
B-Flowrate	-1.07	1	0.1540	-1.41	-0.7322	1.0000
C-Temperature	2.04	1	0.1455	1.72	2.36	1.07
AB	-0.2081	1	0.1886	-0.6232	0.2070	1.07
AC	0.7256	1	0.1722	0.3466	1.10	1.0000
BC	-0.3900	1	0.1540	-0.7289	-0.0511	1.07

APPENDIX C- SAMPLE OF CALCULATIONS

This appendix illustrates the procedures used to calculate the experimental salt removal percentage as well as power density acquired under different conditions.

C.1. Internal Leakage Calculation

High Compartments

$$Leakage\ \% = \left(\frac{V_{mL\ leakage}}{t*Q}\right)*100$$

$$= \left(\frac{0mL}{5min*896mL/mn}\right)*100$$

$$= 0$$

Low Compartments

$$Leakage\ \% = \left(\frac{V_{mL\ leakage}}{t*Q}\right)*100$$

$$= \left(\frac{2mL}{5min*896mL/mn}\right)*100$$

$$=< 0.1$$

C.2. Power Calculations

Based on ohms law: $P = VI$

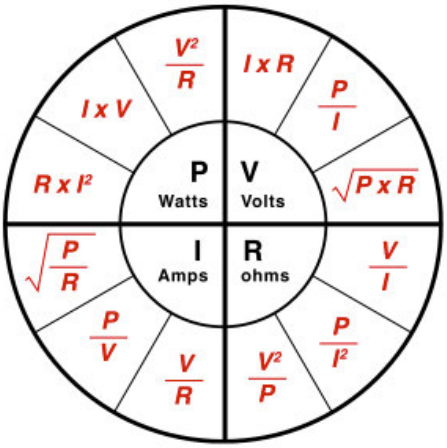

Figure C- 1 Ohm's Law power graph

$$P = \frac{V^2}{R}$$

$$= \frac{(1.063)^2}{10} = 0.11299W$$

C.3. Power density

$$P_d = \frac{P}{A}$$

$$= \frac{0.11299}{0.0297} = 3.80W/m^2$$

C.4. Salt removal percentage

$$R_{removal} = \left(\frac{Z_A - Z_B}{Z_A}\right) * 100$$

$$R_{removal} = \left(\frac{82.1 - 70.8}{82.1}\right) * 100 = 13.76\%$$

C.5. Current Calculation

$$I = \frac{V}{R}$$

$$= \frac{1.063}{10} = 0.01063A$$

C.6. Internal Resistance Calculation

$$\mathrm{R} = \frac{OCV - V}{I}$$

$$= \frac{4.102 - 1.063}{0.01063} = 28.5888\Omega$$

C.7. Power density per cell pair

$$P_d = \frac{P}{A}$$

$$P_d = \frac{0.112997}{0.0297 * 60} = 0.06343.80W/m^2$$

Table C- 1: Experimental results for 18 runs.

H Concentration (M)	Flowrate (mL/min)	Temperature (ºC	Voltage (V)	Resistance(Ω	OCV	Conductivity In	Conductivity Ou	Power (W)	% Salt Remova	Power density (W/m2)	Pd cell pair (W/m2)	Current (A)	Rinternal (Ω)
1	896	20	1.063	10	4.102	82.1	70.8	0.1129969	13.7637028	3.80	0.0634101571	0.1063000000	28.58889934
1	1369	20	1.031	10	4.112	82.7	71.5	0.1062961	13.54292624	3.58	0.0596498878	0.1031000000	29.88360815
1	1550	20	1.012	10	4.191	83.1	72.2	0.1024144	13.11672684	3.45	0.0574716049	0.1012000000	31.41304348
1.5	896	20	1.19	10	4.59	126.9	108.9	0.14161	14.18439716	4.77	0.0794668911	0.1190000000	28.57142857
1.5	1369	20	1.155	10	4.912	126.4	109.2	0.1334025	13.60759494	4.49	0.0748611111	0.1155000000	32.52813853
1.5	1550	20	0.976	10	4.991	127.1	111	0.0952576	12.66719119	3.21	0.0534554433	0.0976000000	41.13729508
2	896	20	1.212	10	4.613	141	120.3	0.1468944	14.68085106	4.95	0.0824323232	0.1212000000	28.06105611
2	1369	20	0.879	10	5.312	140.8	133	0.0772641	5.539772727	2.60	0.0433580808	0.0879000000	50.43230944
2	1550	20	0.829	10	5.645	142	136.4	0.0687241	3.943661972	2.31	0.0385657127	0.0829000000	58.09408926
1	896	40	1.588	10	4.441	80.3	65.7	0.2521744	18.18181818	8.49	0.1415120090	0.1588000000	17.96599496
1	1369	40	1.297	10	4.585	84.5	69.4	0.1682209	17.86982249	5.66	0.0944000561	0.1297000000	25.35080956
1	1550	40	1.241	10	4.596	84.8	70.8	0.1540081	16.50943396	5.19	0.0864242985	0.1241000000	27.03464948
1.5	896	40	1.659	10	4.251	126.7	108.6	0.2752281	14.28571429	9.27	0.1544489899	0.1659000000	15.6238698
1.5	1369	40	1.372	10	4.273	126.8	109	0.1882384	14.03785489	6.34	0.1056332211	0.1372000000	21.14431487
1.5	1550	40	1.36	10	4.321	126.1	109.9	0.18496	12.84694687	6.23	0.1037934905	0.1360000000	21.77205882
2	896	40	1.787	10	4.613	143.2	120.1	0.3193369	16.13128492	10.75	0.1792014029	0.1787000000	15.81421377
2	1369	40	1.563	10	4.628	142	131.5	0.2442969	7.394366197	8.23	0.1370914141	0.1563000000	19.60972489
2	1550	40	1.551	10	4.639	142.2	131.8	0.2405601	7.313642757	8.10	0.1349944444	0.1551000000	19.90973565

Table C- 2: Experimental results for NaCl run at optimum condition.

Monovalent ion	Amount	Voltage (V)	Resistance(Ω)	OCV	Conductivity In	Conductivity Out	Power (W)	% Salt Removal	Power density (W/m2)	Pd cell pair (W/m2)	Current (A)	Rinternal (Ω)
Soduim Chloride	100%	1,787	10	4,231	80	68,34	0,3193369	14,575	10,75208418	0,00016	0,18	13,68

Table C- 3: Experimental results for $CaCl_2$ runs at optimum condition.

Divalent ions	Amount	Voltage (V)	Resistance(Ω)	OCV	Conductivity In	Conductivity Out	Power (W)	% Salt Removal	Power density (W/m2)	Pd cell pair (W/m2)	Current (A)	Rinternal (Ω)
Calcuim Chloride	25%	0,981	10	3,044	180,8	172,4	0,0962361	4,646017699	3,240272727	0,00005	0,10	21,03
Calcuim Chloride	75%	0,543	10	2,012	203,3	198,1	0,0294849	2,55779636	0,992757576	0,00001	0,05	27,05

Table C- 4: Experimental results for Na_2SO_4 runs at optimum condition.

Divalent ions	Amount	Voltage (V)	Resistance(Ω)	OCV	Conductivity In	Conductivity Out	Power (W)	% Salt Removal	Power density (W/m2)	Pd cell pair (W/m2)	Current (A)	Rinternal (Ω)
Soduim sulphate	25%	1,4891	10	4,151	152,7	142,2	0,221741881	6,876227898	7,466056599	0,00011	0,15	17,88
Soduim sulphate	75%	0,978	10	3,056	182	174,4	0,0956484	4,175824176	3,220484848	0,00005	0,10	21,25

C.8. Permeate flux calculation.

$$J_w = \left(\frac{V_p}{A * t}\right)$$

$$J_w = \left(\frac{V_p}{A * t}\right)$$

$$Q = \left(\frac{V_p}{t}\right) = \left(\frac{2.248}{4.16}\right) = 0.54\ L/min$$

$$J_w = \left(\frac{0.54}{0.0297}\right) = 18.194 \frac{L}{m2.min}$$

Table C- 5: Effects of high concentration calculated results.

High concentration M NaCl	Power density (W/m^2)	Salt removal %	OCV	R internal	Mass (g)	Volume (L)	Time (min)	Area (m^2)	(L/min)	Permeate flux
1	3.80	13.76	4.10	28.59	2248	2.248	4.16	0.0297	0.54	18.2
1.5	4.77	14.18	4.59	28.57	2428	2.428	4.37	0.0297	0.56	18.7
2	4.95	14.68	4.61	28.06	2503	2.503	4.39	0.0297	0.57	19.2

Table C- 6: Effects of temperature calculated results.

Temp(ºC)	Power density (W/m^2)	Salt removal %	OCV	R internal	Mass (g)	Volume (L)	Time (min)	Area (m^2)	(L/min)	Permeate flux
20	4.95	14.68	4.613	28.06	2428	2.428	4.03	0.0297	0.60	20.3
30	7.84	15.29	4.625	16.80	2606	2.606	4.11	0.0297	0.63	21.3
40	10.75	16.13	4.629	15.81	2751	2.751	4.09	0.0297	0.67	22.6

Table C- 7: Effects of flowrate calculated results.

Flowrate (mL/min)	Power density (W/m^2)	Salt removal %	OCV	R internal	Mass (g)	Volume (L)	Time (min)	Area (m^2)	(L/min)	Permeate flux
896	4.95	14.68	4.61	28.61	2428	2.428	4	0.0297	0.607	20.44
1369	2.60	5.54	5.31	50.43	2851	2.851	3.41	0.0297	0.8360704	28.15
1550	2.31	3.94	5.65	58.09	3132	3.132	3.12	0.0297	1.0038462	33.80

C.9 Transformation calculation

This sample of calculations is based on Figure D-1, which is the transformation figure for salt removal percentage. The response values for salt removal range from 3.944 to 18.182%. The maximum response ($\hat{y}_{max}$) is 18.182%, whereas the minimum response ($\hat{y}_{min}$) is 3.944. The ratio of maximum to minimum response (T_R) is obtained by the following equation:

$$T_R = \frac{\hat{y}_{\max}}{\hat{y}_{\min}} = \frac{18.182}{3.944} = 4.61$$

This calculation sample is based on Table 5.4, the ANOVA table for salt removal percentage. The total sum of squares (SOS_T) is given by the following equation:

C.10 The ANOVA Table

$$SOS_T = \sum_{i=1}^{N_e} y_i^2 - \left[\frac{\sum_{i=1}^{N_e} y_i}{N_e}\right]^2 = y'y - \left[\frac{\sum_{i=1}^{N_e} y_i}{N_e}\right]^2$$

$$= 281.40$$

The following equation gives the error or residual sum of squares (SOSE):

$$SOS_E = y'y - \left[\frac{\sum_{i=1}^{N_e} y_i}{N_e}\right]^2 - \{\beta' X' y - \left[\frac{\sum_{i=1}^{N_e} y_i}{N_e}\right]^2\} \; y'y - \beta' X' y = \sum_{i=1}^{N_e} [y_i - \hat{y}_i]^2$$

$$= 34.96$$

The following equation calculates the regression or model sum of squares (SOS_R):

$$SOS_R = SOS_T - SOS_E$$

$$SOS_R = 281.40 - 34.96$$

$$SOS_R = 246.44$$

The lack-of-fit sum of squares (SOS_{LOF})

$$SOS_{LOF} = 0$$

The number of variables (n = 3) and the number of centre points is $C_p = 0$. The number of factorial points (nf) is given by the following equation:

$$n_f = 2n(n-1)$$

$$n_f = 2*3(3-1)$$

$$n_f = 12$$

The number of experimental points or observations (Ne) is given by:

$$N_e = n_f + C_p$$

$$N_e = 12$$

The degree of freedom for the numerator (d_{fr}) is:

$$d_{fR} = 6$$

The degree of freedom for the denominator (d_{fE}) is:

$$d_{fE} = 11$$

The mean square for regression (MS_R) is given by:

$$M_{SR} = \frac{SOS_R}{d_{fR}} = \frac{246.44}{6} = 41.0733$$

The mean square for error (MSR) is given by:

$$M_{SE} = \frac{SOS_E}{d_{fE}} = \frac{34.96}{11} = 3.18$$

The F-value for regression (F_R) is given by:

$$F_R = \frac{M_{SR}}{M_{SE}} = \frac{41.0733}{3.18} = 12.92$$

The DOE was measured at 95% confidence intervals, therefore:

1-α = 1-95 = 0.05 = 0.5%

Therefore, The F-value for regression (F_R) from the distribution table can give a critical value at the degree of freedom for the numerator and denominator of F_R (6,11). Then, the F-distribution calculator can obtain the P-value, as shown in the figure below.

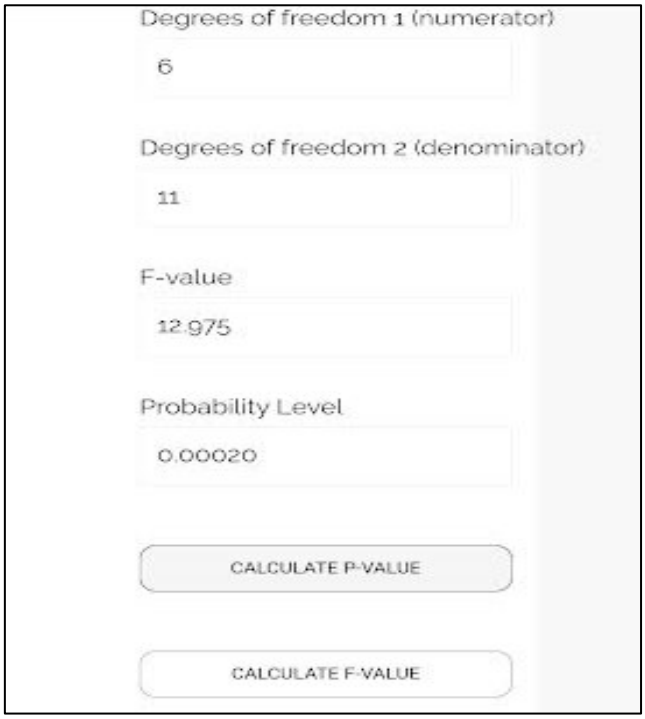

Figure C- 2 P-value calculator

C.11 The collection of summary statistics table

Also, based on the Table, sample calculation for salt removal percentage is presented. The standard deviation (SD)is given by:

$$SD = \sqrt{M_{SE}}$$

$$SD = \sqrt{3.18}$$

$$SD = 1.783$$

The mean (MN) is:

$$MN = \left[\frac{\sum_{i=1}^{N_e} y_i}{N_e} \right]$$

$$MN = \frac{13.7637+13.5429+13.1167+14.1844+13.6076+12.6672+14.6809+5.53977+3.94366+18.1818+17.8698+16.5094+14.2857+14.0379+12.8469+16.1313+7.39437+7.31364}{18}$$

$$MN = \frac{229.61764}{18} = 12.756$$

The coefficient of variance (CV%) is given by:

$$CV\% = \frac{SD}{MN} * 100$$

$$CV\% = \frac{1.783}{12.756} * 100$$

$$CV\% = 13.98$$

R-squared value is obtained by:

$$R^2 = 1 - \frac{SOS_E}{SOS_T}$$

$$R^2 = 1 - \frac{34.96}{281.40} = 0.8758$$

Adjusted R-squared value is obtained by:

$$\text{Adjusted } R^2 = 1 - \frac{\left(1 - R^2\right)\left(N - 1\right)}{N - n - 1}$$

$$\text{Adjusted } R^2 = 1 - \frac{(1 - 0.8758)(18 - 1)}{18 - 3 - 1} = 0.8$$

PRESS value as given by the software:

$$PRESS = \sum_{i=1}^{n} \left[y_i - \hat{y}_i\right]^2 = \sum_{i=1}^{n} \left[\frac{e_i}{1 - h_{i_i}}\right]^2 = 85.87$$

Predicted values R-squared value is obtained by:

$$\text{Predicted } R^2 = 1 - \frac{PRESS}{SOS_{\text{mod}el} + SOS_E}$$

$$\text{Predicted } R^2 = 1 - \frac{PRESS}{SOS_{Rl} + SOS_E}$$

$$\text{Predicted } R^2 = 1 - \frac{85.87}{246.44 + 34.96} = 0.6949$$

There are (6) coefficients in the model. Thus p = 6. The maximum response ($\hat{y}max$) is 18.182%, whereas the minimum response ($\hat{y}min$) is 3.944. adequate precision (AP) is given by:

$$AP = \frac{\hat{y}_{\max} - \hat{y}_{\min}}{\sqrt{p * MS_E / N_e}}$$

$$AP = \frac{18.182 - 3.944}{\sqrt{6 * 3.18/12}} = 11.3$$

The AP ratio was above 4.0, implying satisfactory discrimination.

C.12 The coefficient estimate table

This sample of calculations is based on Table C-8, the coefficient estimate table for

salt removal percentage. There are three process variables for this model, and the equation is as follows:

$$y_i = \beta_o + \beta_1 X_1 + \beta_2 X_2 + \beta_3 X_3 + \beta_4 X_1 X_2 + \beta_5 X_1 X_3 + \beta_6 X_2 X_3$$

Table C- 8: Coefficient estimates

SUBSCRIPT	SUBSCRIPT	COEFFICIENT ESTIMATES
X_1	high concentration (A)	
X_2	flow rate of the solution (B)	
X_3	temperature of the solution(C)	
β_0	coefficient estimate for the intercept,	13.23
β_1	coefficient estimate for high concentration (A),	-2.64
β_2	coefficient estimate for the flow rate of the solution (B)	-1.94
β_3	coefficient estimate for the temperature (C)	-1.07
β_4	coefficient estimates for AB.	-2.15
β_5	coefficient estimates for AC.	-0.4552
β_6	coefficient estimates for BC.	0.0735

C.13 Model equation in terms of coded factors

Salt removal percentages model in terms of coded factors is:

$$y_i = 13.23 - 2.64X_1 - 1.94X_2 + 1.07X_3 - 2.15X_1X_2 - 0.4552X_1X_3 + 0.0735X_2X_3$$

$$y_i = 13.23 - 2.64A - 1.94B + 1.07C - 2.15AB - 0.4552AC + 0.0735BC$$

C.14 Model equation in terms of actual factors

High concentration from 1 to 2mol/L NaCl, with a change of 1 and an average of 1.5. The coded value (C_v) for the high-concentration term (A) is -2.64. The actual high concentration term (A)is therefore:

$$Actual\ A\ terms = C_V * \left[\frac{2*(A-avg)}{\Delta HC}\right]$$

$$= -2.64 * \left[\frac{2*(A-1.5)}{1}\right]$$

$$= -2.64 * \frac{2}{1} * (A - 1.5)$$

$$= -5.28A + 7.92$$

The flow rate was from 896mL/min to 1550mL/min, with a change of 654 and an average of 1223. The coded value (C_v) for the high-concentration term (B) is -1.94. The actual high concentration term (B)is therefore:

$$Actual\ B\ terms = C_V * \left[\frac{2*(B-avg)}{\Delta F}\right]$$

$$= -1.94 * \left[\frac{2*(B-1223)}{654}\right]$$

$$= -1.94 * \frac{2}{654} * (B - 1223)$$

$$= -0.0059B + 7.26$$

Temperature from 20ºC to 40ºC, with a change of 20 and an average of 30. The coded value (C_v) for the high concentration term (C) is 1.07. The actual high concentration term (C)is therefore:

$$Actual\ C\ terms = C_V * \left[\frac{2*(C-avg)}{\Delta T}\right]$$

$$= 1.07 * \left[\frac{2*(C-30)}{20}\right]$$

$= 1.07 * \frac{2}{20} * (C - 30)$

= 0.107C - 3.21

The coded value for the AB term is -2.15. The actual AB term is therefore:

$Actual\ AB\ terms =$ -2.15$* [[\frac{2}{1} * (A - 1.5)]\ ]^* [\frac{2}{654} * (B - 1223)]\ ]$

$= -2.15 * (\frac{2}{1} * \frac{2}{654})[\ (A - 1.5)^* (B - 1223)]$

$= -0.0142(\mathrm{AB} - 1223\mathrm{A} - 1.5\mathrm{B} + 1834.5\ )$

$= -0.0142\mathrm{AB} + 16.0213\mathrm{A} + 0.01999\mathrm{B} - 24.03$

The coded value for the AC term is -0.4552. The actual AC term is therefore:

$Actual\ AC\ terms =$ -0.4552$* [[\frac{2}{1} * (A - 1.5)]\ ]^* [\frac{2}{20} * (C - 30)]\ ]$

$= -0.4552 * (\frac{2}{1} * \frac{2}{20})[\ (A - 1.5)^* (C - 30)]$

$= -0.09104(\mathrm{AC} - 30\mathrm{A} - 1.5\mathrm{C} + 45\ )$

$= -0.09104\mathrm{AC} + 2.73\mathrm{A} + 0.13656\mathrm{C} - 4.2968$

The coded value for the BC term is. 0.0735 The actual BC term is therefore:

$Actual\ BC\ terms =$ 0.0735$* [[\frac{2}{654} * (B - 1223)]\ ]^* [\frac{2}{20} * (C - 30)]\ ]$

$= 0.0735 * (\frac{2}{654} * \frac{2}{20})[\ (B - 1223)^* (C - 30)]$

$= 0.0000224(\mathrm{BC} - 30\mathrm{B} - 1223\mathrm{C} + 36690\ )$

$= 0.0000224\mathrm{BC} + 0.000675\mathrm{B} + 0.0275\mathrm{C} - 0.826$

Therefore, the salt removal percentage mode in terms of actual factors is:

$$=-5.28\mathrm{A} + 7.92 - 0.0059\mathrm{B} + 7.26 + 0.107\mathrm{C} - 3.2 - 0.0142\mathrm{AB} + 16.0213\mathrm{A} + 0.01999\mathrm{B} - 24.03 - 0.09104\mathrm{AC} + 2.73\mathrm{A} + 0.13656\mathrm{C} - 4.2968 + 0.0000224\mathrm{BC} + 0.000675\mathrm{B} + 0.0275\mathrm{C} - 0.826$$

$$y_i = -16.3568 + 14.43A + 0.01409B + 0.214C + 0.0142AB - 0.09104AC + 0.0000224BC$$

The coded value for the constant term is 13.23, whereas else the actual value for the constant term from the above equation is -16.3568. The salt removal percentage equation in terms of actual factors, therefore, becomes:

$$y_i = (13.23 - 16.3568) + 14.43A + 0.01409B + 0.214C + 0.0142AB - 0.09104AC + 0.0000224BC$$

$$y_i = -3.1268 + 14.43A + 0.01409B + 0.214C + 0.0142AB - 0.09104AC + 0.0000224BC$$

C.15 Residual limits

The confidence interval was investigated at 95% CI, and then the alpha value was therefore $\propto =$

$100 - 95 = 5\%$. The tail value is therefore:

$$tails = \frac{\propto}{2N}$$

$$tails = \frac{5/100}{2 * 18}$$

$$tails = 0.00138$$

The degree of freedom is therefore:

$$d_f = N - p - 1$$

$$d_f = 18 - 6 - 1$$

$$d_f = 11$$

From Table B-2 (Appendix B), the limits for the residuals (L_E) at tail = 0.00138 and d_f = 11 is:

C-16 Cook's distance limits

$L_E = \pm t_{(tail, df)} = \pm t_{(0.00138)}$

$= \pm 3.94$

From Table B-3 (Appendix B), the F-value at 0.5%, $d_{fnum} = 6$ and $d_{fden} = 11$ is 6.102

The minimum value is: 6.102.

$$L_{CD} = F^{-1} = \frac{1}{F}$$

$$L_{CD} = \frac{1}{6.102}$$

$$= 0.1639$$

= 0.1639, which is approximately equal to zero

The Cook's minimum and maximum F-critical values are 0 and 1, respectively.

C.17 DBETA

$$L_{DBETA} = \frac{3}{\sqrt{N}}$$

$$L_{DBETA} = \pm \frac{3}{\sqrt{18}} = 0.707$$

APPENDIX D-DESIGN OF EXPERIMENT RAW DATA

D.1 Transformation

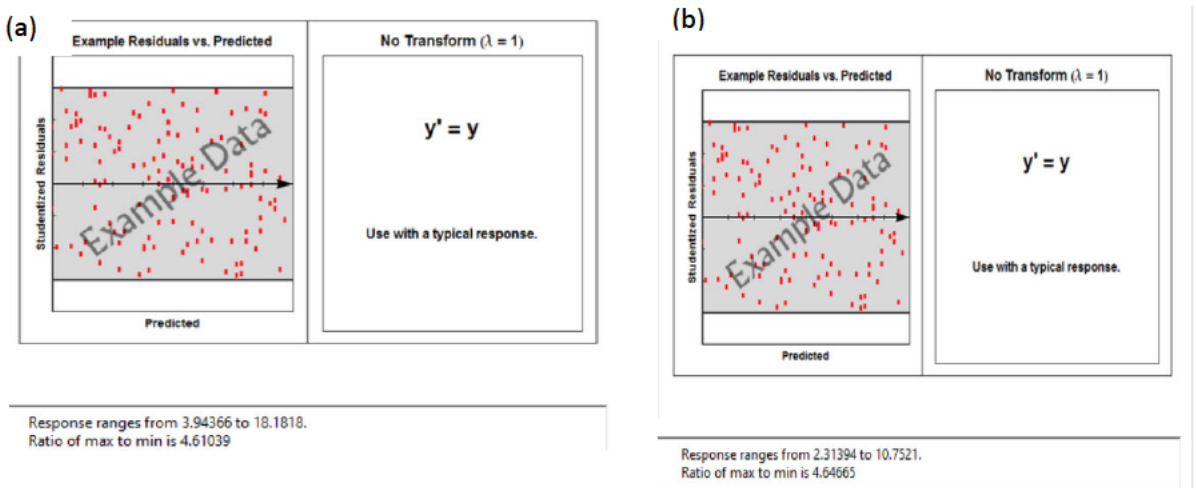

Figure D- 1: Transformation for the (a) salt removal percentage and (b) power density.

Figure D-1 (a and b) depicts the transformation graphs for salt removal percentage and power density, respectively. The response values for salt removal percentage and power density range from 3.944 to 18.182 and 2.314 to 10.7521, respectively. The ratio of maximum to minimum for salt removal percentage and power density are 4.61 and 4.65, respectively. Since the ratios are both below 10, the responses did not need transformation.

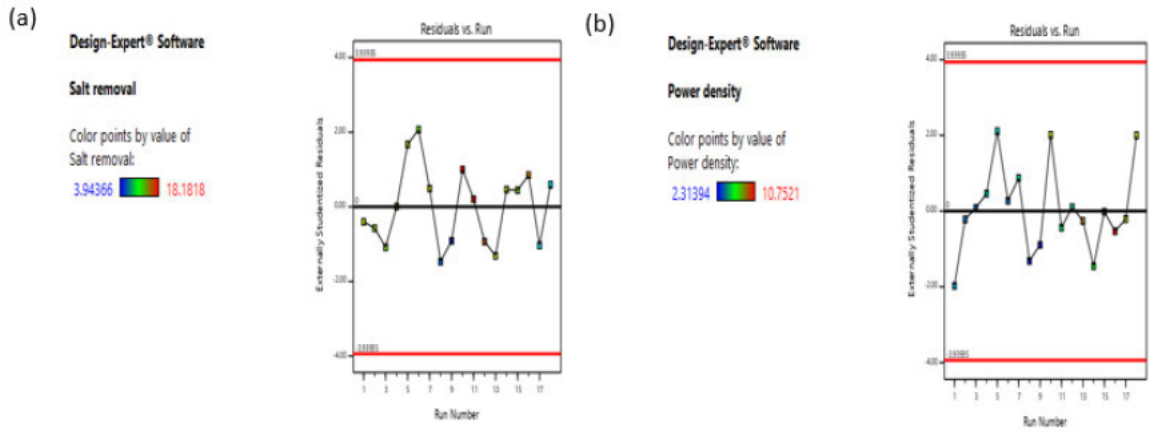

Figure D- 2: Residuals versus run plot for (a) salt removal percentage and (b) power density.

Figure D-2(a and b) depicts residuals versus run plots for salt removal percentage and power density,which is a useful diagnostic tool. Residual limits are ± 3.94, as shown in calculations C-15 and C-16. None of the observational points in both graphs are beyond the residual limits. Thus, it suggests that no response transformation was needed in any runs. A notable random scatter point indicates that no variable lurking in the background is time-related.

D.2 Main effects of variables

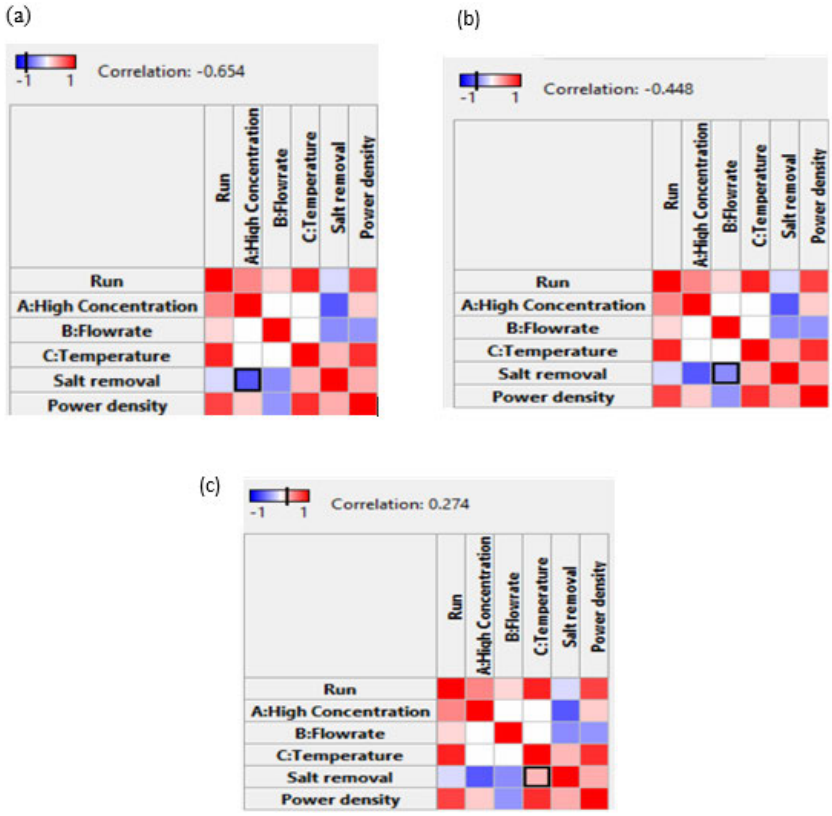

Figure D- 3: Correlation grid of (a) high concentration, (b) flow rate and (c) temperature the on-salt removal percentage.

The correlation grid box is an additional helpful indicator of how a variable affects the response, which in Design-Expert Software is located at the intersection of the variables in the graph columns. Figures D-3a, b and c depict a correlation of high concentration, flow rate, and temperature to salt removal percentage. A correlation between high concentration, flow rate, and temperature and power density is presented in Figures D-4a, b, and c.

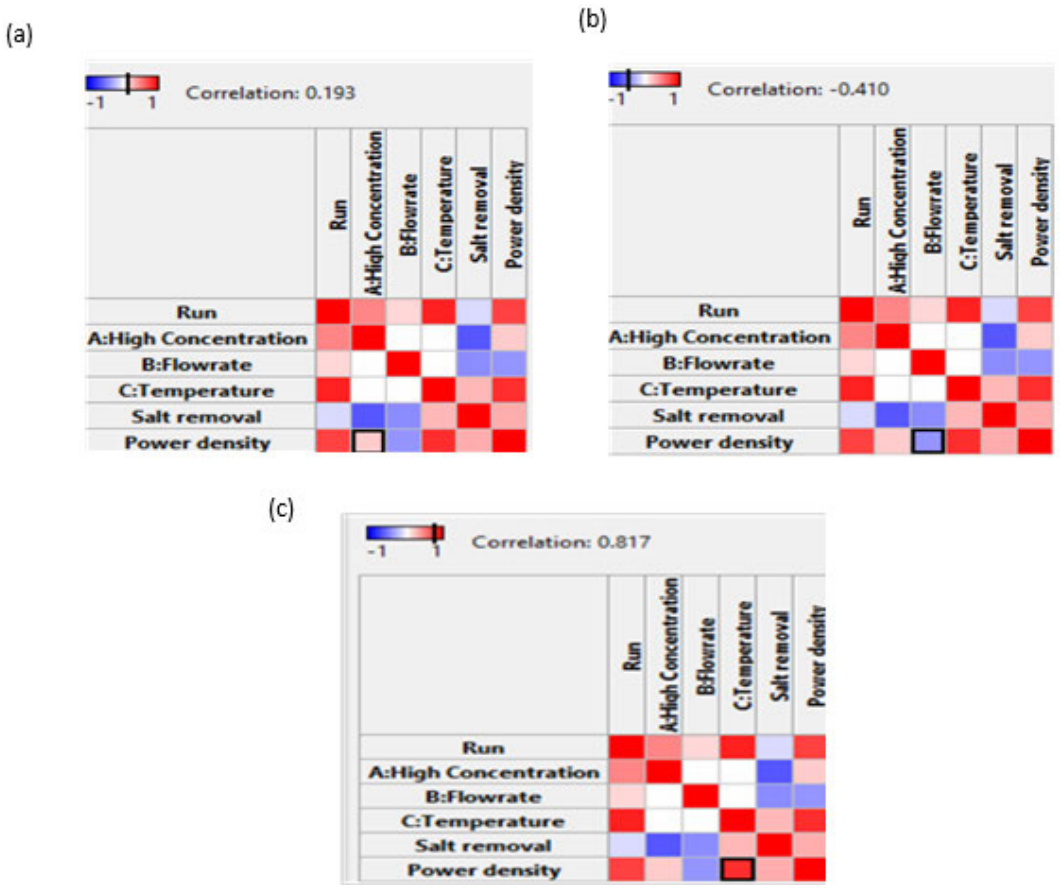

Figure D- 4: Correlation grid of (a) high concentration, (b) flow rate and (c) temperature the on-salt removal percentage.

The correlation value demonstrates the impact of each variable on the response, ranging from -1 to -1. A positive correlation indicates that the response increases with a variable, whereas a negative correlation implies that the response decreases with an increase in a variable. The study reveals that the temperature increase also increased salt removal percentage and power density. The flow rate shows the highest effect on responses, as indicated by the highest correlation (in value) of -0.488 and -0.410 for salt removal percentage and power density, respectively.

D.2 Interaction of variables

A change in the output caused by changes in the variables is generally referred to as an effect or impact. Interaction occurs when the outputs vary depending on the locations of two variables. This happens graphically at the intersection of the two curves. If the curves are parallel, then the two variables do not interact.

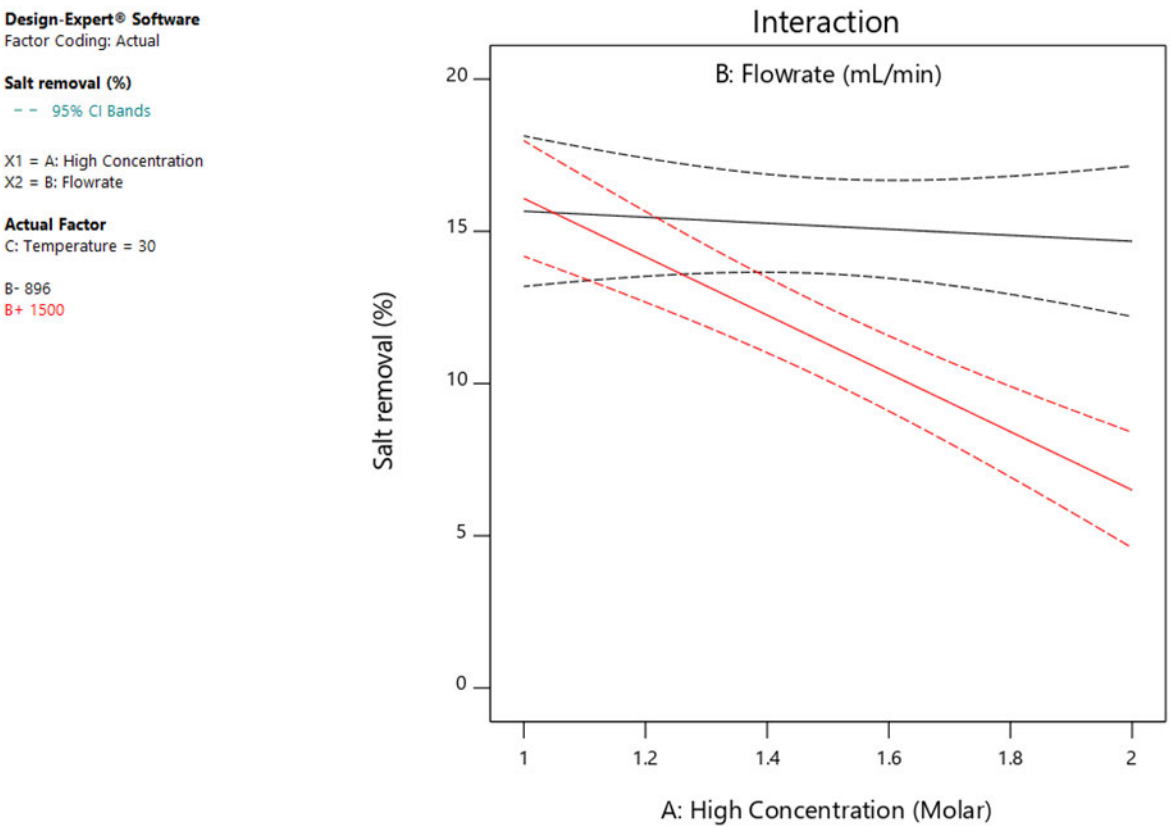

Figure D- 5: Interaction of flowrate and high concentration for salt removal percentage at a temperature of 30ºC.

Figure D-5 depicts the interactions of flow rate and high concentration to salt removal percentage. The flow rate intersects the high concentration at 15.63%. This indicates that the flow rate is not particularly significant at low concentrations. Thus, the experimenters may operate at lower flow rates and increase the concentration of the solution to acquire higher removal.

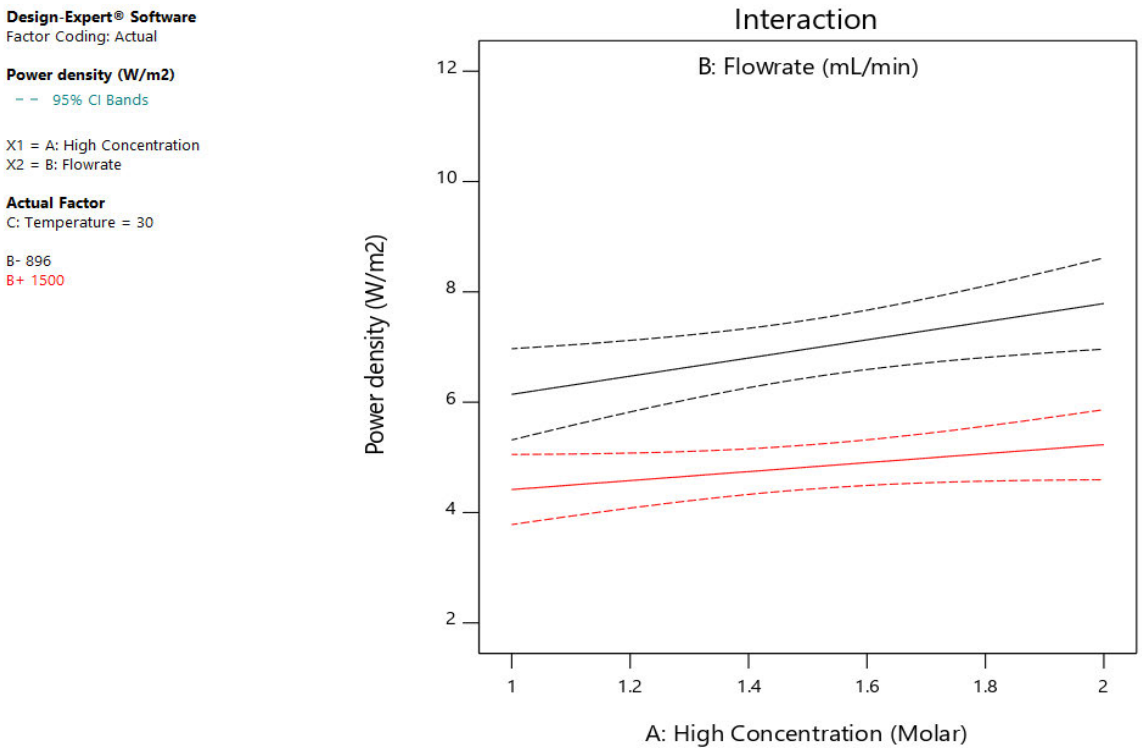

Figure D- 6: Interaction of flowrate and high concentration for power density at a temperature of 30ºC.

Figure D-6 depicts the interactions of flow rate and high concentration to power density. Flowrate curves are parallel, which means there were no interactions between high concentration and temperature.

D.3 Diagnosis in the model

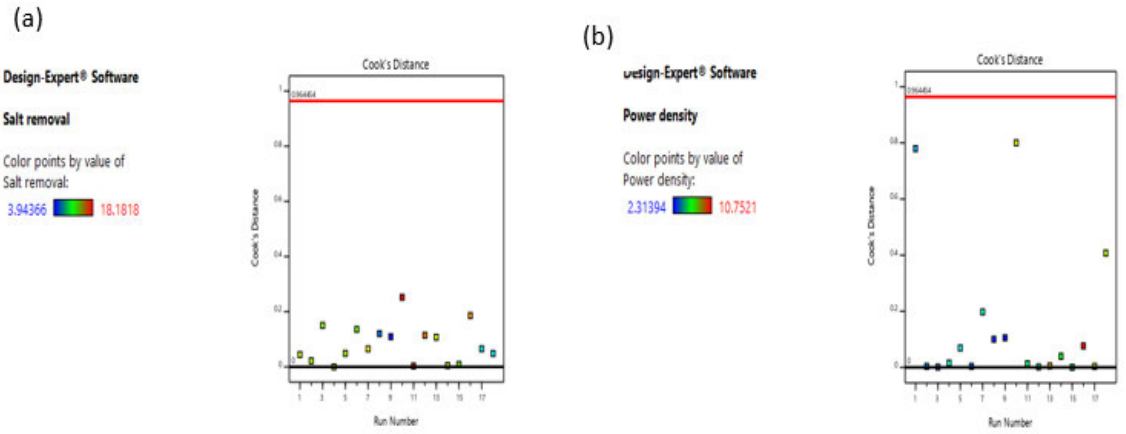

Figure D- 7: Cook's distance versus run number for (a) salt removal percentage and (b) power density.

The Cook's distance versus run number for salt removal percentage and power density are illustrated in Figure D-7 (a and b), respectively. Looking at Cook distance calculations, it ranges from 0 to 1 in both graphs. No runs are outside the limits for both graphs; thus, there is no need to investigate these runs further.

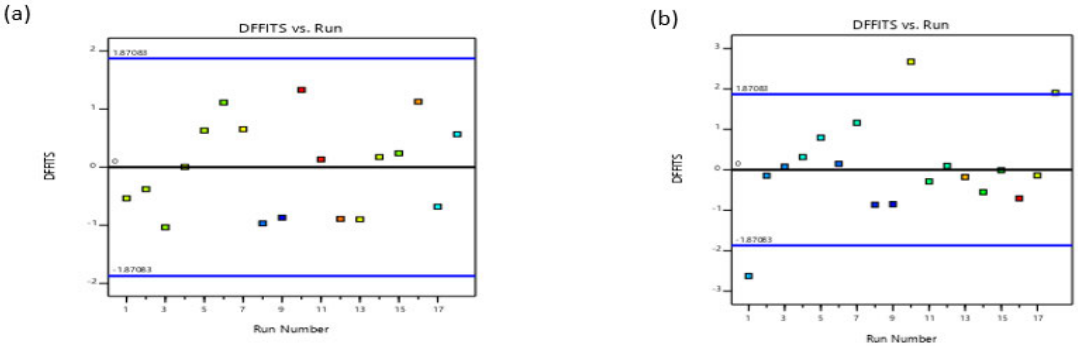

Figure D- 8: DFFITS versus run number for (a) salt removal percentage and (b) power density.

Figures D-9, D-10, D-11, D-12, D-13, and D-14 show the last significant tool, DFBETAS, versus run number for the intercept (A, B, C, AB, AC, and BC for salt removal percentage). As shown by Appendix calculation C-16, DFBETAS limits were ±0.707. From Figure D-9 to Figure D-14, all runs are inside the DFBETAS limits, which indicates that no coefficients for all terms change due to the effect from runs.

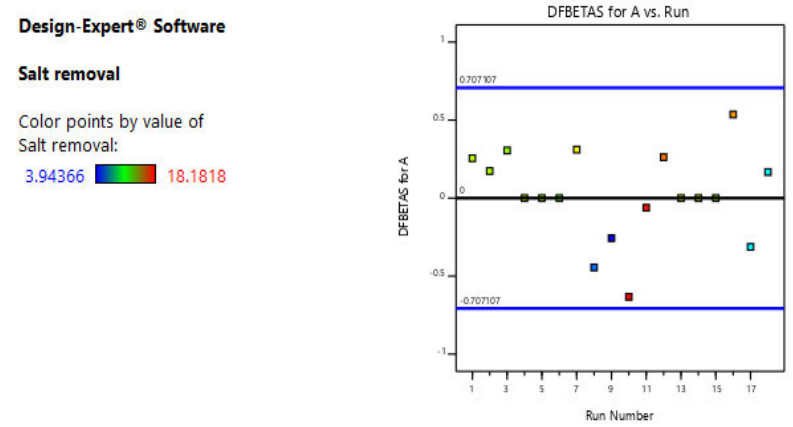

Figure D- 9: DFBETAS for A versus run number for salt removal percentage.

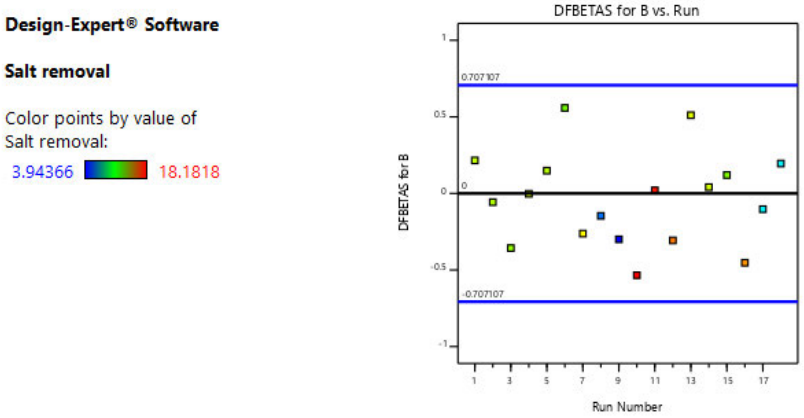

Figure D- 10: DFBETAS for B versus run number for salt removal percentage.

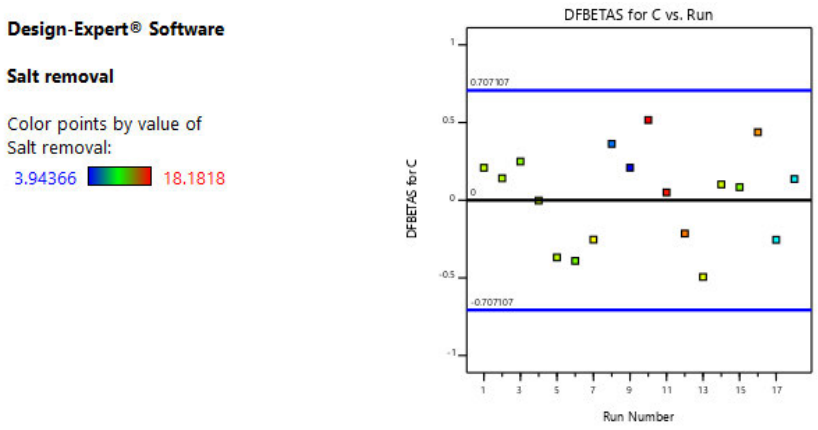

Figure D- 11: DFBETAS for C versus run number for salt removal percentage.

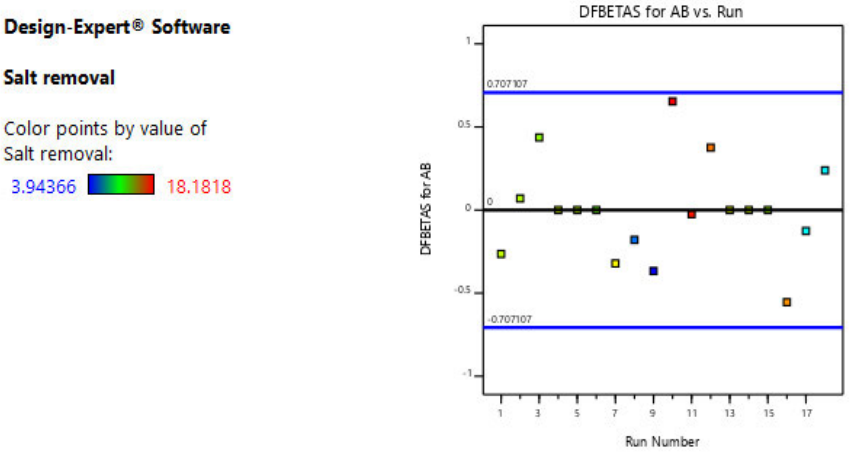

Figure D- 12: DFBETAS for AB versus run number for salt removal percentage.

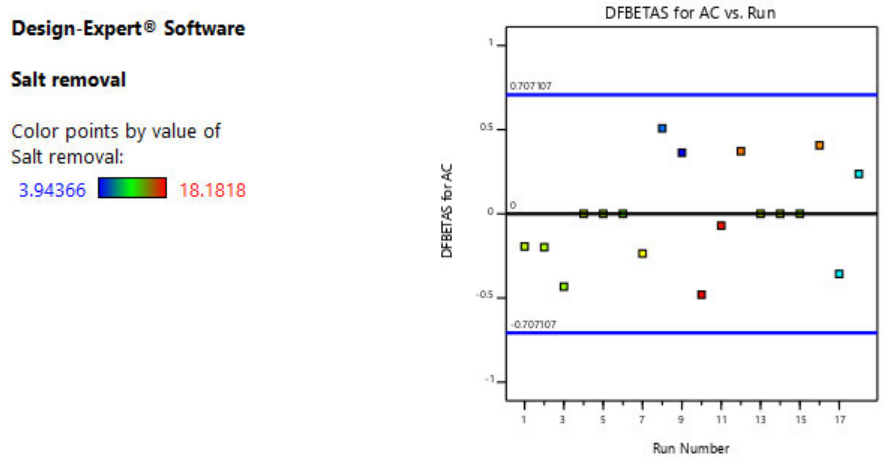

Figure D- 13: DFBETAS for AC versus run number for salt removal percentage.

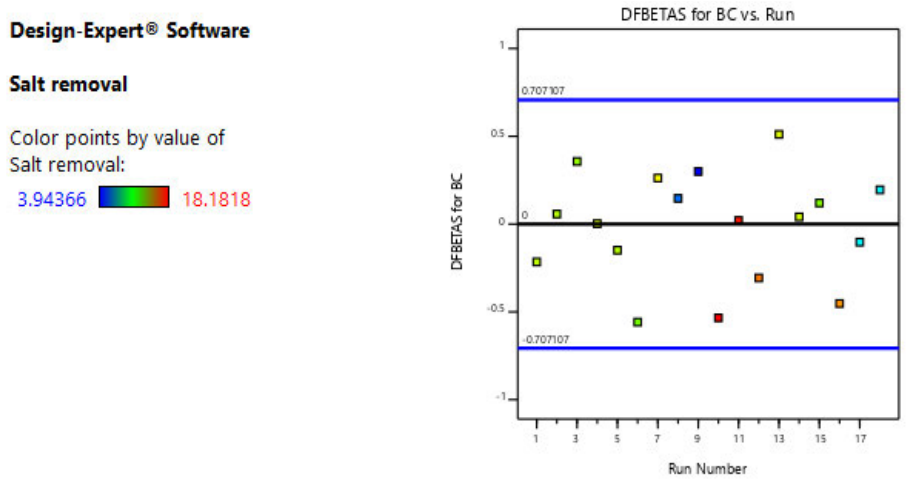

Figure D- 14: DFBETAS for BC versus run number for salt removal percentage.

Figures D-15, D-16, D-17, D-18, D-19, and D-20 depict the DFBETAS verses runs number for the intercepts (A, B, C, AB, AC, and BC for power density). Run 2 and 9 are outside the DFBETAS limits for A, Run 2 and 10 are outside the DFBETAS limits for B, Run 2 and 10 are outside the DFBETAS limits for C, Run 10 and 18 are outside the DFBETAS limits for AB, Run 1,10 and 18 are outside the DFBETAS limits for AC and Run 1 and 10 are outside the DFBETAS limits for BC. The DFBETAS limits outside indicate that the coefficients of those terms vary or change due to the effect of runs.

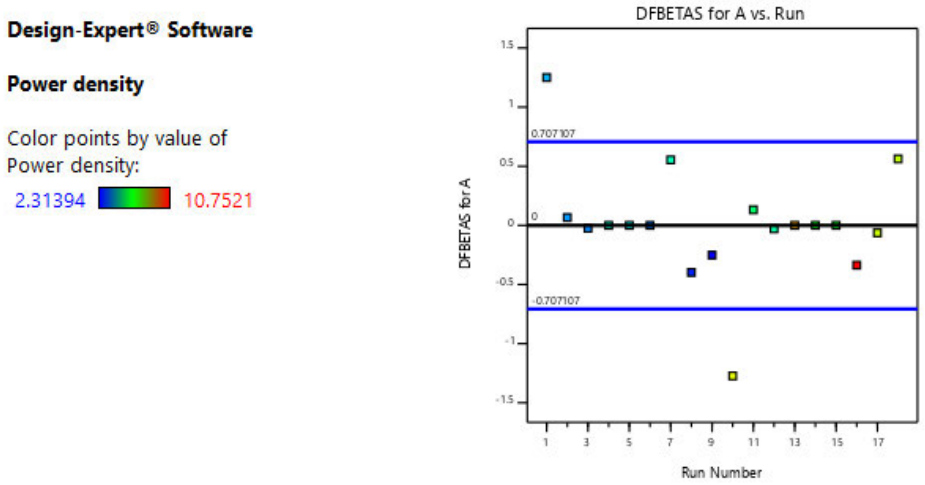

Figure D- 15: DFBETAS for A versus run number for power density.

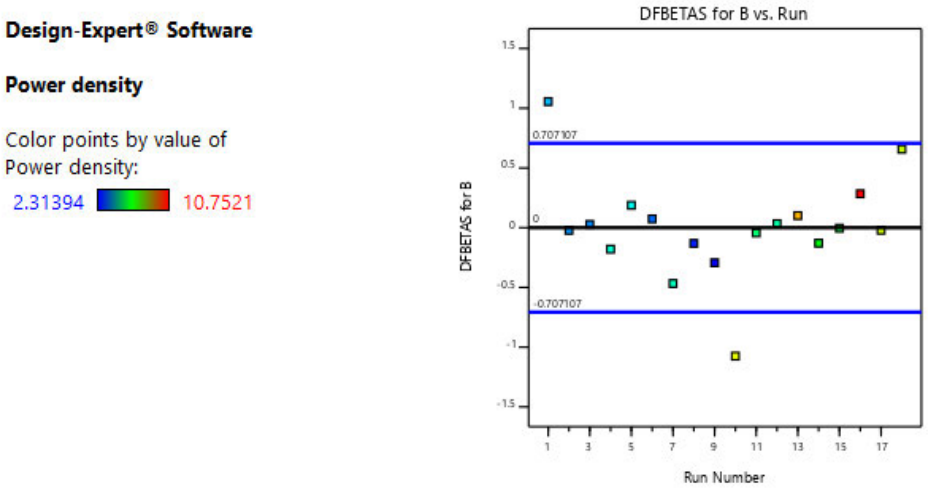

Figure D- 16: DFBETAS for B versus run number for power density.

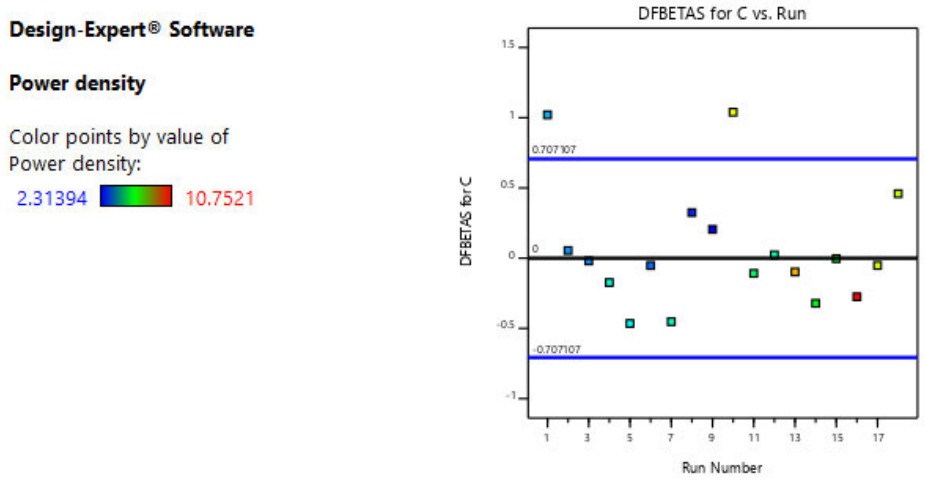

Figure D- 17: DFBETAS for C versus run number for power density.

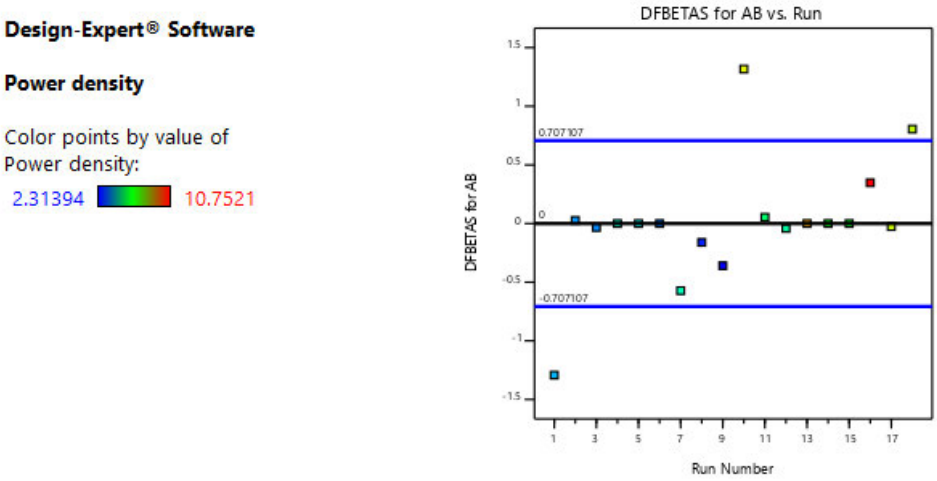

Figure D- 18: DFBETAS for AB versus run number for power density.

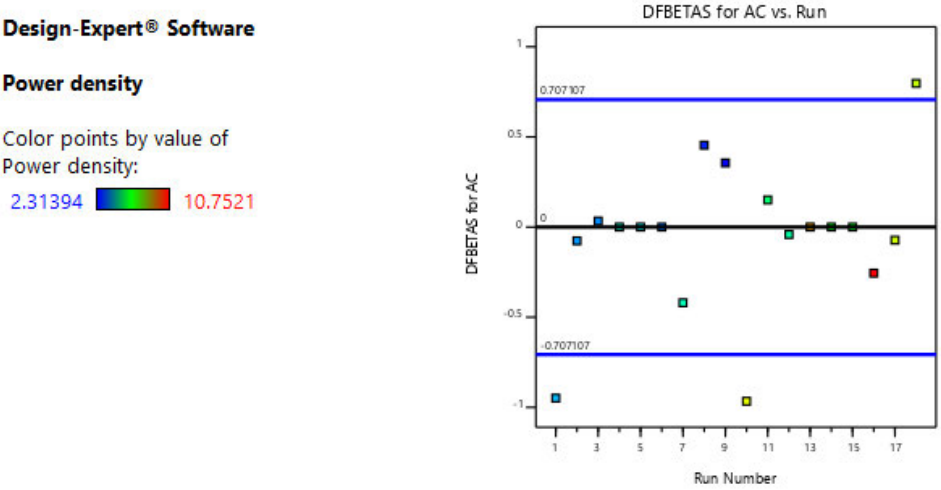

Figure D- 19: DFBETAS for AC versus run number for power density.

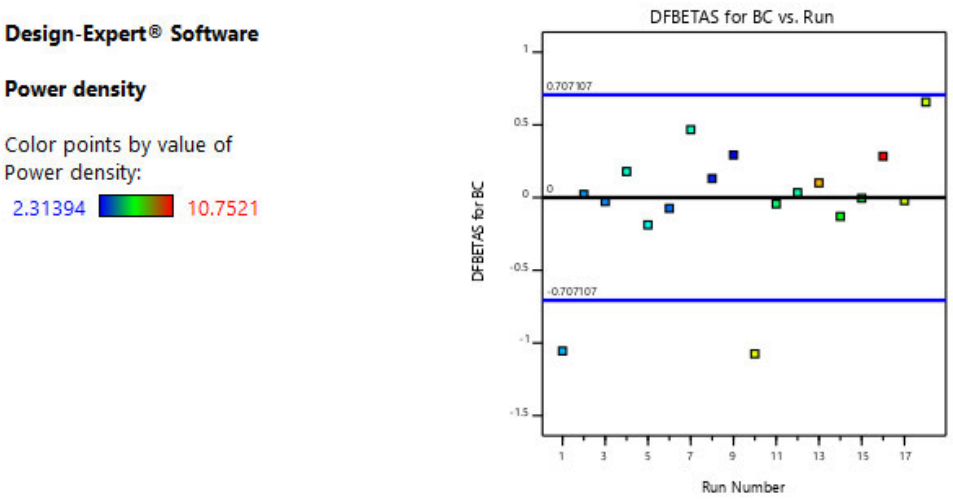

Figure D- 20: DFBETAS for BC versus run number for power density.

Box-Cox Plot is another tool that may be utilized to detect diagnosis in the model "Power Transforms" graph. Figure D-21 and Figure D-23 show the Box-Cox plots for power transformations for salt removal percentage and power density, respectively. The blue line located on the right hand in both graphs elucidates the current transformation (at Lambda =1 for none), and the green line shows the excellent lambda value unless the confidence interval includes 1.

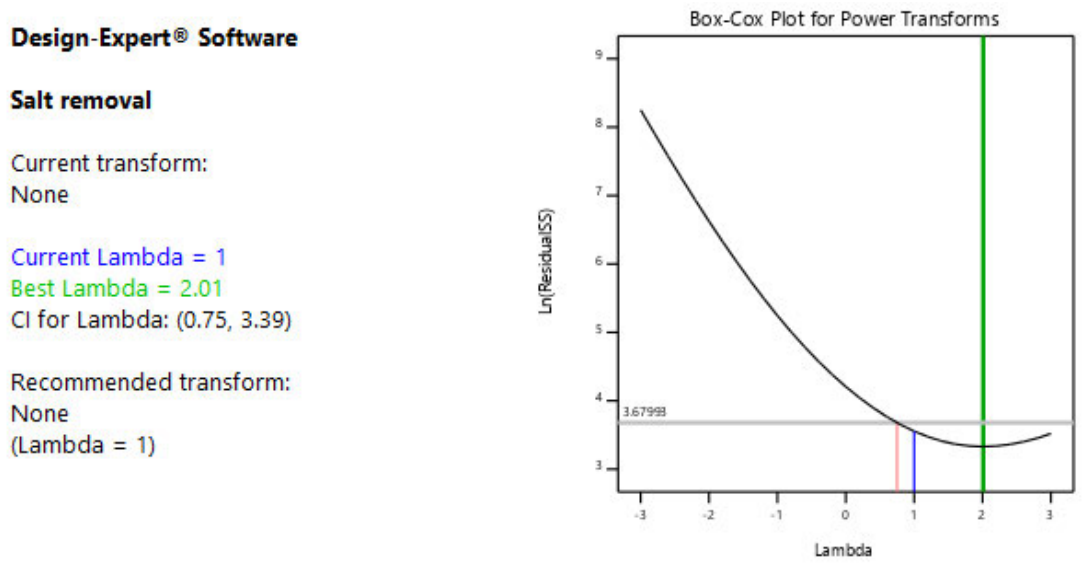

Figure D- 21: Box-Cox plot for power transformation for salt removal percentage.

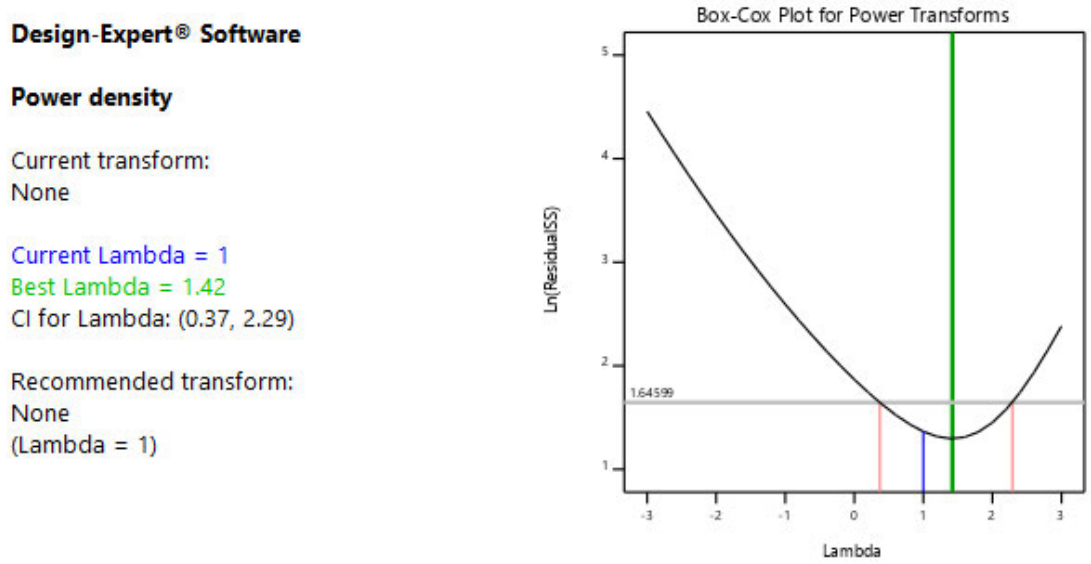

Figure D- 22 Box-Cox plot for power transformation for power density.

The current lambda (λ) is 1 for both salt removal percentage and power density. The software recommends the standard transformation that is nearly closest to the best λ and that which is within the 95% CI. In this case, the Lambda for salt removal percentage and power density are precisely 1, respectively. This best describes that the recommendation will be "None."

Table D-1 Presents the confirmation report that may be utilised to make response estimations for any combinations of process variables. The predicted mean values are similar to the

predicted median, as shown in the confirmations report. Thus, this indicates that the model can predict actual outcomes. The software uses the model acquired from practical results to estimate the interval (PI) and mean for the number (n) of confirmation runs at the conditions employed, yielding the highest salt removal percentage and power density at a lower flow rate.

Table D- 1 Confirmation of best factor settings for salt removal percentage and power density

Two-sided	**Confidence = 95%**		**n=1**					
Factor	**Name**	**Level**	**Low Level**	**High Level**	**Std. Dev.**	**Coding**		
A	High Concentration	1.50	1.0000	2.00	0.0000	Actual		
B	Flowrate	1198.00	896.00	1500.00	0.0000	Actual		
C	Temperature	30.00	20.00	40.00	0.0000	Actual		
Response	**Predicted Mean**	**Predicted Median**	**Observed**	**Std Dev**	**n**	**SE Pred**	**95% PI low**	**95% PI high**
Salt removal	15.3323	15.3323		1.78285	1	2.22827	10.4279	20.2367
Power density	10.7521	10.7521		0.596486	1	0.745511	9.11122	12.3929

APPENDIX E - EQUIPMENTS USED IN EXPERIMENT

Purite water-deionizer

A deionized machine was used to synthesize the solutions.

Figure E- 1: Purite water-deionizer

ICP-OES

ICP-OES was used for the characterization of the solutions.

Figure E- 2: Inductively Coupled Plasma Optical Emission Spectroscopy (ICP-OES)

Test tube rack

A test tube rack was used to store solutions before being transported to UKZN-PMB School of Chemistry.

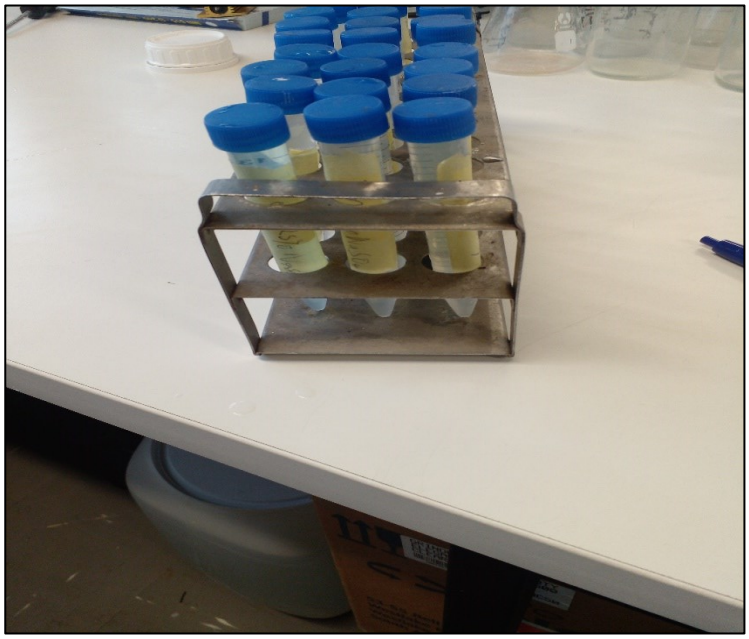

Figure E- 3: Test tube rack.

APPENDIX F – ICP RESULTS

This appendix illustrates conditions selected for characterization and results obtained from ICP-OES.

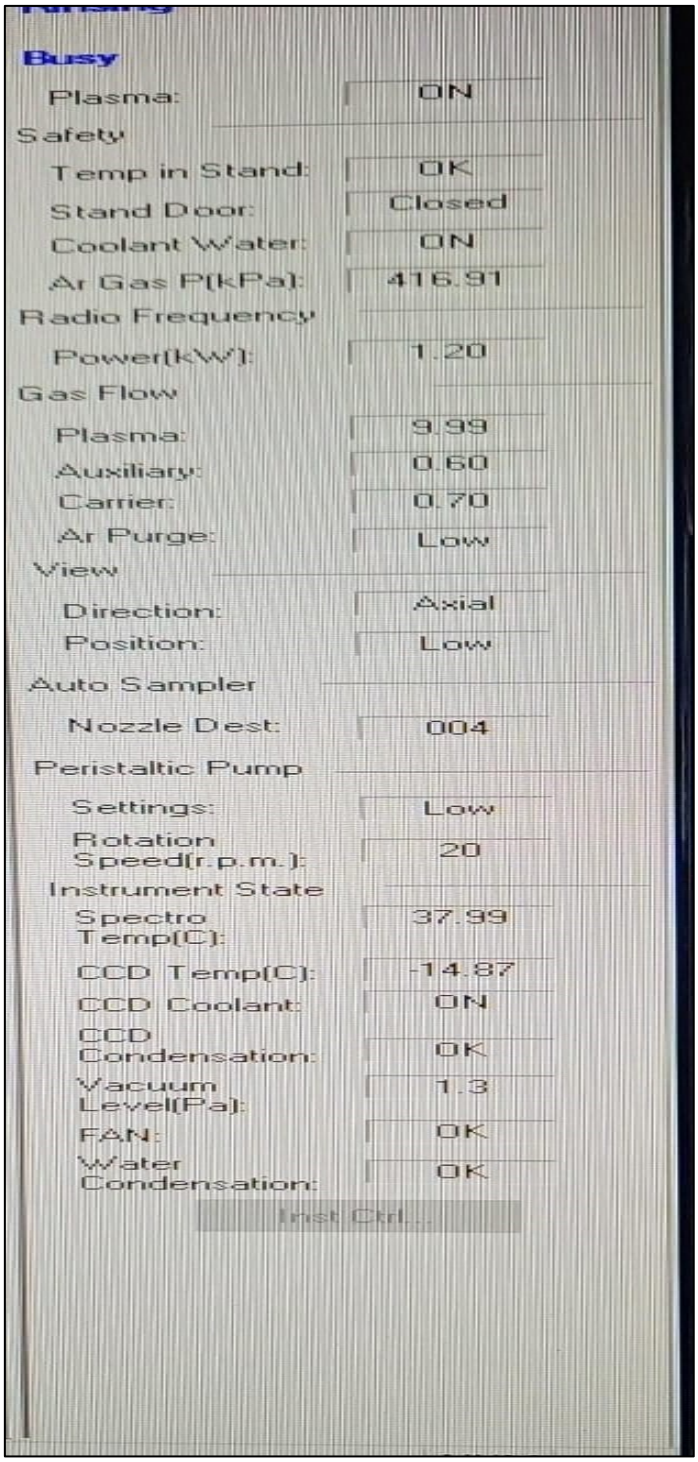

Figure F- 1: Conditions of the instruments provided by (UKZN-PMB School of Chemistry).

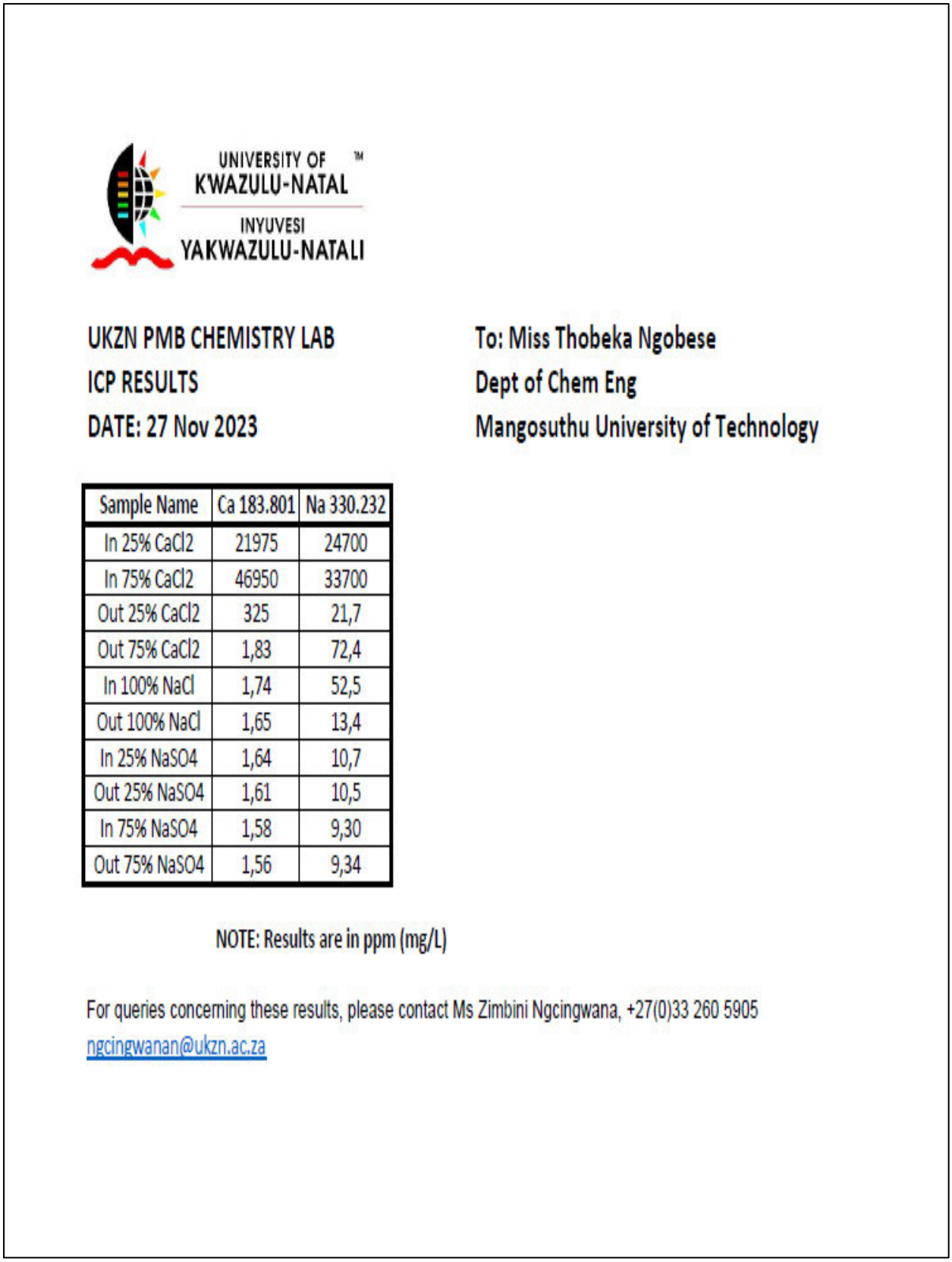

UNIVERSITY OF KWAZULU-NATAL
INYUVESI YAKWAZULU-NATALI

UKZN PMB CHEMISTRY LAB
ICP RESULTS
DATE: 27 Nov 2023

To: Miss Thobeka Ngobese
Dept of Chem Eng
Mangosuthu University of Technology

Sample Name	Ca 183.801	Na 330.232
In 25% CaCl2	21975	24700
In 75% CaCl2	46950	33700
Out 25% CaCl2	325	21,7
Out 75% CaCl2	1,83	72,4
In 100% NaCl	1,74	52,5
Out 100% NaCl	1,65	13,4
In 25% NaSO4	1,64	10,7
Out 25% NaSO4	1,61	10,5
In 75% NaSO4	1,58	9,30
Out 75% NaSO4	1,56	9,34

NOTE: Results are in ppm (mg/L)

For queries concerning these results, please contact Ms Zimbini Ngcingwana, +27(0)33 260 5905
ngcingwanan@ukzn.ac.za

Figure F- 2: ICP Results provided by (UKZN-PMB School of Chemistry).

APPENDIX G - CONFERENCE ABSTRACT

This appendix illustrates the research outputs of this study.

Decarbonization by desalination with reverse electrodialysis: A comparative study

Thobeka Ngobese [a, *], Peterson T. Ngema[a], Tumba A. Kaniki[b], Nkululeko Nkosi[b]

[a]Department of Chemical Engineering, Green Engineering Research Group (GERG), Chemical Thermodynamics, Durban University of Technology, Steve Biko Campus, Durban, 4001, South Africa

[b]Department of Chemical Engineering, Materials and Separations Research Group (TMSRG), Mangosuthu University of Technology, uMlazi, Durban, 4031, South Africa

ABSTRACT

Water shortages hinder economic development, deteriorate health and environmental conditions, and foster political instability. The United Nations (UN) created global sustainable development goals (SDGs) in response to this crisis. The Sustainable Development Goals include a commitment to clean drinking water for everyone as part of sustainable water management. Among the best solutions to the problem of global water shortages is desalination. The technology is, however, expensive to maintain and energy intensive. Approximately 150 countries have embraced this technology, increasing the demand for electricity from conventional power plants. As a result of this high energy consumption, the environment is negatively affected. This impact is expected to increase as global desalination capacity increases at a steep rate. A promising renewable technology for desalination has been proposed as part of the UN's SDGs initiatives: reverse electrodialysis. A competitive advantage of this technology is its ability to desalinate while producing electricity. A comparison of conventional desalination technologies and reverse electrodialysis will be presented in this paper. This review aims to evaluate the underlying challenges of conventional technologies against the benefits of RED technology.

Keywords: Reverse electrodialysis; Desalination; Technologies; Emissions.

*Corresponding author: Thobeka Ngobese; Email: thobekantathu@gmail.com

APPENDIX H - CONFERENCE PAPER

Progress on Strategies to Maximize Reverse Electrodialysis Power Density Using Industrial and Municipal Effluents.

Thobeka Ngobese [1,*], Peterson T. Ngema [1], Kaniki Tumba [2,3], Nkululeko Nkosi [2]

***Abstract*—**High salinity wastewater disposal has adversely affected and degraded aquatic ecosystems. Furthermore, the current wastewater treatment technologies in the Sub-Saharan region are not designed to handle salinized wastewater, which has worsened the water scarcity challenge. Beyond environmental concerns, the agricultural sector is also negatively impacted due to its dependency on clean water for irrigation. Several developed technologies have been used to mitigate these challenges, including desalination as well as membrane, and thermal processes. On the other hand, their reliability when applied to large-scale industrial processes is limited by the high cost of routine maintenance and the intensive energy requirements of such methods. Therefore, scaling these technologies would increase their energy demand, undermining the sustainable development goals (SDGs) initiative taken by the United Nations (UN). The initiative promotes renewable energy while banning fossil fuel-based energy resources. Reverse electrodialysis has emerged as an alternative to treating salinized wastewater effluents. Increasingly, scientists are interested in this technology because of its advantage of harnessing electricity while reducing waste. This technology appears to be in positive alignment with UN SDGs based on studies by other researchers. However, this technology's maximum salinity gradient power is a concern that needs to be addressed. Hence, this paper proposes a critical review of the salinity gradient power production from industrial and municipal effluents. This aims to present the progress of this technology and the strategies used to increase its power-generating capacity.

Thobeka Ngobese [1] is affiliated with the Thermodynamics-Materials-Separations Research Group, in the Department of Chemical Engineering at Mangosuthu University of Technology in Durban (MUT), South Africa, and Green Engineering Research Group (GERG), in the Department of Chemical Engineering at Durban University of Technology, Steve Biko Campus, Durban, 4001, South Africa

Peterson T. Ngema [1] is affiliated with Green Engineering Research Group (GERG), in the Department of Chemical Engineering at Durban University of Technology, Steve Biko Campus, Durban, 4001, South Africa

Kaniki Tumba [2,3] is affiliated with Thermodynamics-Materials and Separations Research Group (TMSRG), in the Department of Chemical Engineering at Mangosuthu University of Technology, uMlazi, Durban, 4031, South Africa; He is also affiliated with the School of Mines at the Official University of Bukavu in the Democratic Republic of Congo

Nkululeko Nkosi[2] is affiliated with Thermodynamics-Materials and Separations Research Group (TMSRG), in the Department of Chemical Engineering at Mangosuthu University of Technology.

***Keywords*—:** Reverse electrodialysis; Salinity gradient power; Renewable energy; Wastewater; Effluent.

I. Introduction

Freshwater and energy are necessary elements for sustaining modern civilization; however, rising population growth and population density have put a strain on many local supplies to sustain water quantity requirements at acceptable water quality standards. The United Nations estimated that by 2025, 1.8 billion people will have a complete water shortage, and 2/3 of the world will be living under water-stressed conditions. Moreover, by 2030, high water stress will affect nearly half of the world's population [1]. This shortage of natural freshwater has promoted desalination to be a major source of freshwater worldwide. It is widely known that the treatment of water or wastewater consumes a large amount of energy, and that wastewater contains thermal energy as well as chemical energy [2]. Desalination, which is a component of treating water or wastewater is broadly categorized as thermal or membrane-based technologies [3].

Desalination has attracted a lot of attention recently due to its potential for recovering potable water from sewage and as well as brackish and seawater, which is why it is seen to be crucial in supplying the world's water needs [4]. Total global capacity to produce fresh water via desalination has increased from around 5 million cubic meters per day (m^3/day) in 1980, to 20 million m^3/day in 2000, to around 90 million m^3/day in 2020, with all major market forecasters anticipating that this tendency will persist over the next few decades [5]. The major drawback with most desalination processes is associated with cost, considering that a power plant is required to provide the energy requirements of the process (electricity may be provided by the national grid) [6]. Desalination is inherently energy-intensive, and energy consumption is a crucial contributor to the overall cost and is also related to environmental impacts. Hence, higher energy consumption also results in a proportional rise in greenhouse gas emissions (GHG) [3]. Therefore, the application of the desalination process such as electromembrane process is critical for lowering the cost of desalination and addressing environmental concerns about GHG emissions from the continuous operation of municipal and industrial desalination plants using conventional fossil fuels as their main energy

https://doi.org/10.17758/IICBE5.C1123044